Deciphering the role of the malectin-like RLK and LRR-RLKs in the liverwort *Marchantia polymorpha*

Inaugural-Dissertation

zur

Erlangung des Doktorgrades

der Mathematisch-Naturwissenschaftlichen Fakultät

der Universität zu Köln

vorgelegt von

Yijia Yan

aus Qiqihar

Köln, September 2024

Die vorliegende Arbeit wurde am Max-Planck-Institut für Pflanzenzüchtungsforschung in Köln in der unabhängigen Forschungsgruppe Grundlegendes Immunsystem der Pflanzen unter der Leitung von Dr. Hirofumi Nakagami angefertigt.

This work described in this thesis was conducted under the supervision of Dr. Hirofumi Nakagami in the independent research group Basic Immune System of Plants at the Max Planck Institute for Plant Breeding Research in Cologne.

Berichterstatterinnen:

Prof. Dr. Jane Parker

Prof. Dr. Alga Zuccaro

Prüfungsvorsitzender:

Prof. Dr. Gunther Döhlemann

Tag der mündlichen Prüfung:

21. Nov. 2024

Publications

Conserved role of the SERK–BIR module in development and immunity across land plants

Yan, Y., J. Mellüh, M. A. Mecchia, H. W. Jeon, K. Melkonian, C. Holzberger, A. Harzen, S. C. Stolze, R. Franzen, Y. Hirakawa, A. I. C. Delgado, and H. Nakagami.

(2024) bioRxiv, Submitted

LysM-mediated signaling in Marchantia polymorpha highlights the conservation of pattern-triggered immunity in land plants

Yotsui, I., H. Matsui, S. Miyauchi, H. Iwakawa, K. Melkonian, T. Schluter, S. Michavila, T. Kanazawa, Y. Nomura, S. C. Stolze, H. W. Jeon, Y. Yan, A. Harzen, S. S. Sugano, M. Shirakawa, R. Nishihama, Y. Ichihashi, S. G. Ibanez, K. Shirasu, T. Ueda, T. Kohchi, and H. Nakagami.

(2023) Current Biology

Abstract

FERONIA (FER) is a member of the malectin-like receptor-like kinase (MLR) family that plays versatile roles in various plant processes such as reproduction, cell growth, and immunity in angiosperms. FER perceives RAPID ALKALINISATION FACTOR (RALF) peptides to modulate development and immunity. While MLRs are conserved among land plants, the molecular and biological functions of FER in non-flowering plants remain largely unexplored. The liverwort *Marchantia polymorpha* encodes a single homologue of FER, known as MpFER, which has been reported to play roles in growth and development. However, its ligands and role in immunity have not yet been described.

In this study, I found that *M. polymorpha* recognises and responds to MpRALF1 and MpRALF3 peptides by producing reactive oxygen species (ROS) in an MpFER-dependent manner. The rhizoids and rhizoid-initiated areas mainly contributed significantly to ROS production, indicating that MpRALFs and MpFER function as a module in *M. polymorpha*. Using the proximity labelling-based interactome analysis, LysM RECEPTOR-LIKE KINASE1, MpLYK1, and LysM RECEPTOR-LIKE KINASE-RELATED, MpLYR, were identified as candidate interactors of MpFER, pointing to a potential crosstalk between MpFER- and MpLYK1-mediated signalling pathways. Transcriptome analysis of *M. polymorpha* treated with MpRALF1 suggested that MpRALF1 positively regulates defence responses. This was supported by the finding that MpRALF1 treatment primed the resistance of *M. polymorpha* against the bacterial pathogen *Pseudomonas syringae* pv. *tomato* DC3000 (*Pto* DC3000). Altogether, this study demonstrates the conservation of the RALF–FER module and its contribution to plant immunity in the liverwort *M. polymorpha*.

The leucine-rich repeat receptor-like kinases (LRR-RLKs) family is the most prominent and best-characterised RLK family in plants. LRR-RLKs are structurally classified into 14 subfamilies. Several subfamily XII LRR-RLKs have been proven to function as pattern-recognition receptors (PRRs) that sense pathogen invasions. Subfamily II LRR-RLKs are generally considered to function as co-receptors, required for LRR-RLK-type PRR-mediated signalling. Within subfamily II, SOMATIC EMBRYOGENESIS RECEPTOR-LIKE KINASES3 (SERK3) was identified as a co-receptor for the PRRs, and thereby plays a role in immunity in the angiosperm *Arabidopsis thaliana*. AtSERK3 also functions with other LRR-RLKs, including BRASSINOSTEROID INSENSITIVE1 (BRI1), to regulate growth and development. The conserved tyrosine residue in AtSERK3 is crucial for signalling specificity in differentiating PRR- and BRI1-mediated pathways. *Marchantia polymorpha* encodes three

subfamily II LRR-RLKs, MpSERK, MpAPEX, and MpCIK, whose functions are poorly characterised.

Here, I investigated the functions of MpSERK and MpAPEX. I found that MpAPEX has a minimal role in growth and development. Mp*apex* mutants tended to be resistant against *Pto* DC3000 compared to wild-type plants, indicating a possible role for MpAPEX in immunity. In contrast, I found that MpSERK plays a crucial role in growth and sexual or vegetative reproduction. Complementation analysis demonstrated that the conserved tyrosine residue of MpSERK is important for thallus growth. Proximity labelling-based interactome analysis identified MpBIR as an MpSERK interactor. Mp*bir* mutants displayed defects in reproductive organ development. Transcriptome analysis revealed that the patterns of development- and immunity-related gene expression in Mp*serk* and Mp*bir* were antagonistic, suggesting that MpBIR functions as an MpSERK repressor. I further found that *Pto* DC3000 barely grew on Mp*bir*, highlighting the significant role of the MpSERK–MpBIR module in immunity. Taken together, this study shows that MpAPEX and MpSERK play roles in immunity. The SERK–BIR working module appears to regulate immunity and development across land plants.

Table of Contents

Acknowledgements

Hiro, thank you for giving me the chance to study here and work on this fantastic project. Over the past nearly four years, I have learnt so much, especially from you. I am deeply grateful for your invaluable advice (both in science and life) and your patience during my PhD journey. There were times when I forgot things and felt really panicked, but you were always kind and supportive. And thank you for your strictness in writing. It was painful, but I felt so great when I finally got through it and learnt a lot. You have always been there whenever I needed support when experiments didn't go right, and I will never forget to 'think deeply.' Thanks a lot!

I also would like to thank my TAC members, Tonni and Alga, for your kind support, guidance, and critical advice on my project.

Thanks to all my group members. Sara and Anne, thank you for the very kind, professional, and efficient support in mass spec. David, thanks for the advice and help in science and bench work. We had great talks about football! Mung, thank you for always being there, for the trips, beers, dinners, all the wonderful times, and the code words! Gabriel, thanks for the help and conversations, and for creating an enjoyable atmosphere in our office, despite the scary plastic spider. Katharina, thank you for everything. You really helped me a lot in science and life, especially when I first came to Germany. I feel so lucky to have had you in my PhD life. You are always the best! I will never forget you, TOO!

A huge thank you to my parents and grandparents for their encouragement, unconditional support, love, and belief in me all along the way. I love you so much. Thanks to XiangXiang Dun for always being there, being patient, having my back, and knowing me so well no matter what! I love you. Thanks to my friends, Shufang, Qiaochu, and Ram. I am incredibly grateful to have had you all in my life. Shufang, you are not here, but I know you are always with me. I love you so much.

Last but not least, thanks to my cats, Mochi and Coffee. Thank you for just being so cute. Whenever I think about you two, I feel so happy and relieved. I love you two forever.

Abbreviations

Abbreviation	Full name
aa	amino acid(s)
ACN	acetonitrile
AHA	H^+-adenosine triphosphatase
Amp	ampicillin
ANOVA	analysis of the variance
At	*Arabidopsis thaliana*
ATP	adenosine triphosphate
BAK	BRI1-ASSOCIATED KINASE
BH	Benjamini and Hochberg
BIR	BAK1-INTERACTING RECEPTOR-LIKE KINASE
BLAST	basic local alignment search tool
bp	base pair(s)
BR	brassinosteroid
BRI1	BRASSINOSTEROID-INSENSITIVE1
CAA	chloroacetic acid
CaMV	cauliflower mosaic virus
Cas9	CRISPR-associated protein 9
CBB	coomassie brilliant blue
cDNA	complementary DNA
CDS	coding sequence
CERK	CHITIN ELICITOR RECEPTOR KINASE
CIK	CLAVATA3 INSENSITIVE RECEPTOR KINASE
cm	centimetre
Col-0	Columbia 0
CRISPR	clustered regularly interspaced short palindromic repeats
CRISPRR	CRISPR resistance
CrRLK1L	*Catharanthus roseus* RECEPTOR-LIKE KINASE 1-LIKE
CS	chlorsulfuron
C-terminus	carboxyl terminus
CWI	cell wall integrity
DAMPs	damage-associated molecular patterns

DEG	differentially expressed gene
DKO	double knock-out
DNA	deoxyribonucleic acid
dpi	day(s) post inoculation
DTT	dithiothreitol
dV	destination vector
ECD	extracellular domain
EDTA	ethylenediaminetetraacetic acid
EFR	EF-Tu RECEPTOR
EF-Tu	elongation factor-Tu
EF1*α*	elongation factor 1*α*
EGF	epidermal growth factor
elf18	N-terminal peptide of EF-Tu, N-acetylated
ETI	effector-triggered immunity
eV	entry vector
FA	ferulic acid
FC	fold change
FDR	false discovery rate
FER	FERONIA
flg22	flagellin-derived 22 amino acid peptide
FLIM	fluorescence lifetime imaging microscopy
FLS2	FLAGELLIN-SENSITIVE2
FMK	mitogen-activated protein kinase of *Fusarium oxysporum*
FRET	Förster resonance energy transfer
GB	Gamborg's B5
Gent	gentamicin
GFP	green fluorescent protein
GMO	genetically modified organism
GO	gene ontology
GPI	glycosylphosphatidylinositol
GST	glutathione-s-transferase
GUS	β-glucuronidases
GW	gateway
h	hour(s)

HCD	higher-energy C-trap dissociation
His	polyhistidine
HR	hypersensitive response
HRP	horseradish peroxidase
HSD	honestly significant difference
Hyg	hygromycin
IgG	immunoglobulin G
IPTG	isopropyl ß-D-1-thiogalactopyranoside
JA	jasmonic acid
Kan	kanamycin
KD	kinase domain
kDa	kilo Dalton
KO	knock-out
L	litre(s)
LB	lysogeny broth
LC	liquid chromatography
LED	light-emitting diode
LFQ	label-free quantification
LLG	LRE-LIKE GPI-ANCHORED PROTEIN
L-O12	luminol-based chemiluminescent probe
LRE	LORELEI
LRR	leucine-rich repeat
LRX	leucine-rich repeat extensin
lux	*luxCDABE* luciferase operon
LYK	LYSM RECEPTOR-LIKE KINASE
LYR	LYSM-KINASE-RELATED
LysM	lysin motif
mA	milliampere
MAMPs	microbe-associated molecular patterns
MAPKs	mitogen-activated protein kinases
MBP	maltose-binding protein
mg	microgram
min(s)	minute(s)
mL	millilitre(s)

mm	millimetre(s)
mM	millimolar
Mp	*Marchantia polymorpha*
MS medium	Murashige and Skoog medium
ms	millisecond(s)
MS	mass spectrometry
mTb	miniTurbo
m/z	mass-to-charge ratio
NB	nucleotide-binding
NLR	nucleotide-binding and leucine-rich repeat
nL	nanolitre(s)
nm	nanometre(s)
ns	not significant
N-terminus	amino terminus
OD	optical density
PAGE	polyacrylamide-gel electrophoresis
PAMPs	pathogen-associated molecular patterns
PCA	principal component analysis
pH	potential of hydrogen
PVFD	polyvinylidene fluoride
RT-PCR	reverse transcription polymerase chain reaction
pep	plant elicitor peptide
PD	plasmodesmata
PR	PATHOGENESIS RELATED
PRR	pattern-recognition receptor
PTI	PRR-triggered immunity
Pto	*Pseudomonas syringae* pv. *tomato*
R	resistance
RALF	RAPID ALKALINISATION FACTOR
RGF	root meristem growth factor
RGI1	RGF1 INSENSITIVE1
RIPK	RPM1-INDUCED PROTEIN KINASE
RLCK	receptor-like cytoplasmic kinase
RLK	receptor-like kinase

RLP	receptor-like protein
RLU	reactive luminescence units
RNA	ribonucleic acid
ROS	reactive oxygen species
rpm	revolutions per minute
RPM	RESISTANCE TO *P. SYRINGAE* PV. *MACULICOLA*
RT	room temperature
SA	salicylic acid
SEM	scanning electron microscope
seq	sequencing
SD	standard deviation
SDS	sodium dodecyl sulfate
SE	standard error
SERK	SOMATIC EMBRYOGENESIS RECEPTOR-LIKE KINASE
sgRNA	single guide RNA
Spt	spectinomycin
strep	streptavidin
S1P	SITE-1 PROTEASE
Tak	Takaragaike
TDIF	TRACHEARY ELEMENT DIFFERENTIATION INHIBITOR FACTOR
TDR	TDIF RECEPTOR
TFA	trifluoroacetic acid
THE	THESEUS
TM	transmembrane domain
Tris	tris (hydroxymethyl) aminomethane
T-DNA	transfer DNA from *Agrobacterium tumefaciens*
UTR	untranslated region
V	volt(s)
v/v	volume per volume
WT	wild-type
X-Gluc	5-bromo-4-chloro-3-indolyl-beta-D-glucuronic acid
µg	microgram(s)

µL	microlitre(s)
µm	micrometre(s)
µM	micromolar
µmol	micromoles
%	percent
°C	degree Celsius

1 Introduction

Land plants, also known as embryophytes, are thought to have evolved from an ancestral lineage of freshwater green algae, the charophycean algae (Delwiche and Cooper 2015; Bowman 2022; Edwards et al. 2014). This transition of plants from aquatic to terrestrial environments marked a pivotal evolutionary event, leading to the emergence of complex terrestrial ecosystems. Extant land plants encompass bryophytes (non-vascular plants) and tracheophytes (vascular plants) (Bowman 2022). Phylogenomics has reached a consensus topology wherein the three bryophyte lineages (hornworts, mosses, and liverworts) form one clade, and the three tracheophyte lineages (lycophytes, ferns, and seed plants) form another clade (Figure 1) (Puttick et al. 2018; Morris et al. 2018; Bowman 2022; Wickett et al. 2014; Nishiyama et al. 2004). Bryophytes, here, as a monophyletic lineage, occupy a unique position compared to tracheophytes, making them valuable for studies on the evolution of land plants. Comparisons between bryophytes and those of tracheophytes provide significant insights into the nature of the ancestral land plant.

Marchantia polymorpha is a species of large thalloid liverwort. Due to its distinct morphology compared to other land plants and its relatively simple genetic background, it has become a prominent model organism. The successful establishment of multiple genomic and genetic tools in *M. polymorpha* has further enhanced its utility for advancing our understanding of genetics and evolutionary processes (Althoff et al. 2014; Ishizaki et al. 2016; Sauret-Gueto et al. 2020; Matsumoto et al. 2021; Iwakawa et al. 2021; Melkonian et al. 2022).

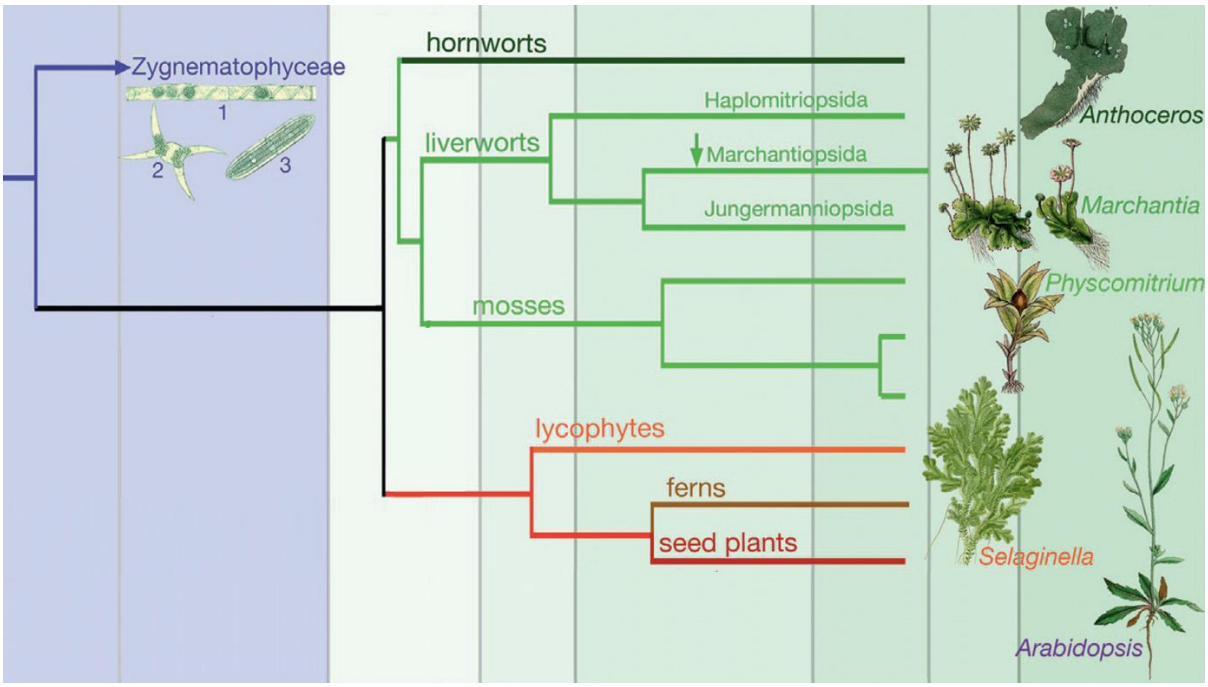

Figure 1. Phylogeny of land plants, modified from Bowman et al. 2022

1.1 The model liverwort *Marchantia polymorpha*

Marchantia polymorpha exhibits a distinct body plan compared to other land plants, comprising a horizontal flattened thallus with dichotomous branching. The upper side of the thallus is equipped with air chambers that have air pores as the entry site for gas exchange (Figure 2). Air chambers are air-filled spaces covered by a single-layered epidermis with a hydrophobic cuticle and contain the assimilatory filaments for photosynthesis (Shimamura 2016; Kohchi et al. 2021). It has been suggested that air chambers are the initial battle fields for pathogens to successfully colonise *M. polymorpha*. This is likely due to the fact that air chambers provide stable humid microenvironments and photosynthetic filament cells, which are beneficial for the growth of pathogenic microbes (Figure 2) (Carella et al. 2018; Iwakawa et al. 2021; Yotsui et al. 2023).

The storage tissue exists in the middle region under the upper side of the thallus, containing oil bodies and parenchymatous cells (Shimamura 2016; Romani et al. 2022). The latter are characterised by their large vacuoles that store starch grains, lipids, and other essential nutrients. The oil body is a specialised structure in liverworts, containing bioactive compounds, such as sesquiterpenoids and cyclic bisbibenzyl compounds (Kanazawa et al. 2020). The oil body was found to be involved in defence mechanisms against herbivores as mutants with defective oil body cell formation are more susceptible to arthropod herbivores compared to wild-type plants (Romani et al. 2020; Kanazawa et al. 2020; Romani et al. 2022).

The lower side of the thallus comprises rhizoids and scales, which contribute to anchorage and the absorption of water (Shimamura 2016). The development and functionality of unicellular rhizoids are crucial for the survival of *M. polymorpha* in terrestrial habitats, especially in damp and shaded areas where they are commonly present (Jones and Dolan 2012). There are two primary types of rhizoids in *M. polymorpha*: smooth-walled and pegged rhizoids (Shimamura 2016). Smooth-walled rhizoids are located on the ventral site of the thallus and are structurally analogous to root hair cells in angiosperms (Jones and Dolan 2012; Shimamura 2016; Kohchi et al. 2021). Smooth-walled rhizoids are elongated and unbranched, primarily functioning in anchorage (Ligrone et al. 2007). In contrast, pegged rhizoids, covered by scales and characterised by internal peg-like projections, are involved in water absorption and retention (Duckett et al. 2014; McConaha 1941). Ventral scales are multicellular structures that overlap to form a protective covering on the lower surface of the thallus. These scales guide the growth and orientation of the rhizoids, ensuring effective attachment to the substrate (Figure 2) (Shimamura 2016).

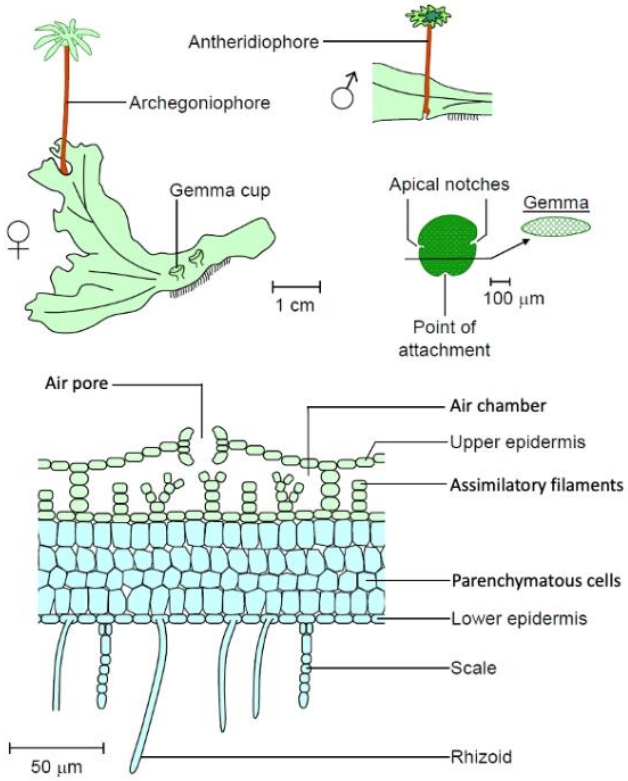

Figure 2. Diagram of *M. polymorpha* structure modified from Cronodon.

Marchantia polymorpha has a typical haploid gametophyte-dominant bryophytic life cycle. The gametophyte is a flat, thalloid structure capable of both sexual and asexual reproduction (Bowman et al. 2017). Both male and female thalli can reproduce asexually by producing multicellular gemmae from gemma cups, which grow into genetically identical gametophytes (Kato, Yasui, and Ishizaki 2020). Sexual reproduction involves the formation of specialised umbrella-like branches named gametangiophores, which bear the gametangia. Gametangiophores can be induced under far-red light irradiation (Chiyoda et al. 2008). Male gametangiophores (antheridiophores) produce antheridia that release motile sperms, while female gametangiophores (archegoniophores) produce archegonia that house the egg cells. After fertilisation, the diploid zygote develops into a sporophyte attached to the gametophyte, producing spores through meiosis. These spores germinate to form new gametophytes, completing the cycle (Shimamura 2016; Yamaoka, Inoue, and Araki 2021; Hisanaga et al. 2019).

The whole-genome sequencing and chromosome genome assembly of *M. polymorpha* were published in 2017 and 2020, respectively (Montgomery et al. 2020; Bowman et al. 2017). It is likely that *M. polymorpha* did not undergo whole-genome duplication during its evolution, leading to low genetic redundancy. The overall simplicity of gene families in *M. polymorpha*

is a valuable attribute that facilitates the dissection of fundamental molecular mechanisms and gene functions in complex biological pathways. Thus, *M. polymorpha* has now been adopted as a modern model plant to uncover conserved and diversified mechanisms in various aspects of plant biology.

Given the simple genetic background and haploid gametophyte of *M. polymorpha*, genome editing can be achieved within a short timeframe. This facilitates the production of transgenic plants that can be utilised directly without additional crossing in *M. polymorpha* compared to other model plants in angiosperms. Techniques such as *Agrobacterium*-mediated stable transformation and CRISPR Cas9-based genome editing for generating knock-out mutants are well-established in *M. polymorpha* (Sugano et al. 2018; Ishizaki et al. 2016; Kubota et al. 2013). Additionally, other broadly applicable tools have been developed in *M. polymorpha*. Transient transformation approaches based on particle bombardment and *Agrobacterium*-mediated methods have been established (Iwakawa et al. 2021; Westermann et al. 2020). A bioluminescence-based quantitative and spatial detection method for bacteria has also been recently introduced, allowing for the direct quantification of *Pto* DC3000 growth on thallus by measuring luminescence from the bacteria (Matsumoto et al. 2021). The miniTurbo-based interactomics approach has been developed in *M. polymorpha* to explore protein networks (Melkonian et al. 2022).

1.2 Plant immune system

In nature, plants as sessile organisms, are constantly exposed to a wide variety of adverse environmental conditions, which can be broadly categorised into biotic stresses, such as attacks by various pathogens including bacteria, fungi, and oomycetes, and abiotic stresses, such as drought, extreme temperature, chemicals, and salinity. Attack by pathogenic microorganisms is one of the most significant challenges to plant growth and development. Extant plants have evolved sophisticated and complex innate immune systems to fend off potentially pathogenic microbes. Extensive studies in angiosperms have revealed that there are two branches of the plant immune system based on the mode of pathogen recognition: pattern-triggered immunity (PTI) and effector-triggered immunity (ETI) (Zhang et al. 2023; Ngou, Ding, and Jones 2022; Alhoraibi et al. 2019; Jones and Dangl 2006; Pruitt et al. 2021).

In PTI, plants utilise cell surface-localised pattern-recognition receptors (PRRs) to perceive evolutionarily well-conserved microbe-/pathogen-/damage-associated molecular patterns (MAMPs/PAMPs/DAMPs) outside the cell, triggering rapid defence responses such as calcium influx, reactive oxygen species (ROS) production, mitogen-activated protein kinase

(MAPK) cascade activation, callose deposition, and defence-related gene expression (Escocard de Azevedo Manhaes et al. 2021; DeFalco and Zipfel 2021; Jian et al. 2024).

Adapted pathogens are able to secrete effector proteins that overcome and/or inhibit PTI. In turn, effectors can be recognised by adapted plants via intracellular resistance (R) proteins to trigger ETI. The main class of R proteins contains nucleotide-binding domain (NB) and leucine-rich repeat (LRR) domains and are referred to as NB-LRR (NLR) proteins (Gao et al. 2018; Jones and Dangl 2006). The activation of intracellular R proteins often results in the hypersensitive response (HR) as a hallmark of ETI, where cells at the site of infection undergo programmed cell death, creating a hostile environment for biotrophic and hemibiotrophic pathogens (Ngou, Ding, and Jones 2022; Coll, Epple, and Dangl 2011; Jones, Vance, and Dangl 2016).

Conventionally, PTI and ETI have been considered as two independent branches within the plant immune system, with PRRs and NLRs differing in their spatial and temporal dynamics. However, recent studies have indicated that crosstalk exists between PTI and ETI, suggesting that plant immunity operates as a unified system containing two interdependent branches (Yuan, Ngou, et al. 2021). ETI increases the protein abundance of PTI signalling components and requires PTI to provide effective resistance to microbial infection. Conversely, the activation of PTI amplifies ETI responses. These findings underscore that plants require both cell surface PRRs and intracellular NLRs to achieve full immunity (Yuan, Jiang, et al. 2021; Ngou et al. 2021; Thomma, Nurnberger, and Joosten 2011).

1.2.1 Immunity in *M. polymorpha*

Key components that have been shown to be essential for immune responses in angiosperms can be found in *M. polymorpha*. Homologues of characterised plasma-membrane localised receptors and their co-receptors were identified in the genome of *M. polymorpha* (Yotsui et al. 2023; Bowman et al. 2017; Mecchia et al. 2022). Lysin motif (LysM) RECEPTOR-LIKE KINASE1, MpLYK1, and LysM RECEPTOR-LIKE KINASE-RELATED, MpLYR, which are homologous to chitin-receptors in *Arabidopsis thaliana*, CHITIN ELICITOR RECEPTOR KINASE1 (AtCERK1) and AtLYK5, respectively, were shown to be required for chitin- and peptidoglycan-induced immune responses (Cao et al. 2014; Miya et al. 2007; Willmann et al. 2011; Yotsui et al. 2023). NLR homologues are also found in the genome of *M. polymorpha* (Bowman et al. 2017).

Marchantia polymorpha offers multiple pathosystems that facilitate investigations into immunity-related functions. Several pathogenic microbes have been reported to elicit immune

responses in *M. polymorpha*. The hemibiotrophic pathogenic bacterium *Pseudomonas syringae* pv. *tomato* DC3000 (*Pto* DC3000), which is an important model system for studying plant–pathogen interactions, can colonise *M. polymorpha* and induce defence-related responses (Gimenez-Ibanez et al. 2019). *Marchantia polymorpha* also exhibits a dynamic molecular response to the hemibiotrophic oomycete pathogen *Phytophthora palmivora*. Additionally, it displays disease symptoms or cell death in response to various fungal pathogens, including *Fusarium oxysporum* (Carella et al. 2019; Redkar et al. 2021; Matsui et al. 2020).

To date, extensive studies have revealed the molecular mechanisms underlying plant immunity across different plant species; however, most insights have been limited to angiosperms. We still lack knowledge of the components and mechanisms involved in the immunity of bryophytes. Studying the immune system in *M. polymorpha* can help us understand how complex immune responses have evolved and diversified in land plants, providing a broader perspective on the evolution of plant immune systems.

1.3 Cell-surface localised receptor

Plant cell surface-localised receptors are crucial for mediating interactions with the external environment, including the detection of pathogens, symbionts, and environmental signals such as pH and light. These receptors play pivotal roles in the regulation of plant growth, development, and defence mechanisms, making them essential for plant survival and adaptation (Ngou, Ding, and Jones 2022; Boutrot and Zipfel 2017).

Plant cell surface-localised receptors can be largely classified into receptor-like kinases (RLKs) and receptor-like proteins (RLPs). RLKs are characterised by an extracellular domain (ECD), a single-pass transmembrane domain (TM), and an intracellular kinase domain (KD) that transduces signals by phosphorylating downstream targets (Osakabe et al. 2013; Boutrot and Zipfel 2017). RLPs, on the other hand, lack the intracellular KD or any other recognisable intracellular domain. Instead, RLPs often associate with RLKs or other signalling components to initiate signal transduction. RLKs and RLPs can be divided into different subgroups based on the structural features of their ECDs that are responsible for ligand perception. These subgroups include LRR, lectin, malectin, LysM, and epidermal growth factor (EGF)-like extracellular types (Bohm et al. 2014). Ligand perception often induces conformational changes and dynamic associations of RLKs and RLPs with specific co-receptors and receptor-like cytoplasmic kinases (RLCKs). The co-receptors are often shared among different receptors (Zipfel 2014; Ngou et al. 2024).

1.3.1 Leucine-rich repeat receptor-like kinases, LRR-RLKs

The leucine-rich repeat receptor-like kinases (LRR-RLKs) family is the most prominent and best-characterised RLK family in plants. LRR-RLKs constitute one of the largest receptor classes in plants and are structurally classified into 14 subfamilies (Zulawski et al. 2014; Xi et al. 2019; Zhang et al. 2006). In angiosperms, several subfamily XII LRR-RLKs have been proven to function as PRRs. These include the well-characterised *A. thaliana* FLAGELLIN-SENSITIVE2 (AtFLS2) and ELONGATION FACTOR-Tu (EF-Tu) RECEPTOR (AtEFR), which are responsible for bacterial flagellin (flg22) and translation elongation factor Tu (elf18) perception, respectively (Gómez-Gómez and Boller 2000; Zipfel et al. 2006). The subfamily II LRR-RLKs are generally considered to function as co-receptors for LRR-type receptors. The PRRs from subfamily XII LRR-RLKs typically require SOMATIC EMBRYOGENESIS RECEPTOR-LIKE KINASES (SERKs) from subfamily II LRR-RLKs as co-receptors for downstream signalling (Ma et al. 2016).

SERK was initially identified as a co-receptor for the brassinosteroid (BR) receptor BRASSINOSTEROID-INSENSITIVE1 (BRI1) (Chinchilla et al. 2009; Heese et al. 2007). BRs are phytohormones that regulate plant growth and development (Fujioka and Yokota 2003). Loss of function mutations in AtSERK3 (also known as BRI1-ASSOCIATED KINASE1, AtBAK1) negatively affect plant growth by impairing cell elongation (Nam 2002; Li et al. 2002). AtSERK3 functions as a common co-receptor for AtFLS2 and AtEFR, as well as AtBRI1, regulating not only PTI but also plant growth and development (Chinchilla et al. 2007; Li et al. 2002; Sun et al. 2013; Fontes 2023). The specificity of these diverse responses is primarily governed by the specificity of the ligand–receptor interaction. Upon ligand perception, SERKs are recruited by PRRs and form complexes with the corresponding PRRs to regulate downstream signalling pathway (Schulze et al. 2010). The tyrosine residue (Y403) located in the kinase domain of AtSERK3, which is widely conserved among SERK homologues, has been shown to be required for immune signalling but not for BR signalling (Perraki et al. 2018). Thus, the immune and developmental signalling mediated by AtSERK3 can be uncoupled by editing the tyrosine residue.

AtSERK3 is also known to interact with AtBIRs (BAK1-INTERACTING RECEPTOR-LIKE KINASE) from subfamily Xa LRR-RLKs (Halter et al. 2014; Imkampe et al. 2017; Gao et al. 2009). The *A. thaliana* genome encodes four AtBIRs: AtBIR1 through AtBIR4. AtBIR1 has been shown to negatively regulate cell death, and disruptions in AtBIR1 abundance impact both plant growth and defence responses, including cell death induction, constitutive expression of the immune-marker genes PATHOGENESIS RELATED1 (AtPR1) and AtPR2, and

enhanced plant resistance to the oomycete *Hyaloperonospora parasitica* (Guzman-Benito et al. 2019; Liu et al. 2016; Gao et al. 2009). Using a dexamethasone (DEX)-inducible expression system, it has been demonstrated that the induction of AtBIR1 in an At*bir1* mutant background at an endogenous level represses the expression of PTI genes and callose deposition at plasmodesmata (PD) in response to the PTI elicitor flg22. Overexpression of AtBIR1 resulted in developmental defects and upregulation of plant defence, similar to the phenotypes observed in At*bir* mutants (Guzman-Benito et al. 2019; Guzmán-Benito et al. 2024).

AtBIR2 and AtBIR3 restrict the binding of AtSERK3 to AtFLS2 and negatively regulate AtSERK3-mediated immunity by constitutively interacting with AtSERK3 in the absence of ligands. This interaction helps to restrict undesired interaction with the corresponding ligand-binding receptors. During ligand perception, AtSERK3 dissociates from AtBIRs and becomes available to form complexes with PRRs (Halter et al. 2014; Imkampe et al. 2017; Gao et al. 2009). The well-balanced expression of BIRs and the tight control of SERKs activities are crucial for plants in coordinating defence responses and growth.

1.3.1.1 LRR-RLKs in *M. polymorpha*

Marchantia polymorpha encodes a total of 107 LRR-RLKs (Bowman et al. 2017). The subfamily XII LRR-RLKs expanded independently in many plant lineages including liverworts, and therefore *M. polymorpha* lacks homologues for FLS2 and EFR (Black in Figure 3A) (Bowman et al. 2017). It has been reported that *M. polymorpha* does not respond to flg22 and elf18, which is in agreement with the genome analysis (Yotsui et al. 2023). It is important to note that *M. polymorpha* does not encode any BRI1 homologues either. The subfamily II LRR-RLKs, including the single SERK homologue, are found to be conserved in *M. polymorpha* (Black in Figure 3B).

The specific roles of subfamily XII LRR-RLKs in *M. polymorpha* are yet to be identified. However, it is tempting to hypothesise that these yet-to-be-characterised LRR-RLKs function as PRRs by recognising unknown MAMPs and forming complexes with the co-receptor homologues. Due to the lack of identified MAMPs and the size of subfamily XII LRR-RLK, it is more feasible to investigate the roles of subfamily XII LRR-RLKs through studying potential co-receptors, the single SERK homologue and two other members (MpAPEX and CLAVATA3 INSENSITIVE RECEPTOR KINASE, MpCIK) (Black in Figure 3B). Given that our collaborators, Yuki Hirakawa's group at Hiroshima University, Japan, are investigating MpCIK (Takahashi et al. 2021), I focused on characterising MpSERK and MpAPEX.

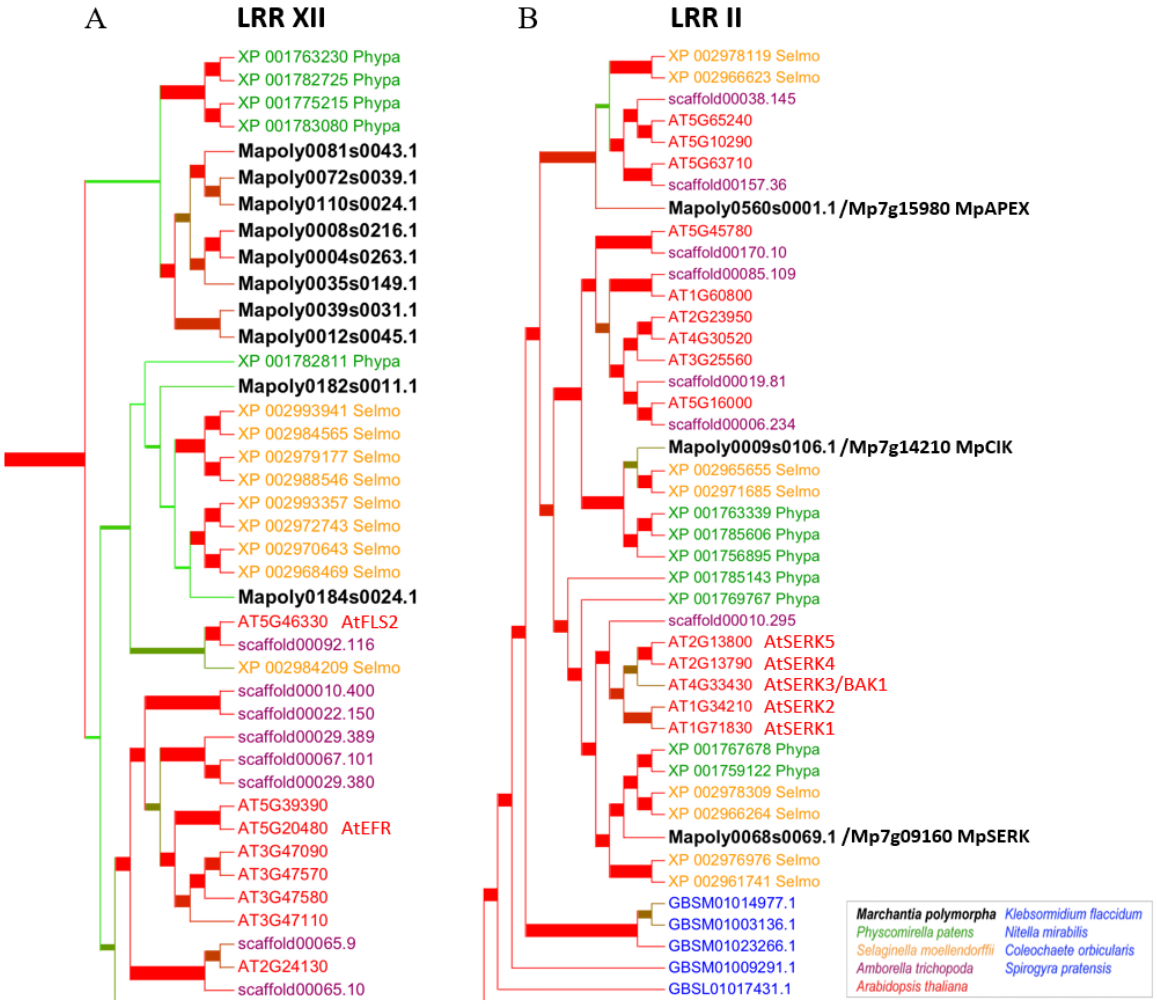

Figure 3. Phylogenetic tree of LRR-RLKs belonging to subfamily XII (A) and II (B) modified from (Bowman et al. 2017).

1.3.2 Malectin-like receptor like kinase, FER

FERONIA (FER) belongs to the malectin-like receptor-like kinases (MLRs) family, also known as the *Catharanthus roseus* RECEPTOR-LIKE KINASE 1-LIKE (CrRLK1L) family (Yang et al. 2021). Proteins in this family are characterised by two tandem malectin-like extracellular domains, a TM, and an intracellular KD. The MLR family proteins play pivotal roles in various plant processes, including reproduction, cell growth, hormone response, and immunity (Ji et al. 2020; Lindner et al. 2012; Zhang et al. 2020; Wang et al. 2022). FER was initially identified as being required for fertilisation in *A. thaliana*, with *fer* mutants exhibiting defects in pollen tube elongation (Escobar-Restrepo et al. 2007). FER recognises numerous types of endogenous signals, mostly rapid alkalinisation factors (RALFs), and participates in a range of processes such as stress responses, H^+-ATPase activity, calcium influx ROS bursts, and root growth

inhibition (Zhu et al. 2021; Gonneau et al. 2018; Stegmann et al. 2017; Haruta et al. 2014b; Liao et al. 2023; Ortiz-Morea et al. 2022).

In the context of plant immunity, FER exerts diverse roles in transducing and mediating immune-related signalling pathways. AtFER is one of the best-characterised MLRs in *A. thaliana* and functions as a receptor for AtRALF1 and AtRALF23 peptides (Haruta et al. 2014a; Stegmann et al. 2017; Bhalla et al. 2024). The interaction of AtFER and AtRALF23 inhibits complex formation between PRRs and their co-receptors, such as that of AtEFR and AtFLS2 with a co-receptor AtBAK1/SERK3, thereby inhibiting elf18- and flg22-induced ROS bursts, respectively (Stegmann et al. 2017). AtFER, here, is considered to act as a scaffold protein that facilitates the formation of different cell-surface receptor complexes essential for transduction of immune signals and thereby functions as a positive regulator of PTI (Stegmann et al. 2017).

This mechanism, whereby RALF negatively regulates immunity in a FER-dependent manner, is utilised by the fungal pathogen *Fusarium oxysporum* f. sp. *lycopersici*. The RALF-like (F-RALF) secreted by *F. oxysporum* hijacks the FER-mediated pathway in plants, activating rapid ROS bursts and inducing alkalinisation of the apoplasts. The upshift of extracellular pH triggers the phosphorylation of the pathogenicity-associated MAPK, FMK1, in *F. oxysporum*, thereby enhancing virulence. The increased surrounding pH facilitates a favourable environment for *F. oxysporum* to further colonise the host plant (Thynne et al. 2017; Masachis et al. 2016).

In contrast, AtRALF22 peptide positively regulates plant immunity via AtFER (He et al. 2023). AtRALF22 elicits a variety of immune responses, including rapid ROS bursts and MAPK cascade activation and amplifies plant elicitor peptides (Pep3)-induced immune responses in an AtFER-dependent manner. AtRALF22 also promotes resistance against the necrotrophic fungal pathogen *Sclerotinia sclerotiorum* (He et al. 2023).

AtRALF1 inhibits the activity of plasma membrane H^+-ADENOSINE TRIPHOSPHATASE2 (AHA2), which secretes protons into the apoplast and thereby regulates cell expansion, in an AtFER-dependent manner (Haruta et al. 2014b). Upon AtRALF1 perception, AtFER interacts with and phosphorylates RLCK, RPM1-INDUCED PROTEIN KINASE (RIPK). This leads to apoplastic alkalinisation, which cooperatively inhibits root growth (Du et al. 2016).

Upon the perception of RALFs, FER requires other receptors, such as LLGs, to assemble heterocomplexes to regulate immune signalling. LORELEI (LRE)-LIKE GLYCOSYLPHOSPHATIDYLINOSITOL (GPI)-ANCHORED PROTEIN1 (LLG1) directly interacts with the extracellular domain of AtFER to assemble the heterocomplexes of

AtRALF1–AtLLG1–AtFER and AtRALF23–AtLLG1–AtFER (Li et al. 2015; Xiao et al. 2019). FER also interacts with the extracellular LEUCINE-RICH REPEAT EXTENSINS (LRXs) upon RALFs mediation. LRXs are chimeric proteins that are insoluble in the cell wall and can form protein–protein interaction platforms (Herger et al. 2019). The interaction between AtRALF1 and AtLRX3/4/5 has been observed in shoots and roots to regulate cell wall signalling and plant growth (Dunser et al. 2019).

1.3.2.1 Rapid alkalinisation factors, RALF peptides

Rapid alkalinisation factors are cysteine-rich, small secretory peptides that are widely recognised as inducible DAMPs (Tanaka and Heil 2021). RALFs were initially identified as endogenous plant peptides, triggering rapid alkalinisation of the apoplast of *Nicotiana benthamiana* and inhibiting plant growth (Pearce et al. 2001). Subsequently, RALFs were identified in most land plants, forming a large family (Cao and Shi 2012; Murphy and De Smet 2014). Fungal pathogens and nematodes have also been found to secrete RALF peptides to modulate plant immune responses, thereby facilitating infection and parasitism, respectively (Zhang, Peng, et al. 2020; Masachis et al. 2016; Thynne et al. 2017).

RALF peptides are firstly translated and secreted as propeptides. Some of these propeptides are cleaved at a SITE-1 PROTEASE (S1P) site by S1P to become mature RALFs. The YISY motif in RALF propeptides is required for receptor binding (Zhang, Yang, et al. 2020; Xiao et al. 2019; Haruta et al. 2014b; Pearce et al. 2010). The mature RALF peptides are then secreted into extracellular spaces, where they interact with the corresponding receptors localised on the plasma membrane and induce rapid alkalinisation (Campbell and Turner 2017).

The genome of *A. thaliana* encodes 37 RALF propeptides, which play versatile roles in plant growth and immunity (Abarca, Franck, and Zipfel 2021). The majority of AtRALF peptides induce ROS production and/or modulate elicitor-induced ROS production in *A. thaliana* (Abarca, Franck, and Zipfel 2021; Stegmann et al. 2017; Olsen, Mundy, and Skriver 2002). AtRALF17 not only induces ROS production but also elevates elf18-induced ROS production, potentially serving as a positive regulator of immune responses (Stegmann et al. 2017). In contrast, AtRALF34 does not induce ROS production and actively inhibits elf18-induced ROS production. Additionally, AtRALF34 functions as a ligand of AtTHESEUS (AtTHE), a homologue of AtFER, to modulate cell wall integrity (CWI) (Gonneau et al. 2018).

AtRALF23 and AtRALF34 were shown to inhibit flg22-induced ROS production and immune responses in an AtFER-dependent manner, but did not induce ROS production on their own (Xiao et al. 2019; Stegmann et al. 2017). However, He et al. demonstrated that AtRALF23

can induce ROS bursts in *A. thaliana* (He et al. 2023). It is important to note that AtRALF23 and AtRALF34 are S1P-cleaved RALF peptides, and both inhibit elicitor-triggered ROS bursts, whereas AtRALF17, lacking S1P cleavage site, induces ROS bursts. However, this dichotomy is not applicable to the entire RALF family. Yet, no clear correlation was found between S1P cleavage and modulation of ROS production across the RALF family (Abarca, Franck, and Zipfel 2021).

Another well-described function of RALF peptides is their role in inhibiting seedling and root growth (Blackburn, Haruta, and Moura 2020; Morato do Canto et al. 2014). Most AtRALFs have the ability to inhibit seedling and root growth, with some of these inhibitory effects being dependent on AtFER. Both AtRALF23 and AtRALF34 have been shown to arrest seedling and root growth in *A. thaliana*, but only the inhibition modulated by AtRALF23 is dependent on AtFER (Abarca, Franck, and Zipfel 2021; Stegmann et al. 2017; Srivastava et al. 2009).

F-RALF secreted by the fungal pathogen *F. oxysporum* exhibits similar effects in inducing ROS bursts and inhibiting root growth in plants. It has been demonstrated that F-RALF significantly arrests root and root hair growth in tomato and *A. thaliana*, with the latter effect being dependent on AtFER (Masachis et al. 2016). Treatment of plants with F-RALF induces robust ROS bursts and alkalinisation in *N. benthamiana* and tomato (Thynne et al. 2017).

1.3.2.2 FER and RALFs in *M. polymorpha*

The *Marchantia polymorpha* genome encodes a single MLR known as MpFER/MpTHE and three RALF propeptides: MpRALF1, MpRALF2, and MpRALF3 (Bowman et al. 2017). MpFER has been shown to be required for various aspects of development, including rhizoid growth, cellular expansion, and morphological integrity of gametophytes (Honkanen et al. 2016; Mecchia et al. 2022). However, its ligands and role in immunity are still unclear.

Phylogenetically, the three MpRALFs are in the same clade and are closely related to AtRALF34 (Figure 7D) (Mecchia et al. 2017; Bowman et al. 2017). MpRALF1 and MpRALF3 are predicted to be processed by S1P, leading to the production of mature peptides. Given the presence of both MpFER and the predicted mature MpRALFs, it is reasonable to hypothesise that the RALF–FER signalling pathway is conserved in *M. polymorpha*.

The RALFs have also been identified in the genome of bryophyte *Physcomitrium patens*. PpRALF1 and PpRALF2 exhibit redundant functions in regulating protonema tip growth, similar to the role of AtRALF1 in root growth (Ginanjar, Teh, and Fujita 2022). Knocking out

PpRALF2 and PpRALF3 led to increased resistance to the bacterial and fungal pathogens, *Pectobacterium carotovorum* and *Fusarium solani*. This suggests that PpRALF2 and PpRALF3 negatively regulate immunity (Mamaeva et al. 2023).

To date, the function of RALFs in *M. polymorpha* remains unknown. Most studies on FER homologue in *M. polymorpha* have focused on its roles in growth and development, with no evidence yet demonstrating its functions in plant immunity as observed in angiosperms. The hypothesised presence of the RALF–FER module raises questions about its contribution and function in immunity of *M. polymorpha*, which remain to be elucidated.

2 Aim of research

The aim of my PhD project is to:

1) decipher the function of MpFER in the *M. polymorpha* immunity;
2) unravel the contribution of the potentially conserved MpRALF–MpFER module in plant immunity;
3) characterise the immune-related functions of subfamily II LRR-RLKs, MpSERK and MpAPEX;
4) identify potential PRRs in *M. polymorpha*;
5) explore the cell-surface immune receptor networks involved in plant–microbe interactions in *M. polymorpha*.

This project is expected to shed light on the ancestral functions of MLRs and LRR-RLKs in plants.

3 Results

3.1 *Marchantia polymorpha* Malectin-like kinase receptor, MpFERONIA

3.1.1 MpFER affects development of *M. polymorpha*

The Mp*fer-1* mutant was isolated in a screen of T-DNA insertion lines that was targeted at identifying genes required for rhizoid growth (Honkanen et al. 2016). To generate the insertion lines, spores from a cross between wild-type Tak-1 (male) and Tak-2 (female) were used. It appeared that the T-DNA was inserted in the 3' UTR of Mp*FER*, which does not affect Mp*FER* expression level (Mecchia et al. 2022). Because of the mixed genetic background and possible MpFER expression in Mp*fer-1*, we generated a Mp*FER* disruptant in a Tak-1 background using the CRISPR-Cas9 system, for a better understanding of MpFER functions. During this study, other Mp*fer* mutants, Mp*fer-2* to Mp*fer-8*, were generated and reported (Mecchia et al. 2022), and thus I named our mutant Mp*fer-9*. The Mp*fer-9* mutant had a single base-pair deletion at the beginning of the Mp*FER* coding sequence, resulting in a nonsense translation of MpFER protein after 13 amino acids and an early stop translation after 21 amino acids (Figure 4A). Four-week-old Mp*fer-9* exhibited strong defects in thalli growth and rhizoids development (Figure 4B). The defects in rhizoid formation is consistent with previous reports (Honkanen et al. 2016; Mecchia et al. 2022). Mp*fer-9* engaged in asexual propagation and formed the cup-shaped receptacle, namely gemma and gemma cup, respectively, indicating that MpFER is dispensable for asexual reproduction in *M. polymorpha* (Figure 4B).

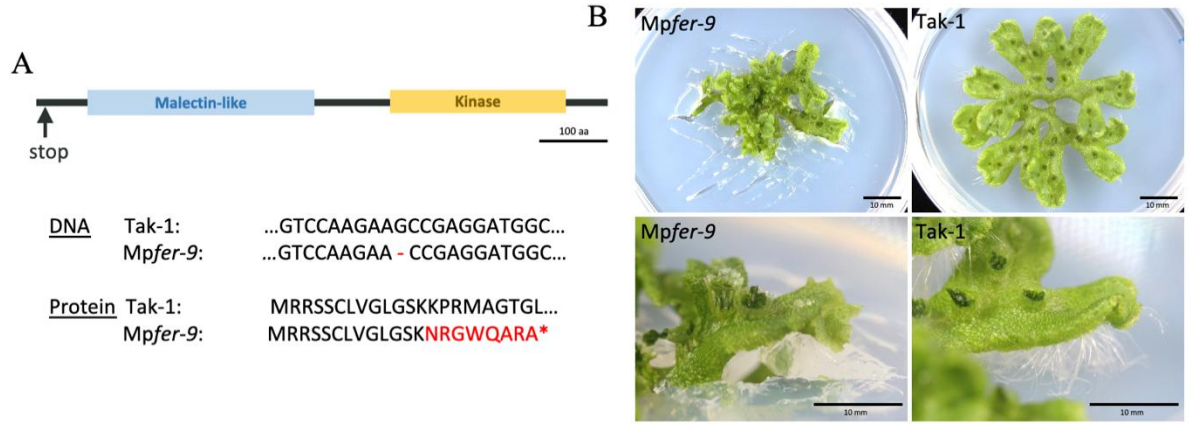

Figure 4. Phenotypes and genome editing site of the Mp*fer-9* mutant

A. Schematic representation of Mp*FER* disruption in Mp*fer-9*. The early stop of protein translation at the N-terminus of MpFER caused by a guanine deletion is indicated by an arrow.

B. Four-week-old Mp*fer-9* compared to Tak-1. Thalli were grown from single gemma under constant white light.

To investigate the expression profile of Mp*FER*, I cloned a 5-kb DNA fragment upstream of the start codon and fused it to a β-glucuronidases (GUS)-reporter gene. Three independent transgenic lines expressing $_{pro}$Mp*FER*:*GUS* were established in a Tak-1 background. GUS-staining was performed through cross-sectional and top-view analysis. In 3-day-old gemma, GUS-staining was prominently confined to rhizoids and the central region of the gemma (Figure 5A). At later stages, GUS staining was observed in the meristem, rhizoids, assimilatory filaments, and rhizoid-initiated areas along midribs (Figure 5). Tak-1, serving as a negative control, did not exhibit any GUS staining at any of these growth stages. These observations align with the functional involvement of MpFER in rhizoid formation and in thallus growth.

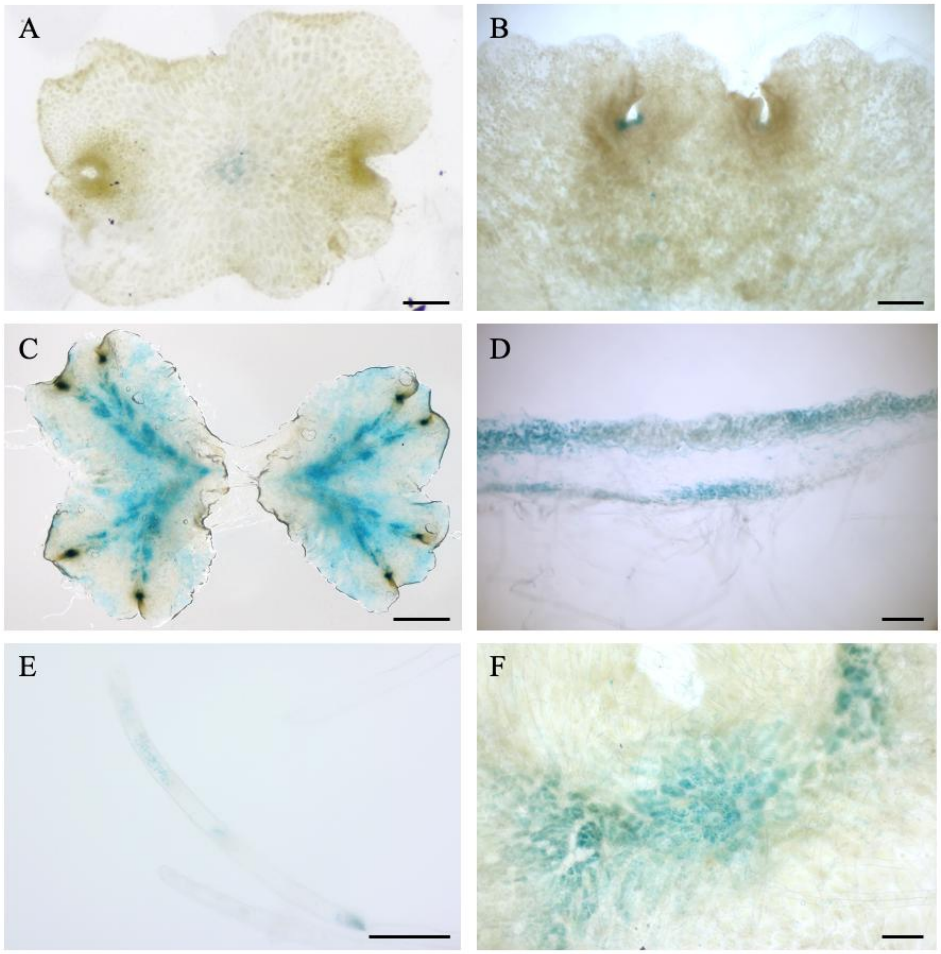

Figure 5. Gene expression profile of Mp*FER*

Histochemical GUS staining of transgenic lines expressing a GUS gene under Mp*FER* promoter.

A. Top view of 3-day-old gemmaling. Scale bar, 250 μm.

B. Top view of 7-day-old thallus. Scale bar, 200 μm.

C. Top view of 15-day-old thalli. Scale bar, 200 μm.

D. Cross-sectional view of 15-day-old thallus. Scale bar, 200 μm.

E. Top view of 7-day-old rhizoids. Scale bar, 100 μm.

F. Top view of 7-day-old thallus. Scale bar, 50 μm.

3.1.2 The kinase activity and protein level of MpFER is important for thallus growth

In order to investigate the contribution of MpFER kinase activity to the development of *M. polymorpha*, I generated transgenic plants overexpressing MpFER or MpFER kinase-dead mutant (MpFER-KD). Proteins were tagged with miniTurbo and Myc at their C-termini and expressed under an Mp*FER* promoter in the Tak-1 background ($_{pro}$Mp*FER*:Mp*FER-miniTurbo-Myc* and $_{pro}$Mp*FER*:Mp*FER-KD-miniTurbo-Myc*). The overexpression of MpFER, but not MpFER-KD, severely affected the growth of *M. polymorpha* (Figure 6A). Immunoblot analysis confirmed that MpFER and MpFER-KD proteins were expressed in the transgenic plants (Figure 6B). MpFER-KD tended to accumulate to slightly higher levels than MpFER (Figure 6B). These results indicate that the kinase activity of MpFER is responsible for the observed growth defects in MpFER-overexpressing plants. At the same time, these results imply that kinase activity is indispensable for MpFER functions in *M. polymorpha*.

To further validate the significance of MpFER kinase activity, MpFER-miniTurbo-Myc and MpFER-KD-miniTurbo-Myc were overexpressed under the ubiquitous Mp*EF1α* promoter in Tak-1 ($_{pro}$Mp*EF1α*:Mp*FER-miniTurbo-Myc* and $_{pro}$Mp*EF1α*:Mp*FER-KD-miniTurbo-Myc*). Overexpression lines of MpFER-KD, but not of MpFER, were successfully obtained. This suggests that the overaccumulation of MpFER is detrimental to thallus growth, underscoring the importance of both the kinase activity and the protein level of MpFER in the growth and development of *M. polymorpha*.

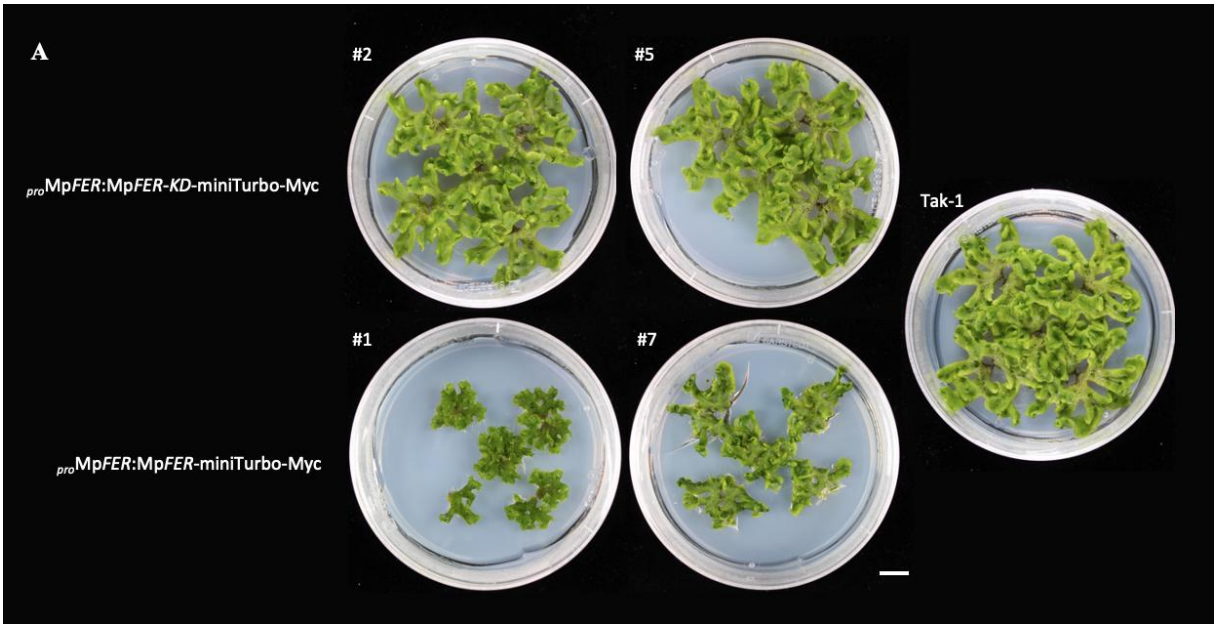

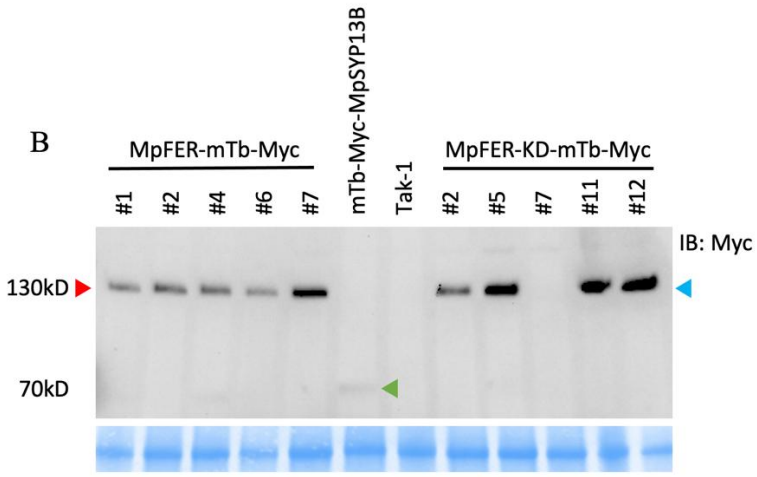

Figure 6. Mp*FER*-overexpressing plants

A. Transgenic lines with $_{pro}$Mp*FER*:Mp*FER-miniTurbo-Myc* or $_{pro}$Mp*FER*:Mp*FER-KD-miniTurbo-Myc* compared to Tak-1. Four-week-old plants are shown. Thalli were grown from single gemma under constant white light. Scale bar, 10 mm.

B. Immunoblot analysis of MpFER accumulation in $_{pro}$Mp*FER*:Mp*FER-miniTurbo-Myc* and $_{pro}$Mp*FER*:Mp*FER-KD-miniTurbo-Myc* transgenic plants. Wild-type Tak-1 and miniTurbo-Myc-MpSYP13B-expressing plants served as controls. Red, blue, and green arrows indicate MpFER-miniTurbo-Myc, MpFER-KD-miniTurbo-Myc, and miniTurbo-Myc-MpSYP13B, respectively. Anti-Myc antibody was used to detect the fusion proteins. A coomassie brilliant blue (CBB)-stained membrane is shown as loading control.

3.1.3 MpRALF and MpFER function as a module in *M. polymorpha*

3.1.3.1 MpRALF1 triggers ROS bursts in *M. polymorpha*

Marchantia polymorpha encodes three MpRALF propeptides, MpRALF1, MpRALF2, and MpRALF3, which are phylogenetically related to AtRALF34 (Figure 7D). In *A. thaliana*, RALF peptides trigger ROS bursts or suppress MAMP-induced ROS bursts in an AtFER-dependent manner (Abarca, Franck, and Zipfel 2021; Stegmann et al. 2017). AtRALF34 does not trigger ROS bursts on its own but suppresses flg22- or elf18-induced ROS bursts in *A. thaliana*. The functions of MpRALFs and their relationship with the single MLR, MpFER, are not yet described.

In order to determine whether *M. polymorpha* can sense and respond to RALF peptides, predicted mature MpRALF1 (Mp7g07270) and MpRALF3 (Mp1g27120) peptides were chemically synthesised (Figure 7A). Wild-type Tak-1 gemmae were treated with MpRALF1 and MpRALF3, and ROS bursts were monitored. I found that both MpRALF1 and MpRALF3

can trigger ROS bursts in Tak-1 (Figure 7B and 7C). The level of ROS production triggered by MpRALF3 was significantly lower compared to MpRALF1 (Figure 7B, 7C, and 10A).

To investigate whether MpFER is required for sensing MpRALF1 and MpRALF3, a ROS production assay was performed in Mp*fer*-9. As shown in Figure 7B and 7C, MpRALF1 and MpRALF3 failed to trigger ROS bursts in Mp*fer*-9. These results suggest that MpFER functions as a receptor for MpRALF1 and MpRALF3 in *M. polymorpha*. This also means that RALF and FER function as a module in liverworts or in bryophytes, suggesting that the RALF–FER module is widely conserved in land plants.

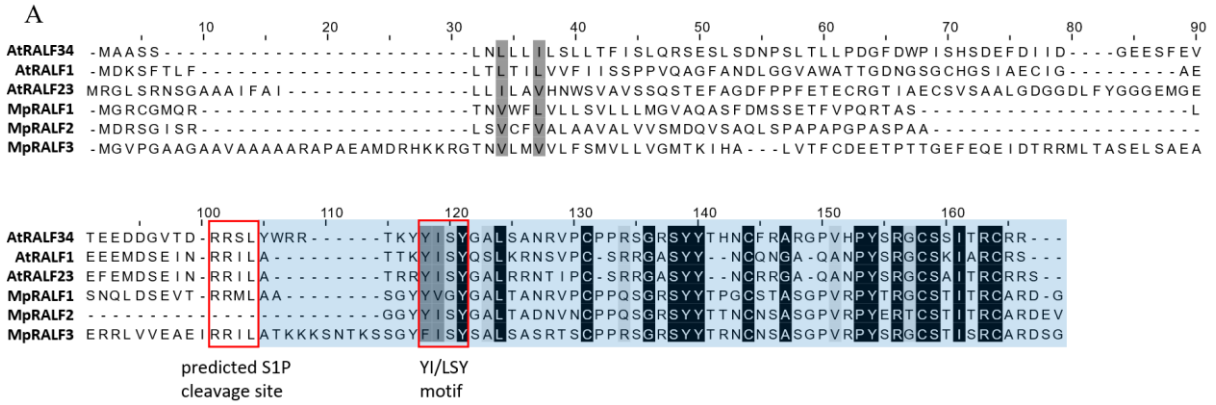

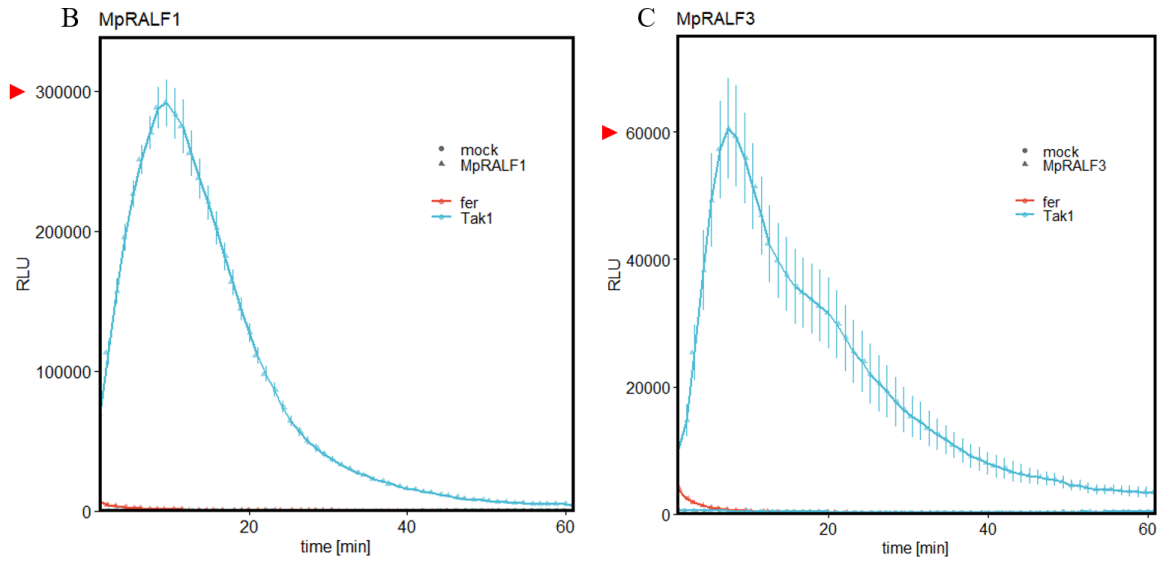

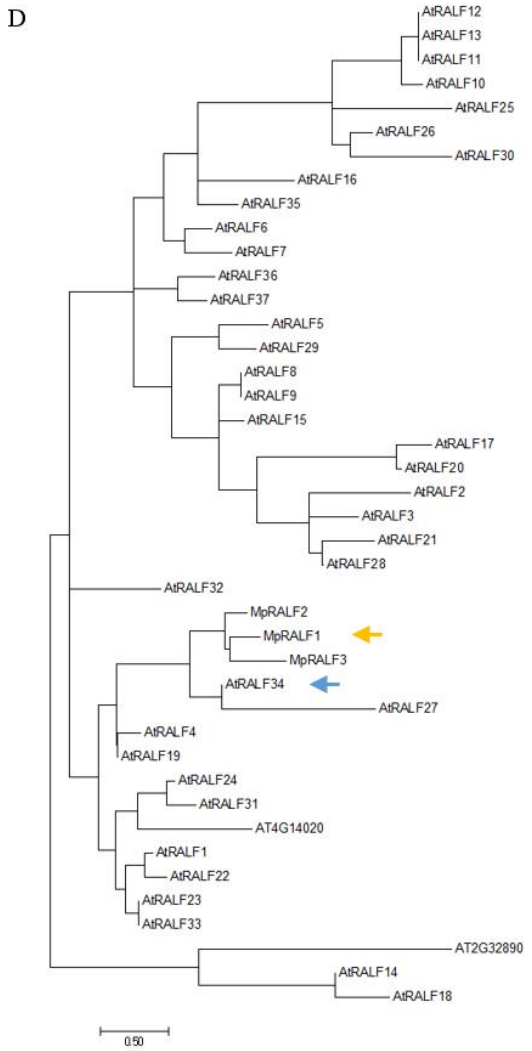

Figure 7. MpRALF1 and MpRALF3 trigger ROS bursts in an MpFER-dependent manner

A. Sequence alignment of MpRALFs, AtRALF1, AtRALF23, and AtRALF34. Colour-coding based on sequence conservation: the darker the colour, the more conserved the residue. Sequences shaded in blue indicate the predicted mature peptides. Red boxes highlight conserved motifs.

B and C. Gemmae were treated with 1 µM MpRALF1 **(B)** or 1 µM MpRALF3 peptides **(C)**. Seven-day-old liquid-cultured gemmae from Mp*fer-9* and wild-type Tak-1 were used. ROS production over time was monitored with a plate reader by luminescence (RLU) (n=3, mean +/- SE). The peaks of ROS production triggered by either MpRALF1 or MpRALF3 are indicated by arrows.

D. Phylogenetic analysis of RALF peptides from *A. thaliana* and *M. polymorpha*. The evolutionary history was inferred using the Maximum Likelihood method based on the JTT matrix-based model. MpRALF1 and AtRALF34 are indicated by arrows.

3.1.3.2 MpRALF1 and chitin induce different ROS production patterns

Chitin, one of the typical MAMPs inducing multiple immune responses in angiosperms, has recently been reported to be recognised by *M. polymorpha* resulting in induction of immune

responses, including ROS bursts (Yotsui et al. 2023). In comparison to chitin-induced ROS bursts, which peaked around 5 mins after treatment, MpRALF1-induced ROS bursts peaked around 10 mins after treatment (Figure 7B and 8A). To further investigate the difference between MpRALF1- and chitin-induced ROS production, I monitored which regions of thallus are responding to these elicitors and producing ROS. The comparison was conducted at the time point where the ROS bursts peaked in each condition (Figure 7B and 8A).

Most of ROS bursts triggered by chitin originated from the dorsal side and were concentrated around the meristematic apical notch of thalli, with few ROS bursts observed on the ventral side. In contrast, MpRALF1-triggered ROS bursts were more intense overall compared to chitin and mainly derived from the ventral side rather than the dorsal side of plants (Figure 8B). The majority of ROS bursts were detected in regions coinciding with the presence of rhizoids or sites of rhizoids initiation (Figure 8B and Figure 5C to 5E). These findings are in agreement with the Mp*FER* expression profile indicated by the promoter-GUS analysis (Figure 5) and suggest that MpRALF1 perception by MpFER primarily occurs in rhizoids and/or the rhizoid-initiated regions.

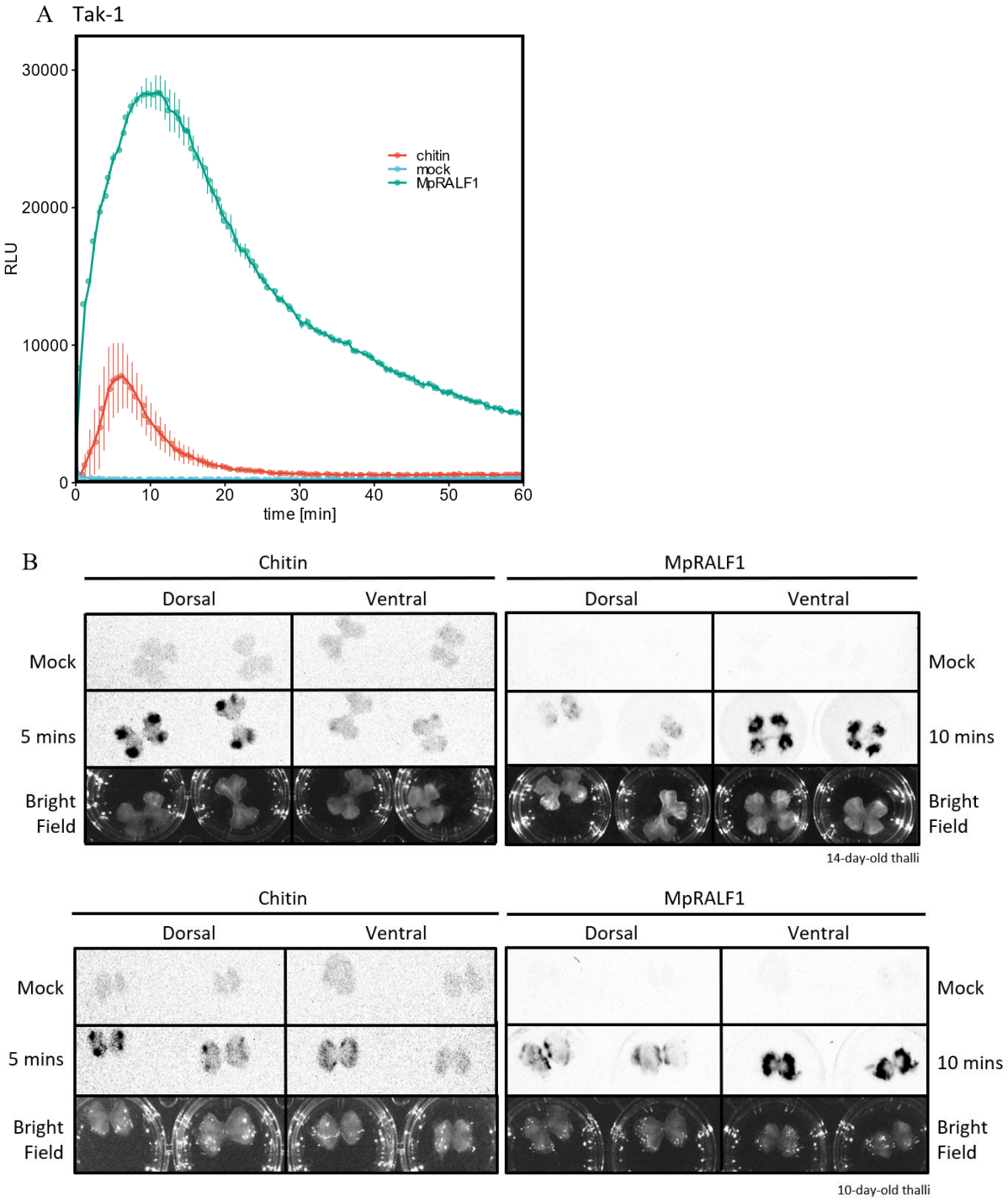

Figure 8. ROS production patterns upon chitin and MpRALF1 treatment

A. Gemmae were treated with 1 µM MpRALF1 or 1 µM chitin. Seven-day-old liquid-cultured gemmae from wild-type Tak-1 were used. ROS production over time was monitored with a plate reader by luminescence (RLU) (n=3, mean +/- SE).

B. Ten (bottom)- and 14 (top)-day-old thalli of wild-type Tak-1 were treated with 1 µM chitin and 1 µM MpRALF1 compared to mock. Luminescence images were captured by a gel documentation system (Bio-Rad) at indicated exposure times.

3.1.3.3 Mp*FER* and Mp*LYK1* expression patterns during thallus growth

I investigated whether Mp*FER* and Mp*LYK1* expression patterns could explain the differences in ROS production patterns triggered by MpRALF1 and chitin. To this end, I compared the gene expression patterns of Mp*LYK1* and Mp*FER* at various growth stages. The results showed that the Mp*LYK1* gene was expressed in meristematic areas, particularly at younger stages, such as 3- and 7-day-old gemmae. It was expressed across the entire dorsal surface of mature thalli after 10 days of growth. Additionally, Mp*LYK1* gene expression patterns became more distinct and intense as the thalli matured (10, 14, and 21-day-old) (Figure 9). In contrast, *MpFER* gene expression, besides the patterns mentioned above (Figure 5), also occurred on the dorsal surface of thalli, excluding the central regions, differing from the patterns of Mp*LYK1* at the same ages (Figure 9). Altogether, these results show differential expression patterns of Mp*LYK1* and Mp*FER*, although there are overlaps in the expression patterns of Mp*LYK1* and Mp*FER* at specific growth stages. Together with the ROS production pattern shown in Figure 8, MpFER on the dorsal side of *M. polymorpha* appears to be less active in detecting MpRALF1 to elicit ROS bursts compared to its activity on the rhizoid side. Chitin perception by MpLYK1 primarily occurs in the meristematic regions at the apical notches of *M. polymorpha*.

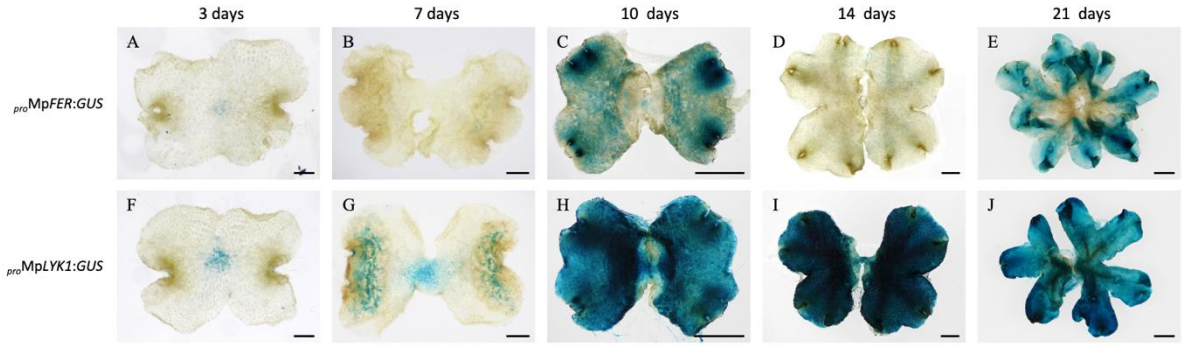

Figure 9. Comparison of gene expression patterns between Mp*FER* and Mp*LYK1*

Histochemical GUS staining of transgenic lines expressing a GUS gene under the respective promoters. The dorsal surfaces of all plants are shown.

A and F. Three-day-old gemmalings. Scale bars, 250 μm.

B and G. Seven-day-old gemmalings. Scale bars, 500 μm.

C and H. Ten-day-old thalli. Scale bars, 2 mm.

D and I. Fourteen-day-old thalli. Scale bars, 2 mm.

E and J. Twenty-one-day-old thalli. Scale bars, 5 mm.

3.1.3.4 The specificity of RALF–FER pairs

AtRALF34 and AtRALF23 were reported to suppress MAMP-triggered ROS bursts and, therefore, negatively regulate PTI in *A. thaliana* (Stegmann et al. 2017). F-RALF secreted by *F. oxysporum* induces ROS bursts in tomato and *N. benthamiana*. To investigate the specificity of ligand–receptor pairs for understanding the evolution of the RALF–FER module, AtRALF23 (AT3G16570), AtRALF34 (AT5G67070), and F-RALF (FOXG_21151) peptides were chemically synthesised (Data S1), and I tested whether these peptides can trigger ROS production in *M. polymorpha*. As shown in Figure 10A, AtRALF34 and F-RALF could trigger ROS bursts, whereas AtRALF23 failed to trigger ROS bursts in *M. polymorpha*. It is worth mentioning that although both AtRALF34 and F-RALF triggered ROS bursts in *M. polymorpha*, the levels of ROS production were significantly lower than that triggered by MpRALF1 (Figure 10A). Although AtRALF34 does not trigger ROS bursts in *A. thaliana*, it could induce ROS bursts in *M. polymorpha* to the same extent as closely related MpRALFs (Figure 7D).

Previous studies have shown that AtRALF34, AtRALF23, and F-RALF can inhibit root growth in *A. thaliana*. To validate whether AtRALF34, AtRALF23, and F-RALF peptides used in this study are functional, I treated *A. thaliana* seedlings with these peptides and measured root growth. I also used MpRALFs to investigate whether *A. thaliana* can recognise RALFs from *M. polymorpha*. Five-day-old seedlings were treated with the RALF peptides for 2 days, and then root lengths were measured. At a concentration of 1 µM, AtRALF34, AtRALF23, and MpRALF1 peptides inhibited root growth (Figure 10B). This result confirmed that these peptides are functional and indicates that MpRALF1 can be sensed by *A. thaliana*.

Masachis et al. showed that F-RALF inhibits root growth of *A. thaliana* at a high concentration (10 µM) (Masachis et al. 2016). Therefore, I conducted a root inhibition assay with a higher concentration (10 µM) of F-RALF. As shown in Figure 10C, 10 µM F-RALF inhibited root growth of *A. thaliana*, indicating that F-RALF can be sensed by *A. thaliana* at higher concentration. With respect to MpRALF3, 1 µM MpRALF3 did not inhibit root growth (Figure 10B). As in the case of F-RALF, this could be due to the lower concentration used. Taken together, these results highlight the specificity of the RALF–FER module and further suggest that the physiological and molecular roles of the module have diversified during land plant evolution.

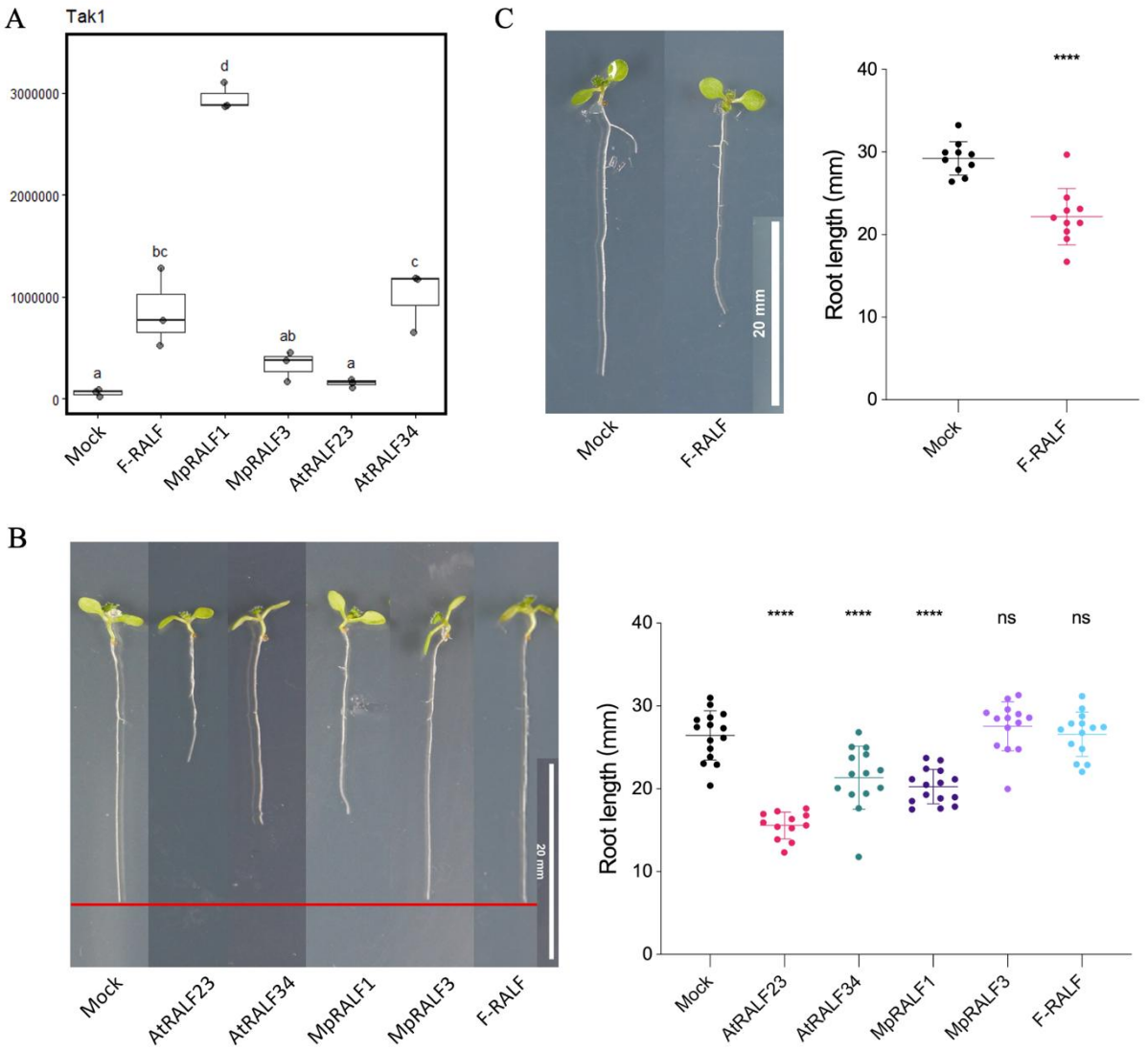

Figure 10. ROS production and root growth inhibition induced by different RALFs

A. Total ROS bursts over time triggered by 1µM of F-RALF, MpRALF1, MpRALF3, AtRALF23, and AtRALF34. Total ROS production over time was monitored with a plate reader by luminescence (RLU) (n=3, mean +/- SE). Letters indicate the significant differences calculated using an ANOVA and Tukey HSD, p-value < 0.05.

B and C. Primary root lengths of 5-day-old seedlings grown on ½ MS medium with 1% agar were transferred to liquid ½ MS medium in the absence (mock) or presence of 10 µM F-RALF peptides **(C)**, or 1 µM AtRALF23, AtRALF34, MpRALF1, MpRALF3, and F-RALF **(B)**. Asterisks indicate significant difference of one-way ANOVA test; each treatment was compared with its corresponding mock. ns, not significant; ****, p-value < 0.0001.

3.1.4 RALF–FER module regulates defence responses in *M. polymorpha*

3.1.4.1 MpRALF1- and chitin-induced DEGs partially overlap

Due to the rather severe developmental defects of Mp*fer-9* (Figure 4B), it was not feasible to properly compare pathogen growth in Mp*fer-9* and Tak-1, making it difficult to investigate the

contribution of MpFER to immunity. To gain insights into whether and how the MpRALF1–MpFER module contributes to immunity, I profiled transcriptome changes following MpRALF1 treatment. Chitin can trigger immune responses resulting in defence-related gene expression in *M. polymorpha* (Yotsui et al. 2023). Therefore, I compared transcriptional reprograming upon MpRALF1 and chitin treatment. Fourteen-day-old Tak-1 thalli were treated with either MpRALF1 or chitin for 1 or 3 hours.

Principal component analysis (PCA) of differentially expressed genes (DEGs) revealed distinct patterns of DEGs between 1-hour and 3-hour treatments. Additionally, there were distinct patterns observed among MpRALF1, chitin, and mock treatments within the same treatment duration, indicating significant transcriptional reprogramming in each condition (Figure 11A). DEGs from different comparisons are presented in Table S1. After 1 hour of treatment, 628 and 167 genes were regulated by chitin and MpRALF1, respectively (Figure 11B and 11C). Among these genes, 93 genes were found to be commonly regulated by both treatments. At 3 hours, 128 and 97 genes were regulated by chitin and MpRALF1, respectively, with an overlap of 49 genes (Figure 11B and 11C).

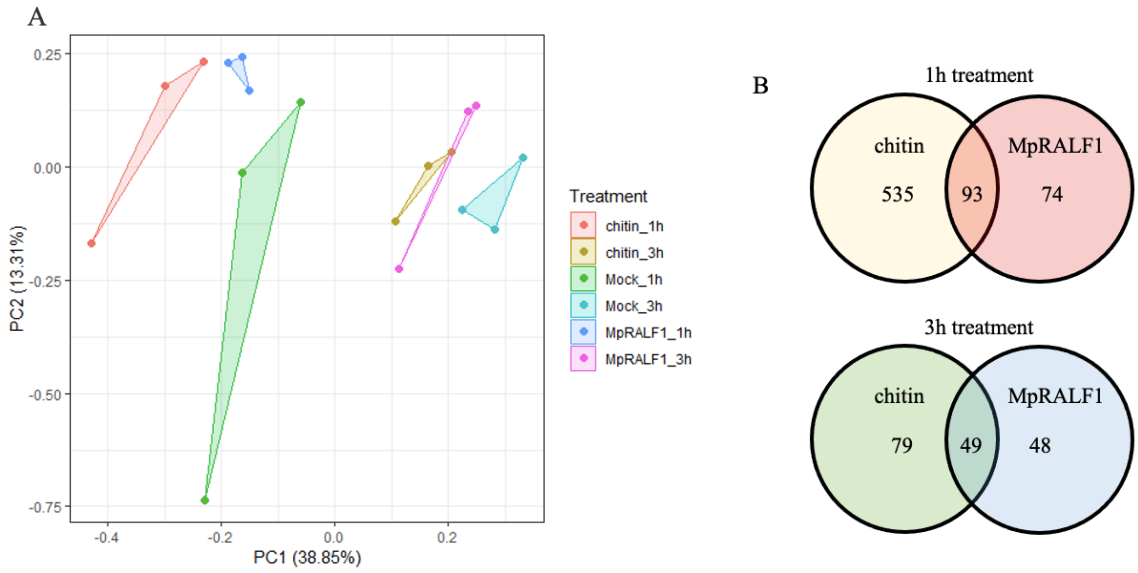

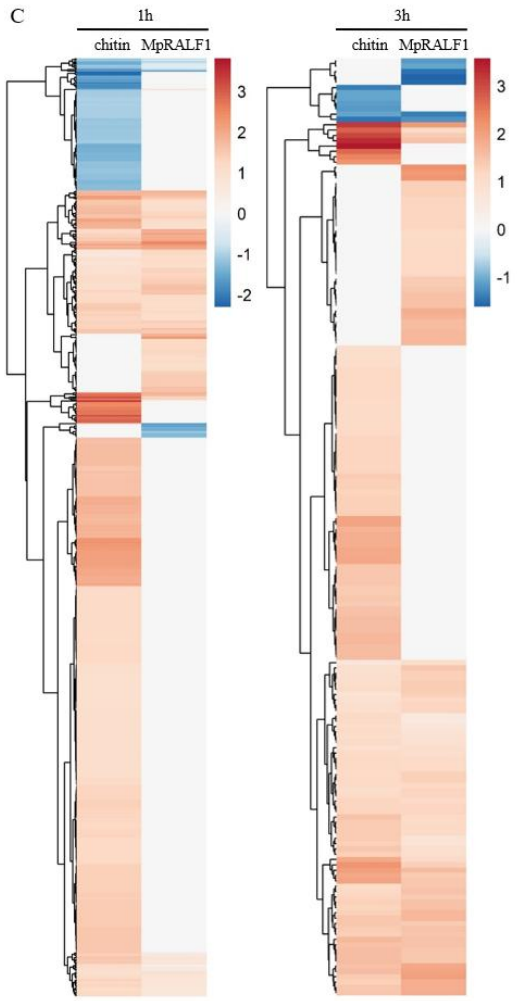

Figure 11. Transcriptome analysis of *M. polymorpha* upon MpRALF1 and chitin treatments

A. Principal component analysis (PCA) plot of DEGs observed in MpRALF1, chitin, and mock treatments for 1 hour and 3 hours. Three technical replicates were performed for each condition.

B. Venn diagram of the total numbers of DEGs upon chitin and MpRALF1 treatments for 1 hour and 3 hours. Overlaps indicate the shared DEGs between chitin and MpRALF1 treatments.

C. Heatmap of 628 chitin-regulated and 167 MpRALF1-regulated DEGs identified after 1-hour treatment, and 128 chitin-regulated and 97 MpRALF1-regulated DEGs identified after 3-hour treatment. Up-regulated and down-regulated DEGs are coloured red and blue, respectively. $|\log2FC| \geq 1$, adjusted p-value < 0.05.

The gene ontology (GO) enrichment analysis of DEGs, which were regulated upon chitin treatments, found terms related to defence responses, confirming the results of a previously published study (Yotsui et al. 2023). The GO terms such as ‘Response to chemical’, ‘Cellular response to toxic substance’, and ‘Phenylpropanoid metabolic process’ were identified after 1-hour chitin treatment (Figure 12A), and ‘Defence response’, ‘Response to other organism’, and ‘Response to external biotic stimulus’ were identified after 3-hour treatment (Figure 12B).

To investigate the function of genes commonly induced by MpRALF1 and chitin treatments, I performed GO enrichment analysis of the overlapping DEGs. GO terms such as ‘Reactive oxygen species metabolic process’, ‘Response to oxidative stress’, ‘Cellular response to stimulus’, and ‘Cellular response to toxic substance’ were among the top 25 GO terms of the overlapped DEGs after 1 and 3 hours. The GO terms ‘Chitin metabolic process’ and ‘Chitin catabolic process’ were found in the overlapping DEGs at 1 hour and ‘Response to toxic substance’, ‘Response to external biotic stimulus’, ‘Defence response to other organism’, ‘Defence response to fungus’, and ‘Phenylpropanoid metabolic process’ were exclusively enriched after 3 hours of treatment (Figure 12C and 12D). These results suggest that MpRALF1-induced DEGs overlapping with chitin-induced DEGs play roles in defence responses, implying a role for the MpRALF1–MpFER module in immunity.

Upon MpRALF1 treatment, a greater number of defence-related GO terms were enriched after 3 hours compared to 1 hour, including ‘Innate immune response’, ‘Defence response’, and ‘Defence response to other organism’ (Figure 12E and 12F). Additionally, the DEGs induced by MpRALF1 are related to CWI. For instance, GO terms such as ‘Cell wall organisation’ and ‘Cell wall biogenesis’ were identified both at 1 and 3 hours (Figure 12E and 12F).

Taken together, these results indicate that MpRALF1 induces multiple genes that function in defence responses, implying that MpRALF1 positively regulates defence through MpFER. This suggests that the MpRALF1–MpFER module plays an important role in immunity.

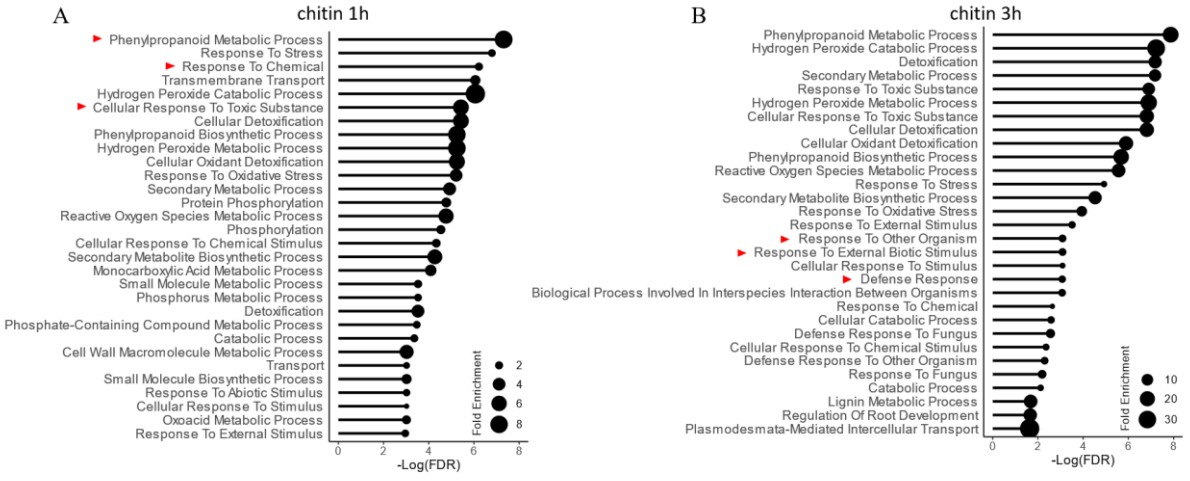

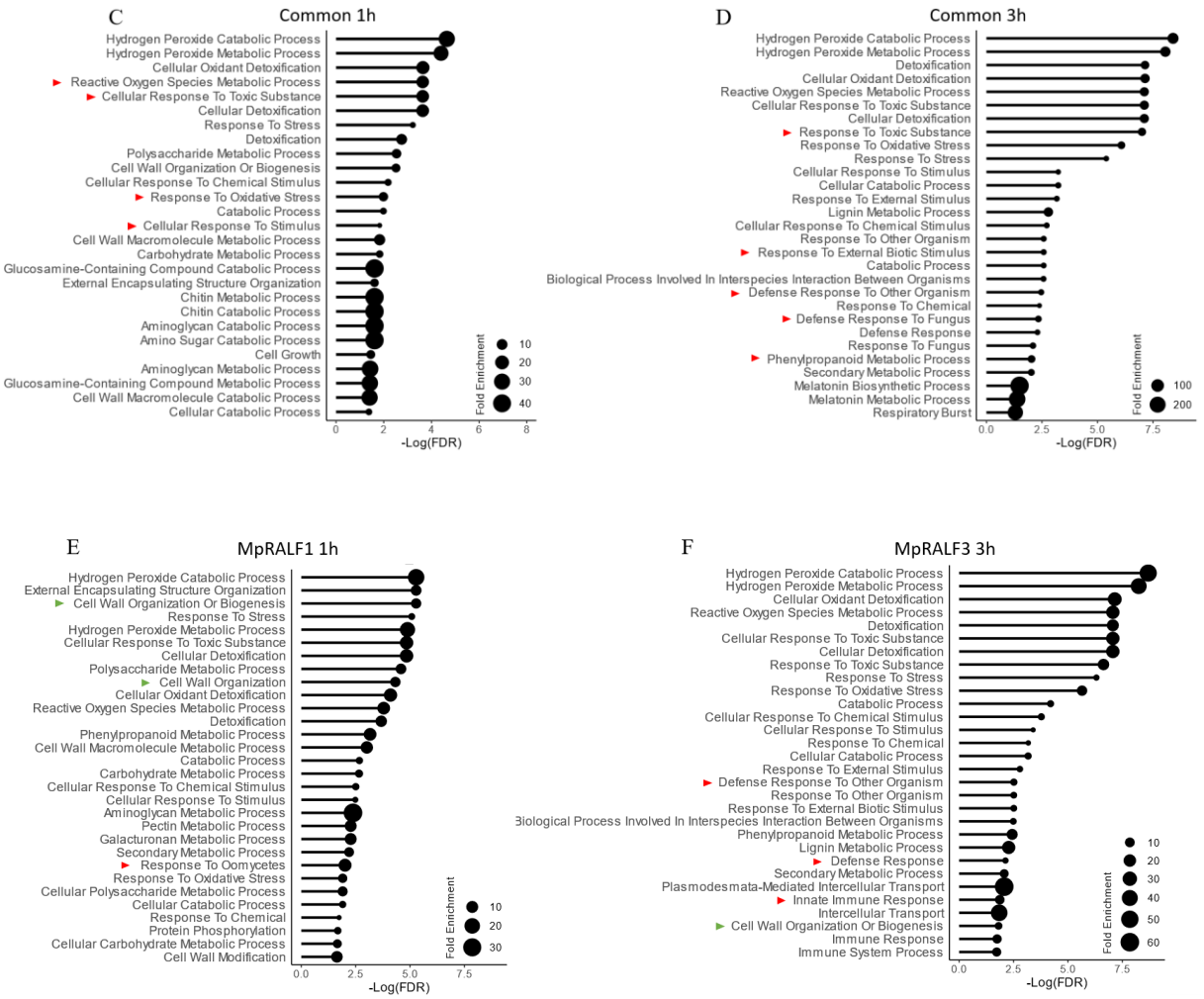

Figure 12. GO enrichment analysis of DEGs induced by MpRALF1 and chitin

The GO enrichment analysis was performed using ShinyGO in the pathway database of GO biological process. The size of closed circles indicates the fold enrichment in each condition. False discovery rate (FDR) < 0.05. GO terms related to defence responses are indicated by red arrows, while GO terms related to cell wall biogenesis are indicated by green arrows.

Having found that DEGs induced by MpRALF1 are partly related to defence responses, I looked into the expression of reported defence-related marker genes in my transcriptome dataset. As shown in Figure 13A, MAMP-responsive or defence-related genes were significantly up-regulated (Log2FC ≥ 1) following either 1 or 3 hours of MpRALF1 treatment (Carella et al. 2019; Gimenez-Ibanez et al. 2019). To further confirm the RNA-seq results, I performed the quantitative RT-PCR analysis of the selected two defence-related genes Mp*PR3* (Mp4g20440) and Mp*WRKY14* (Mp6g16800). The housekeeping gene Mp*ACTIN7* (Mp6g11010) was used as an internal reference. Compared to the mock treatment, the expression of both Mp*PR3* and Mp*WRKY14* was significantly increased after MpRALF1 treatment for 1 hour (Figure 13B).

Collectively, these results suggest that MpRALF1 positively regulates defence in *M. polymorpha*.

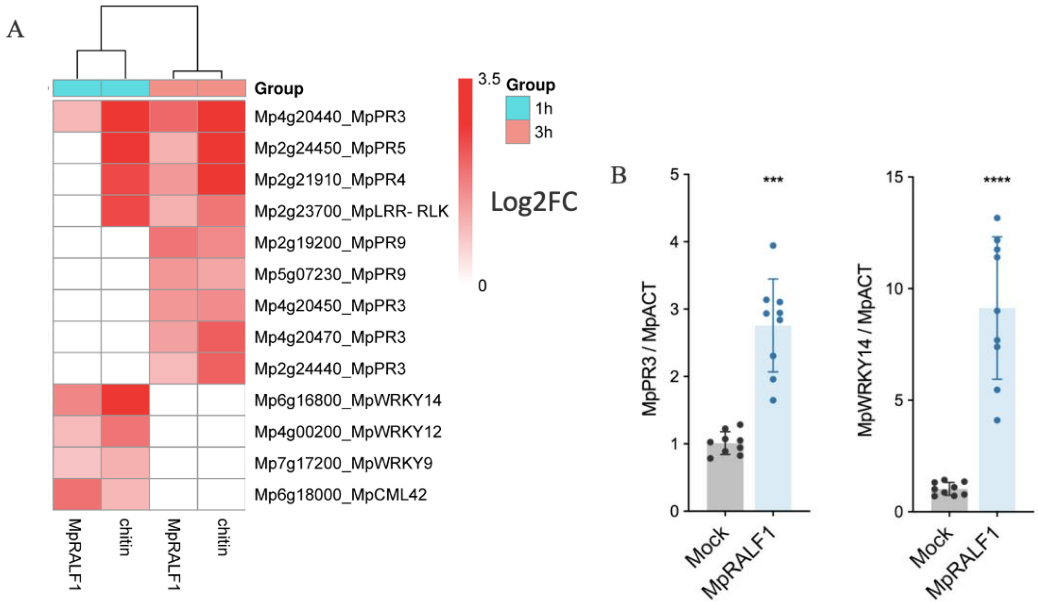

Figure 13. MpRALF1-induced defence-related gene expressions

A. Differential expression of defence-related genes up-regulated by chitin and MpRALF1 after 1-hour and 3-hour treatments. |log2FC| ≥ 1, adjusted p-value < 0.05.

B. qRT-PCR analysis of defence-related gene transcripts induced by MpRALF1 for 1 hour. Expression values are shown relative to internal Mp*ACT* control. Asterisks indicate statistically significant differences calculated using the one-way ANOVA test. Error bars represent standard deviation (SD) (n=9). ***, p-value < 0.001; ****, p-value < 0.0001.

3.1.4.2 MpRALF1 treatment primes resistance against a bacterial pathogen in *M. polymorpha*

To ascertain whether MpRALF1 positively regulates immunity in *M. polymorpha*, I conducted a priming assay. Fourteen-day-old thalli were pre-treated with MpRALF1 peptides for 3 and 24 hours, and then inoculated with the bioluminescent bacterial pathogen *Pto* DC3000-lux (Matsumoto et al. 2021). AtRALF23 was used as a negative control, as it could not be sensed by *M. polymorpha* to trigger ROS bursts (Figure 10A). As shown in Figure 14, pre-treatment with MpRALF1 for both 3 and 24 hours significantly reduced the growth of *Pto* DC3000-lux compared to mock and AtRALF23 treatments. I confirmed that the pH of the surrounding buffer remained constant during peptide treatment (Data S2). This result indicates that MpRALF1 primes defence in *M. polymorpha* and thereby positively regulates immunity in *M. polymorpha*.

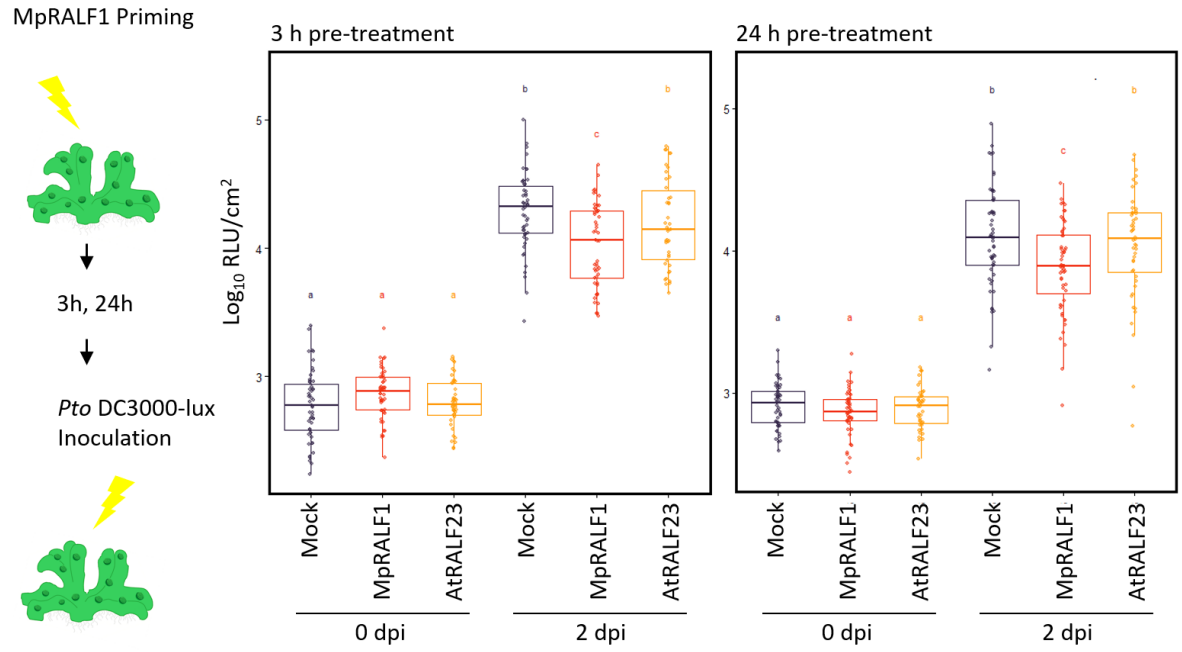

Figure 14. MpRALF1 primes *M. polymorpha* resistance against *Pto* DC3000-lux

Quantification of bacterial growth in the middle region of 14-day-old thalli, inoculated with the bioluminescent *Pto* DC3000-lux. dpi, days post-inoculation. Boxes show upper and lower quartiles of the values, and lines in boxes represent the medians. Statistical analysis was performed using Student's t test with p-values adjusted by the Benjamini and Hochberg (BH) method (n = 44). Statistically significant differences are indicated by different letters. p-value < 0.05.

3.1.5 Crosstalk between MpRALF- and chitin-triggered pathway

3.1.5.1 MpFER interactome analysis identifies MpLYK1 and MpLYR as potential interactors

To explore molecular links or mechanisms by which MpFER contributes to defence amplification, I performed an interactome analysis of MpFER using a miniTurbo-based proximity labelling approach (Melkonian et al. 2022). Transgenic plants expressing $_{pro}$Mp*FER*:Mp*FER-miniTurbo-Myc* were used for interactome analysis. Wild-type Tak-1 plants were used as controls. I confirmed the expression of bait protein (MpFER-miniTurbo-Myc) in these plants by immunoblotting using an anti-Myc-tag antibody (Figure 6B). Fourteen-day-old thalli of $_{pro}$Mp*FER*:Mp*FER-miniTurbo-Myc* transgenic plants and Tak-1 plants were treated with biotin for 24 hours at room temperature. Protein biotinylation in cell extracts was determined by immunoblotting using a streptavidin-HRP (Figure 15A). Immunoblot analysis confirmed that the corresponding transgenic plants are suitable for identifying potentially interacting proteins by mass spectrometry (MS) followed by pulldown. Line No.2 of transgenic

plants expressing $_{pro}$Mp*FER*:Mp*FER-miniTurbo-Myc* was used for further MS analysis (Figure 6B and 15A).

The MS analysis identified 789 potential interactors of MpFER, including MpFER itself, indicating the success of the analysis (Figure 15B). Interestingly, MpLYK1 and MpLYR, which play roles in sensing chitin in *M. polymorpha*, were identified as potential interactors of MpFER (Figure 15B and Table S2). Reciprocally, interactome analysis of MpLYK1 identified MpFER as a candidate interactor (Figure S1). These results suggest the interaction between MpFER and MpLYK1.

To investigate the interaction between MpLYK1 and MpFER, I transiently expressed mCherry- or GFP-tagged proteins under the CaMV 35S promoter in *N. benthamiana* and performed Förster resonance energy transfer with fluorescence lifetime imaging microscopy (FRET–FLIM) analysis. MpLYK1 and MpLYR were tagged with mCherry at their C-termini, while MpFER was tagged with GFP at its C-terminus. The mean fluorescence lifetime (τ) of MpFER-GFP as the donor molecule was firstly measured. An average fluorescence lifetime of 2.491 ns was determined from 42 measurements conducted on the plasma membrane. Subsequently, FLIM-based FRET analysis was performed by expressing MpFER-GFP along with MpLYK1-mCherry or MpLYR-mCherry as the acceptor molecules. Co-expression of MpLYK1-mCherry or MpLYR-mCherry with MpFER-GFP significantly decreased the fluorescence lifetime of the donor MpFER-GFP to 2.408 ns and 2.426 ns, respectively (Figure 15C). This result indicates that MpFER interacts with MpLYK1 and MpLYR *in vivo*.

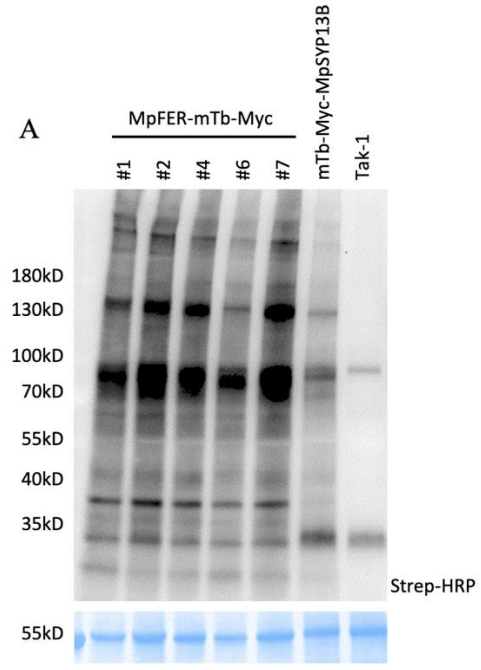

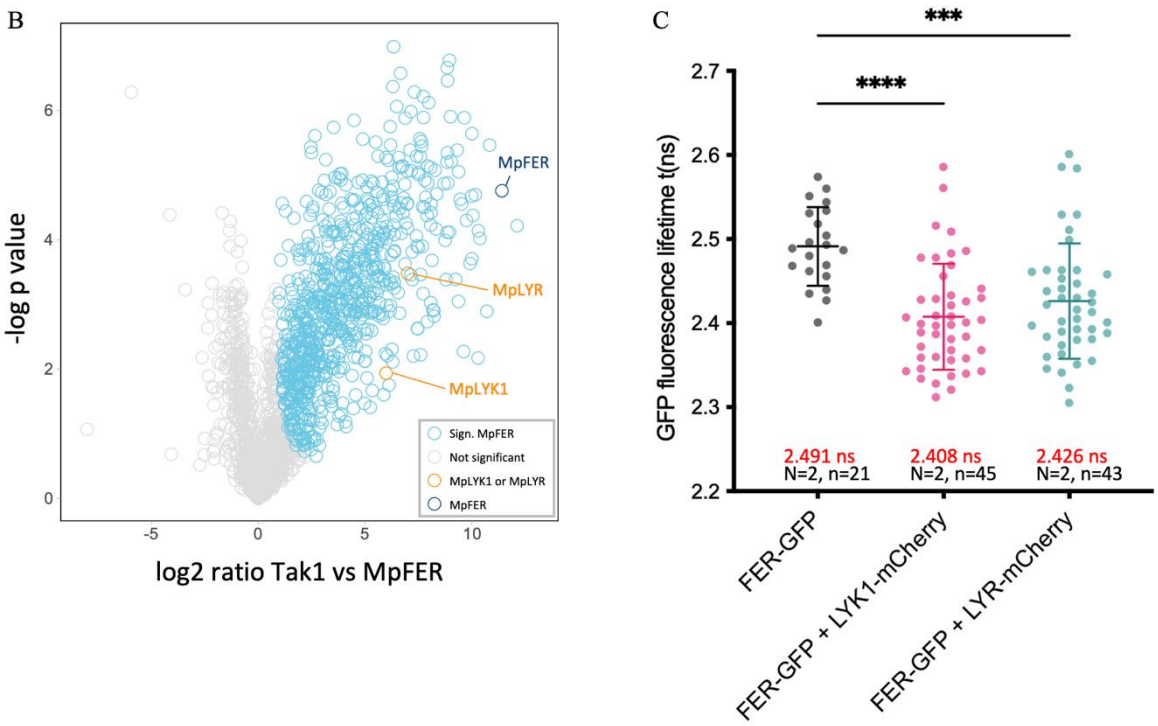

Figure 15. Interactome and FRET–FLIM analysis of MpFER

A. Protein biotinylation was detected by immunoblotting using the streptavidin-HRP. A CBB-stained blot is shown as loading control.

B. Identification of MpFER-interacting proteins by the miniTurbo-based proximity *in vivo* labelling approach. Wild-type Tak-1 was used as a control. Three biological replicates were used for the analysis. All candidate interactors are shown in blue; MpLYR and MpLYK1 are shown in orange and the bait protein MpFER is shown in dark blue.

C. Mean fluorescence lifetime (τ, ns) of MpFER-GFP when expressed alone or along with MpLYK1-mCherry or MpLYR-mCherry. Significant differences calculated by one-way ANOVA are indicated with asterisks. Error bars, S; n, number of measurements; N, number of independent experiments. ***, p-value < 0.001****, p-value < 0.0001.

3.1.5.2 MpFER is phosphorylated upon chitin treatment

Considering the interactions between MpFER and LysM receptors in *M. polymorpha*, I asked whether crosstalk exits between MpFER- and MpLYK1-mediated signalling pathways. Based on phosphoproteome analysis in a published study from our group, MpFER can be phosphorylated upon chitin treatment, suggesting a potential contribution of MpFER to the MpLYK1-mediated signalling pathway (Figure S2) (Yotsui et al. 2023).

To investigate how MpFER is involved in the chitin-induced signalling pathway, I examined whether MpLYK1 can directly phosphorylate MpFER *in vitro*. An *in vitro* kinase assay between MpFER and MpLYK1 was performed. The MBPHis-tagged kinase-dead mutant of MpFER cytoplasmic domain (MBPHis-FER-KD), GST-tagged MpLYK1 cytoplasmic

domain (GST-LYK1) and its kinase-dead mutant (GST-LYK1-KD) were prepared using an *Escherichia coli* expression system. It should be noted that my attempts to clone the MBPHis-tagged MpFER cytoplasmic domain (MBPHis-FER) were unsuccessful, possibly due to the toxicity of MpFER kinase activity in *E. coli* cells.

While performing the *in vitro* kinase assay, I found that MBPHis-FER-KD was phosphorylated in *E. coli* in the absence of MpLYK1. This was likely due to the action of endogenous *E. coli* kinases. Therefore, I treated MBPHis-FER-KD with FastAP thermosensitive alkaline phosphatase for use as a substrate. Subsequently, in the kinase reaction, the phosphatase-treated MBPHis-FER-KD was incubated with either GST-MpLYK1 or GST-MpLYK1-KD. As shown in Figure 16, no phosphorylation-dependent mobility band shift of MBPHis-FER-KD was detected in the presence of GST-LYK1 compared to negative controls. Clear band shifts of GST-LYK1 were observed, but not of GST-LYK1-KD, indicating that the used GST-LYK1 was kinase-active.

At the same time, proteins from the *in vitro* kinase assay were subjected to MS analysis. We did not detect GST-LYK1-dependent phosphorylation of MpFER also by MS analysis either. Taken together, these results suggest that MpLYK1 does not directly phosphorylate MpFER.

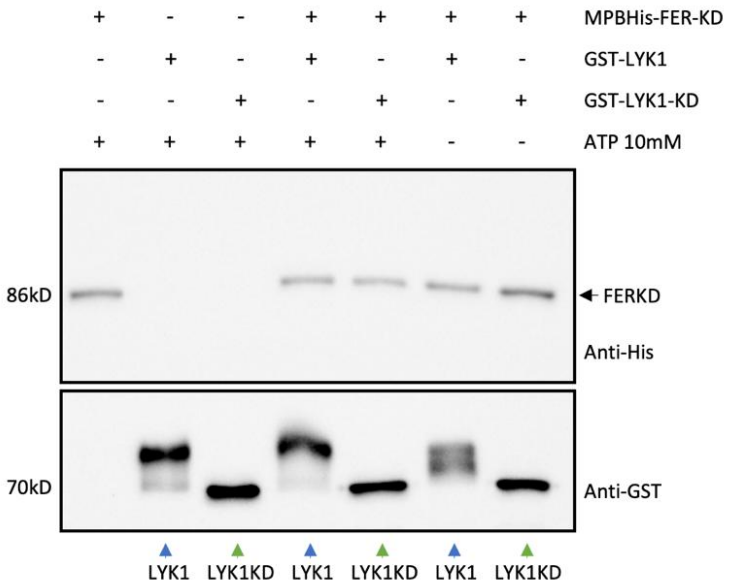

Figure 16. Phosphorylation between MpFER and MpLYK1

In vitro kinase assay against MBPHis-FER-KD in the absence or presence of GST-LYK1 or GST-LYK1-KD proteins. Proteins were subjected to Phos-tag SDS-PAGE gel after the *in vitro* kinase reaction with (+) or without (−) ATP. Equal amounts of each recombinant protein were used. Immunoblot analysis was carried out using antibodies against the indicated tags. Target proteins are indicated by arrows.

3.1.5.3 MpRALF1-induced ROS production is compromised in Mp*lyk1* and Mp*lyr* mutants, and chitin-induced ROS production is compromised in the Mp*fer* mutants

Phosphoproteome analysis implicates MpFER in the chitin-induced signalling pathway (Yotsui et al. 2023). To investigate the potential crosstalk, I assessed ROS production in Mp*fer-9*, Mp*lyk1*, and Mp*lyr* mutants. Five-day-old gemmae from the Mp*fer-9* mutant were treated with chitin (Figure 17B), while gemmae from Mp*lyk1* and Mp*lyr* mutants were treated with MpRALF1 peptides (Figure 17A). I found that ROS bursts triggered by chitin were compromised in the Mp*fer-9* mutant compared to Tak-1 (Figure 17B). Similarly, the ROS bursts triggered by MpRALF1 were compromised in both Mp*lyk1* and Mp*lyr* mutants (Figure 17A). Taken together, these findings imply that there is a potential crosstalk between MpRALF1- and chitin-induced signalling pathways.

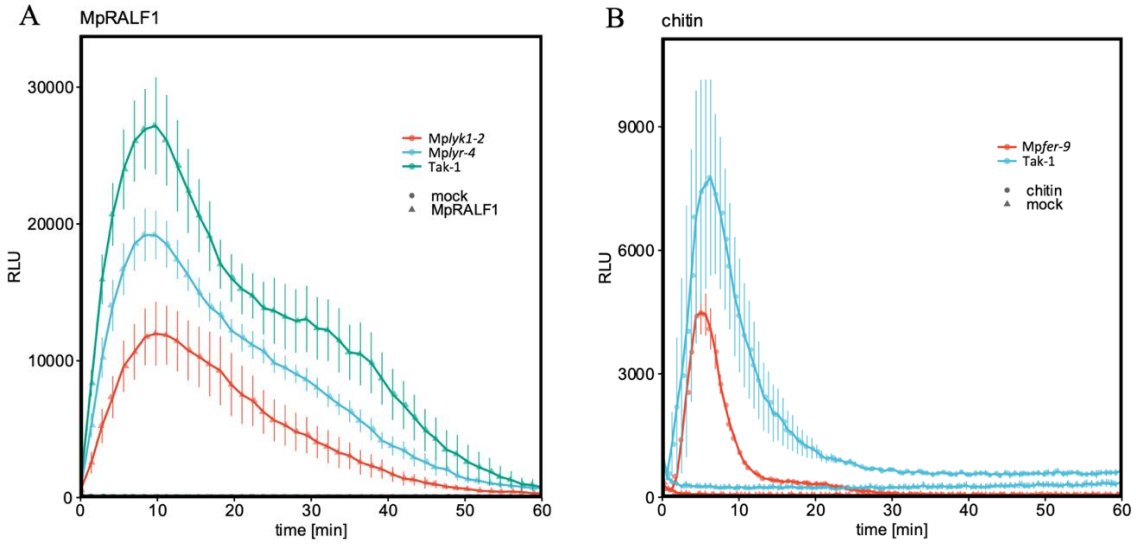

Figure 17. ROS bursts in Mp*fer*, Mp*lyk1*, Mp*lyr* mutants triggered by chitin and MpRALF1.
Gemmae were treated with mock and 1 µM MpRALF1 **(A)** or 1 µM chitin **(B)**. Five-day-old liquid cultured gemmae from indicated genotypes and wild-type Tak-1 were used. ROS production over time was monitored with a plate reader by luminescence (RLU) (n=3, mean +/- SE).

3.2 Leucine-rich repeat receptor-like kinases, LRR-RLKs

3.2.1 Subfamily II LRR-RLKs, MpSERK and MpAPEX

3.2.1.1 MpSERK plays roles in development

To investigate the functions of MpSERK and MpAPEX from subfamily II LRR-RLKs in *M. polymorpha*, we obtained Mp*serk* and Mp*apex* disruptants generated by the CRISPR-Cas9 system in Tak-1 background from Prof. Ana I. Caño-Delgado (Centre for Research in

Agricultural Genomics, Spain) and Prof. Yuki Hirakawa (Hiroshima University, Japan), respectively (Figure 18). The Mp*apex-1* mutant had a single base-pair insertion at the beginning of the Mp*APEX* coding sequence, leading to a nonsense translation of MpAPEX after 21 amino acids and premature translation termination (Figure 18A). The Mp*apex-2* mutant had a single base-pair deletion at the beginning of the intracellular domain of MpAPEX, leading to premature translation termination with lack of a large part of the intracellular domain (Figure 18A). The growth of Mp*apex* was comparable to Tak-1, suggesting that MpAPEX has little or no influence on vegetative growth and development (Figure 18B).

The Mps*erk* mutants lacked most of the intracellular domain of MpSERK and, thus, likely cannot fulfil their proper function (Figure 18C). Three independent Mps*erk* lines, Mps*erk-1*, Mps*erk-2*, and Mps*erk-3*, could develop air pores and rhizoids, but exhibited developmental defects in thallus branching and gemma cup formation compared to Tak-1 (Figure 18D and 18E). Sexual organs of *M. polymorpha* can be induced after transfer to far-red light conditions for 2–3 weeks (Chiyoda et al. 2008). Under far-red light irradiation, Mps*erk-1* did not develop the sexual gametangiophore organ up to the 38-day-old stage (Figure 18F). These results indicate that MpSERK plays a role in initiating vegetative growth and sexual reproduction.

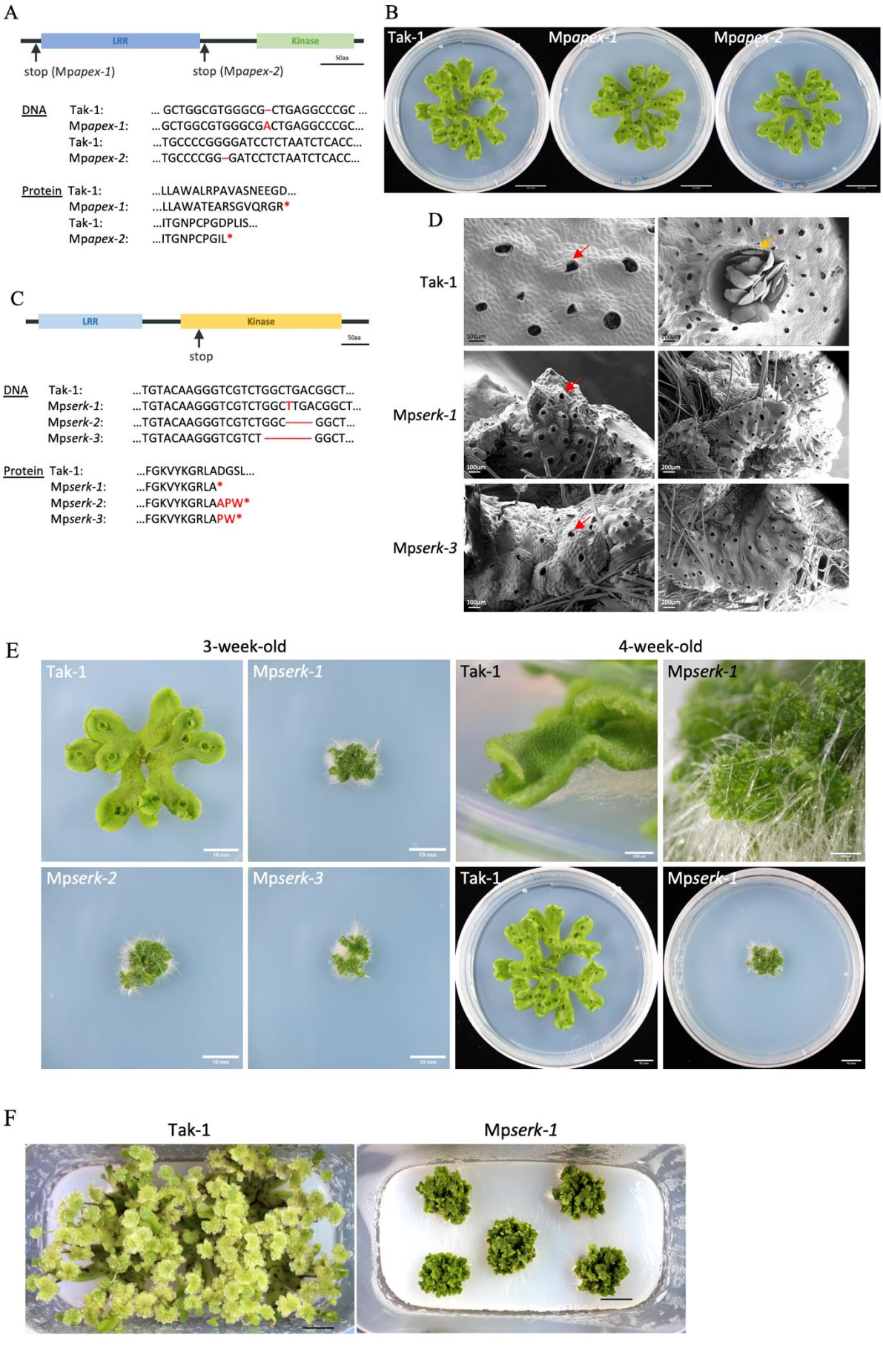
A
LRR
Kinase
50aa
stop (Mpapex-1)
stop (Mpapex-2)
DNA Tak-1: ... GCTGGCGTGGGCG–CTGAGGCCCGC ...
Mpapex-1: ...GCTGGCGTGGGCGACTGAGGCCCGC...
Tak-1: ...TGCCCCGGGGATCCTCTAATCTCACC...
Mpapex-2: ...TGCCCCGG–GATCCTCTAATCTCACC...
Protein Tak-1: ...LLAWALRPAVASNEEGD...
Mpapex-1: ...LLAWATEARSGVQRGR*
Tak-1: ...ITGNPCPGDPLIS...
Mpapex-2: ...ITGNPCPGIL*
B
Tak-1
Mpapex-1
Mpapex-2
C
LRR
Kinase
50aa
stop
DNA Tak-1: ...TGTACAAGGGTCGTCTGGCTGACGGCT...
Mpserk-1: ...TGTACAAGGGTCGTCTGGCTTGACGGCT...
Mpserk-2: ...TGTACAAGGGTCGTCTGGC—— GGCT...
Mpserk-3: ...TGTACAAGGGTCGTCT —————— GGCT...
Protein Tak-1: ...FGKVYKGRLADGSL...
Mpserk-1: ...FGKVYKGRLA*
Mpserk-2: ...FGKVYKGRLAAPW*
Mpserk-3: ...FGKVYKGRLAPW*
D
Tak-1
Mpserk-1
Mpserk-3
100µm
200µm
E
3-week-old
4-week-old
Tak-1
Mpserk-1
Mpserk-2
Mpserk-3
F
Tak-1
Mpserk-1

Figure 18. Phenotypes and genome editing sites of Mp*apex* and Mp*serk* mutants

A. Schematic representation of Mp*APEX* disruptions in Mp*apex-1* and Mp*apex-2*. Early stop of protein translation caused by gene editing is indicated by arrows.

B. Four-week-old Mp*apex-1* and Mp*apex-2* compared to Tak-1. Thalli were grown from single gemma under constant white light.

C. Schematic representation of Mp*SERK* disruptions in Mp*serk-1*, Mp*serk-2*, and Mp*serk-3*. Early stop of protein translation at the intracellular domain of MpSERK is indicated by an arrow.

D. Scanning electronic microscope (SEM) images of thalli surfaces from Mp*serk-1*, Mp*serk-3*, and Tak-1. Air pores are indicated by red arrows, gemma cup is indicated by a yellow arrow.

E. Three- and four-week-old Mp*serk-1*, Mp*serk-2*, and Mp*serk-3* compared to Tak-1. Thalli were grown from single gemma (Tak-1) or small pieces of thalli (Mp*serk* mutants) under constant white light.

F. Gametangiophore induction in Mp*serk-1* and Tak-1. All plants were 38-day-old. Thalli were grown from single gemma (Tak-1) or small pieces of thalli (Mp*serk-1*) under constant far-red and white light. Scale bar, 15 mm.

3.2.1.2 Expression patterns of Mp*SERK* and Mp*APEX*

To investigate the expression profiles of Mp*SERK* and Mp*APEX*, 5-kb DNA fragments upstream of the start codons of Mp*SERK* and Mp*APEX* were cloned and fused to a GUS-reporter gene. Four independent transgenic plants expressing $_{pro}$Mp*SERK*:*GUS* or $_{pro}$Mp*APEX*:*GUS* were established in the Tak-1 background. As shown in Figure 19A–D and 19I, Mp*SERK* was primarily expressed in the meristematic regions and assimilatory filaments, supporting a role in growth and development.

Mp*APEX* expression was hardly detected until the plants were 7 days old (Figure 19F). At the later growth stages, patchy GUS staining was observed, which typically suggests the staining of assimilatory filaments in air chambers (Figure 19G and 19H). This was confirmed by the cross-sectional analysis (Figure 19J). Wild-type Tak-1, used as a negative control, did not exhibit any GUS staining at any of these growth stages. Air chambers and assimilatory filaments have been suggested to support fungal and bacterial colonisation in *M. polymorpha* (Carella et al. 2018; Matsui et al. 2020). Thus, the observed Mp*SERK* and Mp*APEX* expression in assimilatory filaments may imply contributions to plant–microbe interactions.

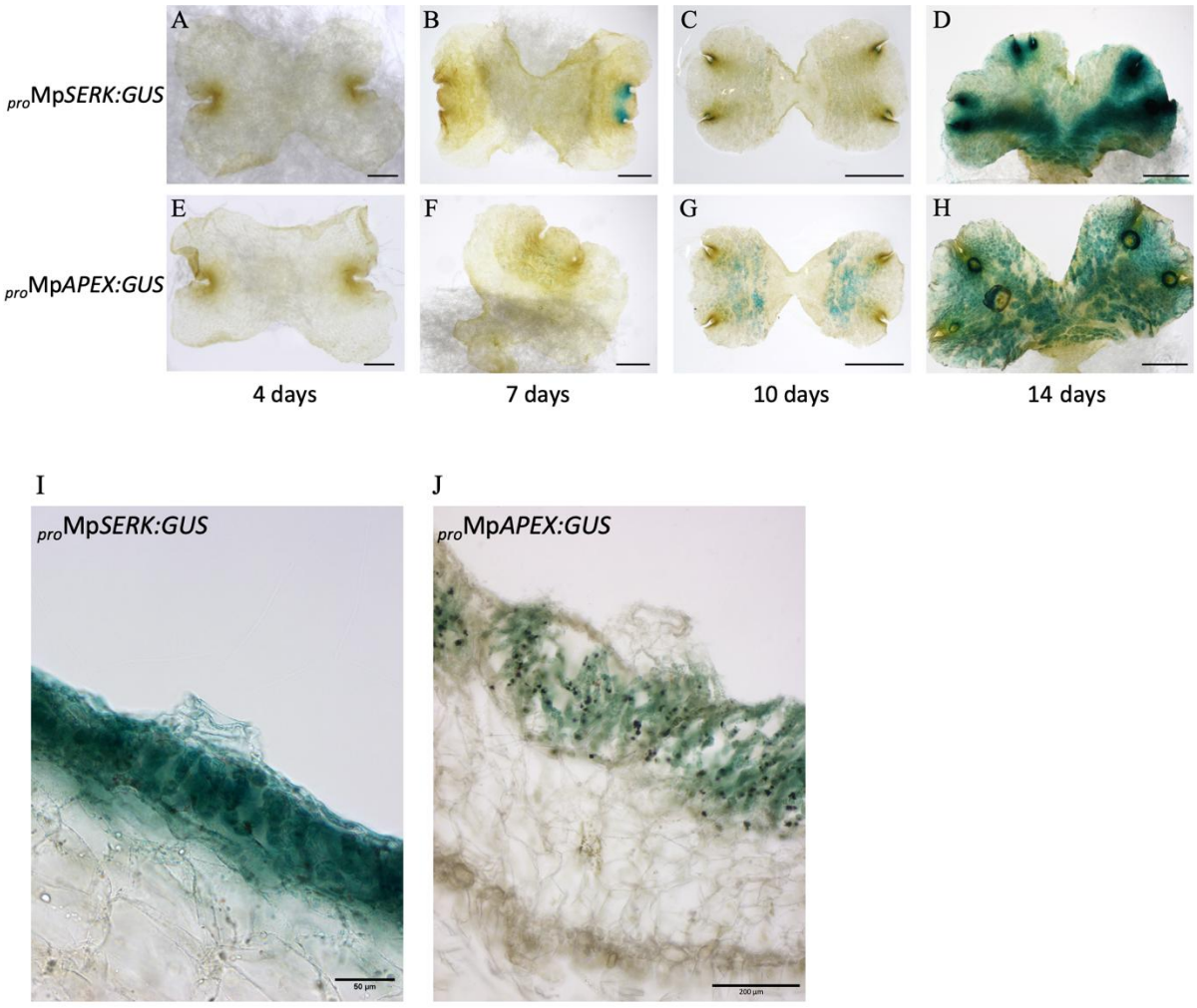

Figure 19. Gene expression patterns of Mp*SERK* and Mp*APEX*

Histochemical GUS staining of transgenic lines expressing the GUS gene under the indicated promoters.

A and E. Top view of 4-day-old gemmalings. Scale bars, 250 μm.

B and F. Top view of 7-day-old gemmalings. Scale bars, 500 μm.

C and G. Top view of 10-day-old thalli. Scale bars, 2 mm.

D and H. Top view of 14-day-old thalli. Scale bars, 2 mm.

I. Cross-sectional view of 14-day-old thalli.

J. Cross-sectional view of 14-day-old thalli.

3.2.1.3 Growth of *Pto* DC3000 in Mp*apex* mutants

In order to investigate the role of MpAPEX in defence against bacterial pathogens, I monitored the growth of *Pto* DC3000 in the Mp*apex* mutants. Fourteen-day-old thalli of Mp*apex-1*, Mp*apex-2*, and Tak-1 were inoculated with the bioluminescent *Pto* DC3000-lux. Bacterial growth on the apical regions of thalli at 0 and 2 dpi were determined by measuring luminescence. The Mp*apex-1* and Mp*apex-2* mutants tended to be resistant against *Pto* DC3000-lux compared to Tak-1 (Figure 20). This result suggests that MpAPEX may negatively regulate immunity.

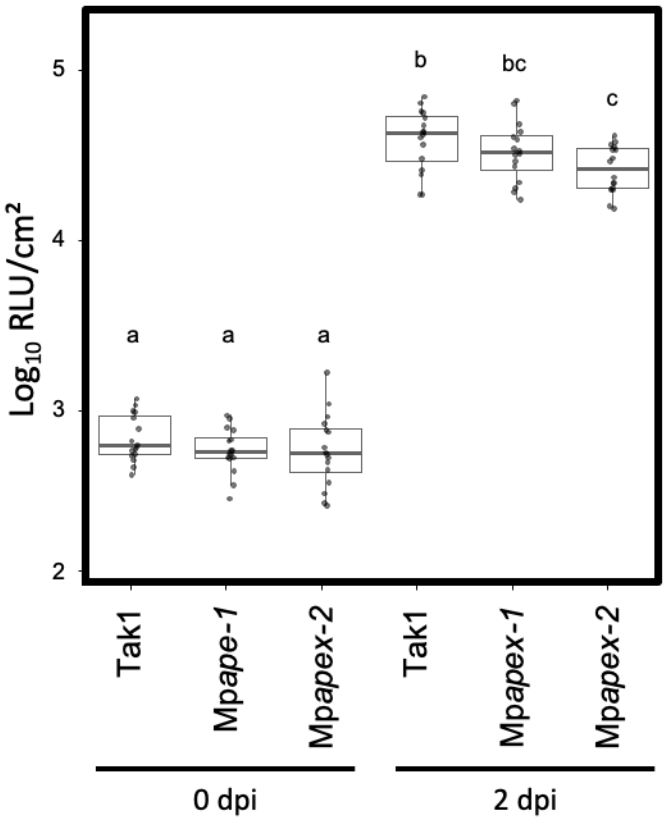

Figure 20. Growth of *Pto* DC3000-lux in Mp*apex-1*, Mp*apex-2*, and Tak-1.

Quantification of bacterial growth in the apical regions of 14-day-old thalli, inoculated with *Pto* DC3000-lux (n = 16). Boxes show upper and lower quartiles of the values, and lines in boxes represent the medians. Statistical analysis was performed using Student's t test with p-values adjusted by the BH method. Statistically significant differences are indicated by different letters. p-value < 0.05.

3.2.1.4 The conserved tyrosine residue in MpSERK is required for its function in growth and development

In *A. thaliana*, a conserved tyrosine residue Y403 located at the kinase domain of AtSERK3 has been shown to be required for immune signalling but not for BR signalling. This tyrosine residue – Y418 – is well-conserved in MpSERK (Perraki et al. 2018). To investigate whether this conserved Y418 residue contributes to MpSERK function in *M. polymorpha*, I generated transgenic plants expressing MpSERK or MpSERK^{Y418F}, tagged with miniTurbo and Myc at their C-termini, under the native Mp*SERK* promoter in the Mp*serk-3* mutant background ($_{pro}$Mp*SERK*:Mp*SERK-miniTurbo-Myc*/Mp*serk-3* and $_{pro}$Mp*SERK*:Mp*SERK*^{Y418F}*-miniTurbo-Myc*/Mp*serk-3*).

As shown in Figure 21A, plants expressing $_{pro}$Mp*SERK*:Mp*SERK-miniTurbo-Myc* almost fully rescued the developmental defects, while plants expressing $_{pro}$Mp*SERK*:Mp*SERK*^{Y418F}*-miniTurbo-Myc* only partially rescued Mp*serk* phenotypes (Figure

21B). These results suggest that the conserved tyrosine residue is required for MpSERK function in growth and development. Protein expression of MpSERK-miniTurbo-Myc and MpSERK^{Y418F}-miniTurbo-Myc in all transgenic lines was confirmed by immunoblot analysis (Figure 21C). Tak-1 and transgenic plant expressing MpSYP13B tagged with miniTurbo and Myc at its N-terminus were used as controls for immunoblot analysis. Although variations in protein expressions among four independent transgenic lines of $_{pro}$Mp*SERK*:Mp*SERK*^{Y418F}-*miniTurbo-Myc* were detected (Figure 21C), they all displayed similar developmental defects compared to transgenic lines expressing $_{pro}$Mp*SERK*:Mp*SERK-miniTurbo-Myc* and Tak-1. This result shows that lower accumulation of MpSERK^{Y418F}-miniTurbo-Myc was not the reason for the poor complementation. Taken together, these results indicate that the conserved tyrosine residue in MpSERK plays a role in growth and development, which is likely to be different from its role in immunity in AtSERK3.

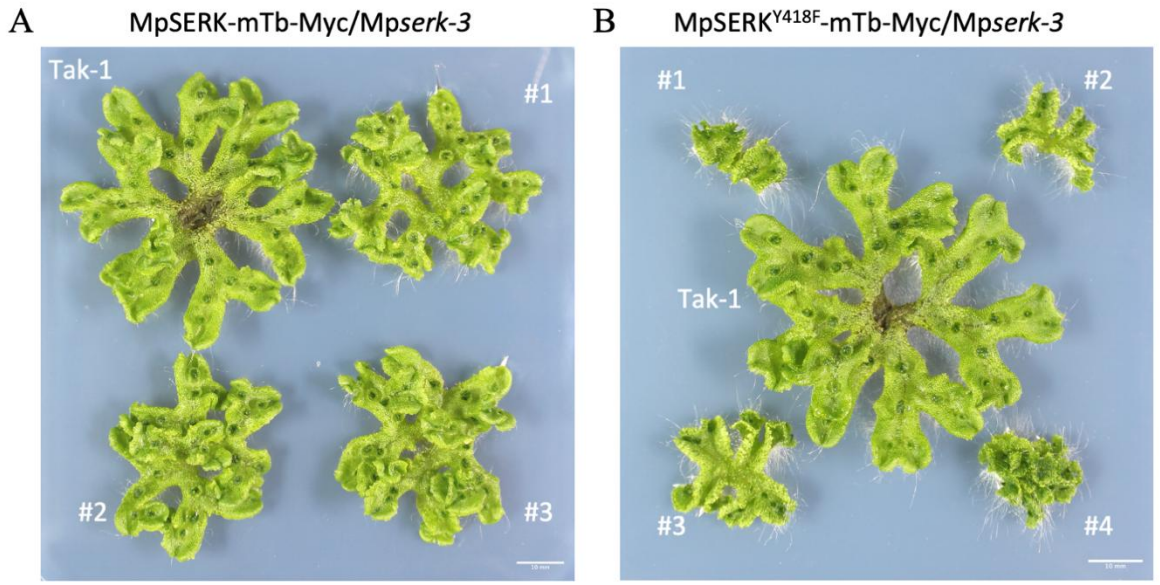

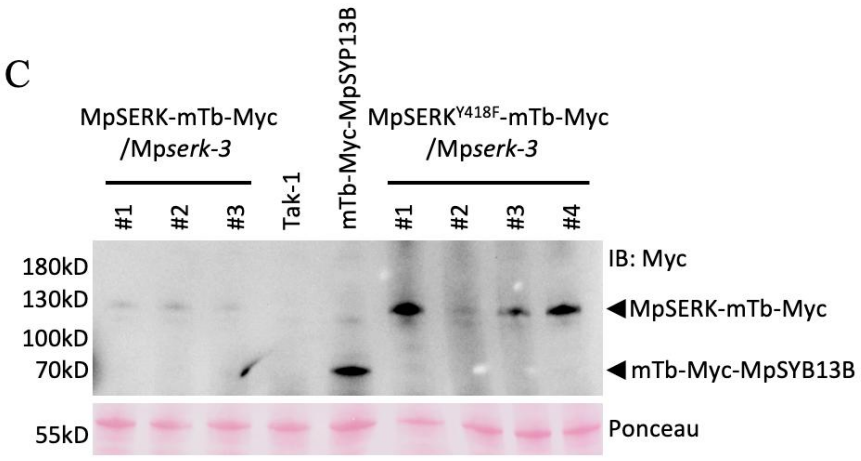

Figure 21. Phenotypes of $_{pro}$Mp*SERK*:Mp*SERK-miniTurbo-Myc*/Mp*serk-3* and $_{pro}$Mp*SERK*:Mp*SERK*^{Y418F}-*miniTurbo-Myc*/Mp*serk-3* transgenic lines

A and B. Transgenic lines $_{pro}$Mp*SERK*:Mp*SERK-miniTurbo-Myc*/Mp*serk-3* **(A)** and $_{pro}$Mp*SERK*:Mp*SERK*^{Y418F}-*miniTurbo-Myc*/Mp*serk-3* **(B)** compared to Tak-1. All plants were 31 days old. Thalli were grown from single gemma under constant white light.

C. MpSERK-miniTurbo-Myc and MpSERK^{Y418F}-miniTurbo-Myc protein expression was confirmed by immunoblotting with an anti-Myc antibody. Target proteins and miniTurbo-Myc-MpSYP13B as the control are indicated by black arrows. A ponceau red-stained blot is shown as a loading control.

3.2.2 LRR-RLKs are found in the interactome profiling of MpSERK

One of the aims of this project was to identify potential PRRs in *M. polymorpha* from subfamily XII LRR-RLKs, which may detect unknown MAMPs. SERKs function as co-receptors for PRRs in angiosperms. Therefore, I performed miniTurbo-based interactome analysis of MpSERK to identify LRR-RLKs that form complexes with MpSERK.

The $_{pro}$Mp*SERK*:Mp*SERK-miniTurbo-Myc* and $_{pro}$Mp*SERK*:Mp*SERK*^{Y418F}*-miniTurbo-Myc*-expressing plants described above were used for interactome analysis. Wild-type Tak-1 and transgenic plants expressing $_{pro}$Mp*SYP13B*:*miniTurbo-Myc*-Mp*SYP13B* were used as controls (Melkonian et al. 2022). Fourteen-day-old thalli of these transgenic and Tak-1 plants were treated with biotin for 24 hours at room temperature. Protein biotinylation in cell extracts was determined by immunoblotting using streptavidin-HRP (Figure 22A). Line No. 2 of $_{pro}$Mp*SERK*:Mp*SERK-miniTurbo-Myc*/Mp*serk-3* and line No. 4 of $_{pro}$Mp*SERK*:Mp*SERK*^{Y418F}-*miniTurbo-Myc*/Mp*serk-3* were chosen for further MS analysis.

The MS analysis identified 235 and 433 potential interactors of MpSERK and MpSERK^{Y418F}, respectively (Figure 22B, 22C, and Table S3). Among the candidate interactors, 16 LRR-RLKs that belong to subfamily I, II, III, V, VIII, IX, X, or XI were identified. Eight of them belong to subfamily I LRR-RLKs. I did not identify potential interactors from subfamily XII LRR-RLKs. This could be because the plants used in this experiment were not subjected to elicitor induction. AtFLS2 and AtEFR are known to form a complex with AtBAK1/AtSERK3 upon flg22 and elf18 treatment, respectively (Chinchilla et al. 2007; Heese et al. 2007; Roux et al. 2011). Thus, it is possible that MpSERK was not recruited by potential PRRs under my experimental conditions. MpRGI and MpTDR from subfamily XI LRR-RLKs were found to specifically interact with MpSERK^{Y418F} (Figure 22B–D). This suggests that the conserved Y418 of MpSERK plays a role in MpTDR- and MpRGI-mediated signalling pathways.

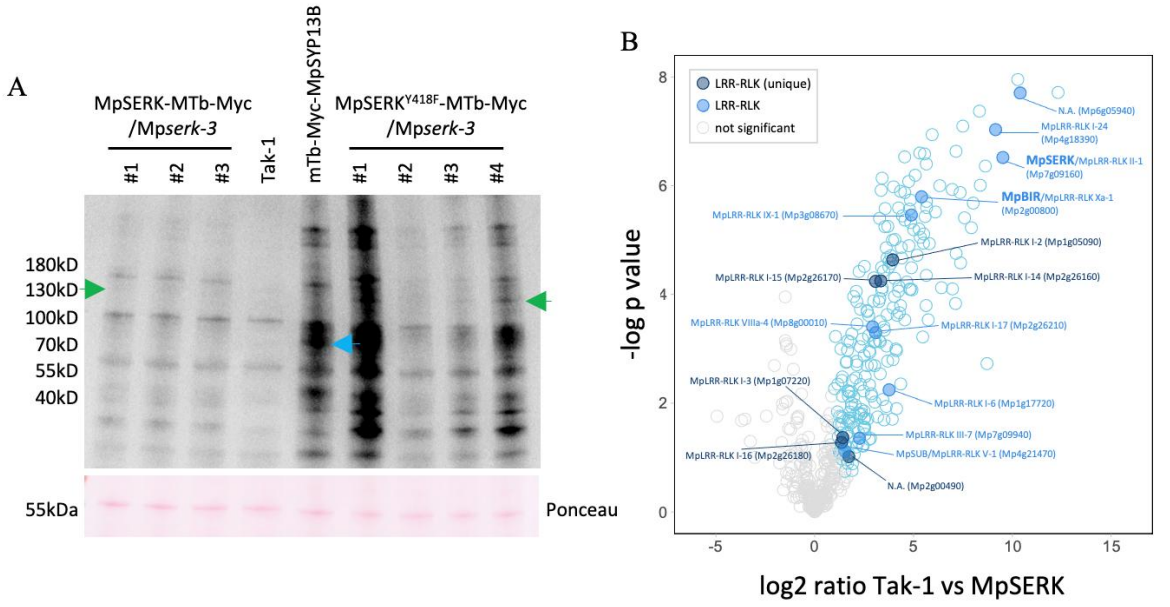
A
MpSERK-MTb-Myc /Mpserk-3
Tak-1
mTb-Myc-MpSYP13B
MpSERK^Y418F-MTb-Myc /Mpserk-3
#1
#2
#3
#1
#2
#3
#4
180kD
130kD
100kD
70kD
55kD
40kD
55kDa
Ponceau
B
LRR-RLK (unique)
LRR-RLK
not significant
-log p value
log2 ratio Tak-1 vs MpSERK

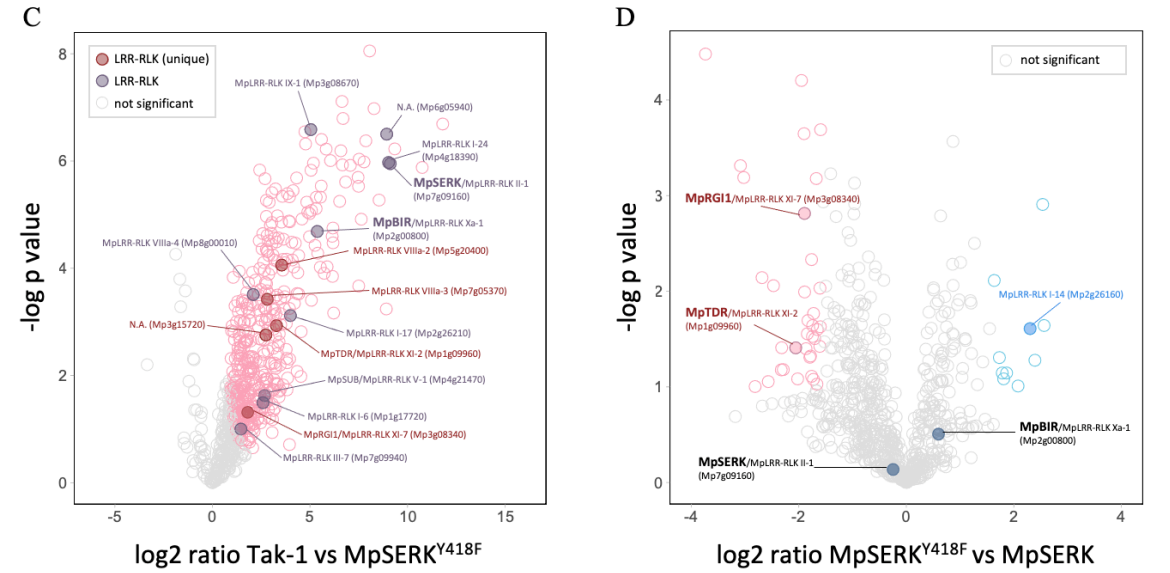
C
LRR-RLK (unique)
LRR-RLK
not significant
-log p value
log2 ratio Tak-1 vs MpSERK^Y418F
D
not significant
-log p value
log2 ratio MpSERK^Y418F vs MpSERK

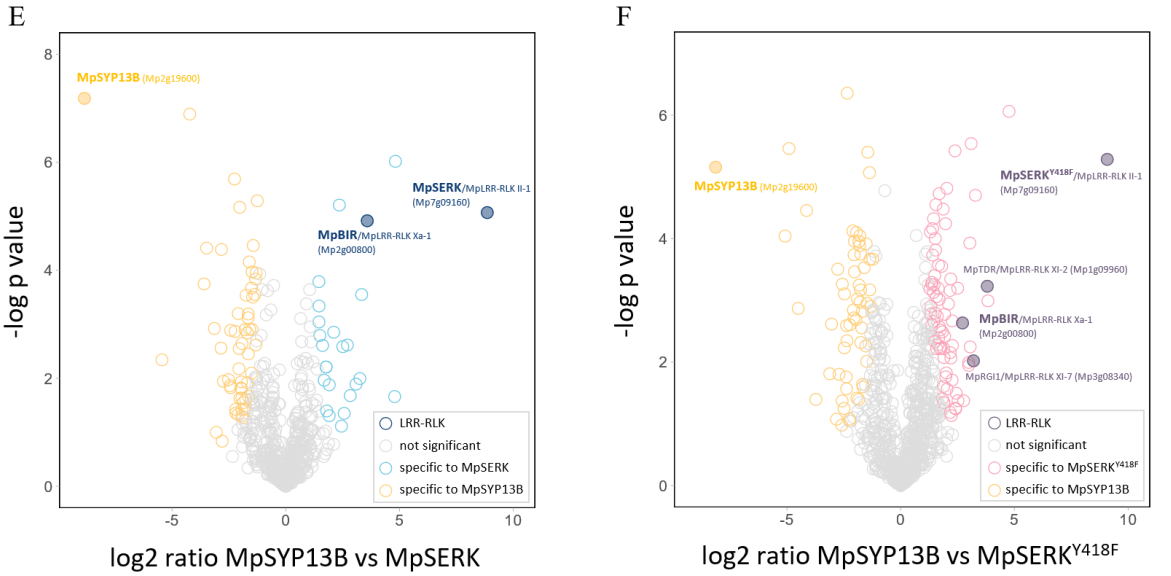
E
MpSYP13B (Mp2g19600)
-log p value
LRR-RLK
not significant
specific to MpSERK
specific to MpSYP13B
log2 ratio MpSYP13B vs MpSERK
F
MpSYP13B (Mp2g19600)
-log p value
LRR-RLK
not significant
specific to MpSERK^Y418F
specific to MpSYP13B
log2 ratio MpSYP13B vs MpSERK^Y418F

Figure 22. Interactome analysis of MpSERK and MpSERK^{Y418F}

A. Protein biotinylation was detected by immunoblotting using streptavidin-HRP. Biotinylated MpSERK-miniTurbo-Myc and MpSERK^{Y418F}-miniTurbo-Myc proteins are indicated by green arrows, biotinylated miniTurbo-Myc-MpSYP13B protein is indicated by a blue arrow. Ponceau red-stained blot is shown as loading control.

B and C. Identification of MpSERK **(B)** and MpSERK^{Y418F} **(C)** potential interacting proteins compared to Tak-1 condition by a miniTurbo-based proximity *in vivo* labelling approach. Four biological replicates were used for the analysis. Potential interacting proteins from subfamilies of LRR-RLKs are labelled with gene IDs and subfamily numbers. Unique and shared LRR-RLKs candidates in each condition are shown in different colours.

D. Identification of specific potential interactors in 'MpSERK vs MpSERK^{Y418F}' condition by miniTurbo-based proximity *in vivo* labelling approach.

E. Proteins significantly enriched using MpSERK as a bait are indicated in blue circles. LRR-RLKs are highlighted as filled dark blue circles.

F. Proteins significantly enriched using MpSERK^{Y418F} as a bait are indicated in pink circles. LRR-RLKs are highlighted as filled dark pink circles.

3.2.3 The MpSERK–MpBIR module regulates immunity

3.2.3.1 MpSERK interacts with MpBIR

Among the candidate interactors of MpSERK, MpBIR from subfamily X LRR-RLKs was identified to interact with MpSERK. Further comparison to the interactome analysis of MpSYP13B suggested that MpBIR could be the single very specific LRR-RLK that interacts with MpSERK in the resting state (Figure 22B, 22E, and 22F). To further validate the interaction between MpBIR and MpSERK, FRET–FLIM analysis was performed. Full lengths versions of MpBIR and MpSERK were tagged with fluorescent protein GFP and mCherry at their C-termini, respectively. The chimeric proteins were transiently expressed in *N. benthamiana* leaves using the *Agrobacterium*-mediated transformation method. MpBIR-GFP localised at the plasma membrane as expected (Figure 23C).

Firstly, the mean fluorescence lifetime (τ) of MpBIR-GFP as the donor molecule was measured. An average fluorescence lifetime of 2.508 ns was determined from 60 measurements conducted on the plasma membrane. Subsequently, FLIM-based FRET analysis was performed by expressing MpBIR-GFP along with MpSERK-mCherry as the acceptor molecule. Co-expression of MpSERK-mCherry significantly decreased the fluorescence lifetime of MpBIR-GFP, reducing this value to 2.272 ns (Figure 23A and 23B). This result indicates that MpBIR interacts with MpSERK *in vivo*.

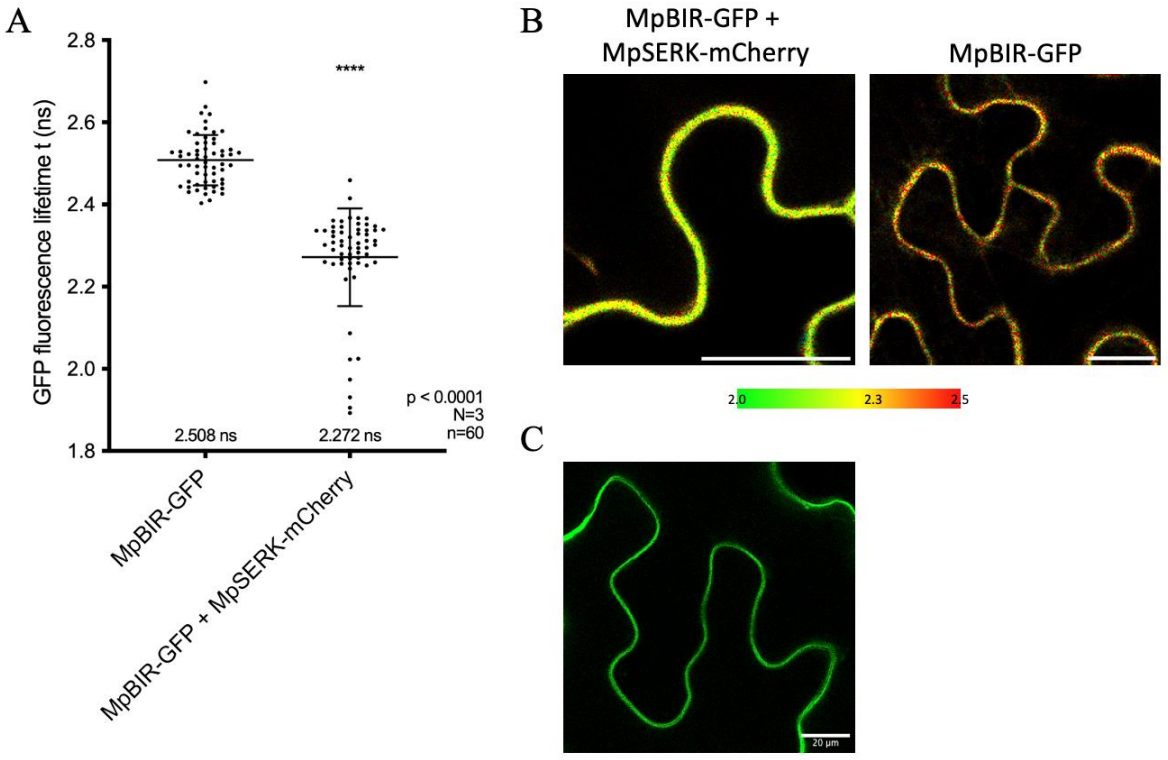

Figure 23. Interaction of MpBIR and MpSERK detected by FRET–FLIM

A. Mean fluorescence lifetime (τ, ns) of MpBIR-GFP when expressed alone or along with MpSERK-mCherry. Significant differences calculated by one-way ANOVA are indicated with asterisks. Error bars, SD; n, number of measurements; N, number of independent experiments. ****, p-value < 0.0001.

B. Lifetime images are represented as pseudo-colour according to the colour code ranging from 2.0 ns (green) to 2.5 ns (red). The respective lifetime values measured for MpBIR-GFP alone or upon co-expression with MpSERK-mCherry are indicated on the colour scales. Scale bar, 25 µm.

C. Subcellular localisation of MpBIR-GFP in an *N. benthamiana* leaf cell.

3.2.3.2 MpBIR functions in MpSERK-dependent growth and development

The *M. polymorpha* genome encodes a single BIR homologue, MpBIR. To analyse the functions of MpBIR and its relationship with MpSERK, MpBIR knock-out mutants were generated using the CRISPR-Cas9 system. The sgRNA was designed to target the beginning of the extracellular LRR domain in MpBIR. Among the obtained three independent lines (Mp*bir-1*, Mp*bir-2*, and Mp*bir-3*), Mp*bir-2* and Mp*bir-3* had an early stop codon leading to the premature translation termination in the LRR domain of MpBIR, whereas Mp*bir-1* only had a three-amino acid (TSL: 95-97) deletion at the LRR domain (Figure 24A). All these Mp*bir* mutants exhibited similar phenotypes, including growth retardation, a reduced formation of gemma cups, defects in formation of serrated rim of gemma cup, and uncurled thalli compared to Tak-1 (Figure 24B to 24D). These results indicate that gene editing, including the TSL

deletion, led to a loss of function of MpBIR. Under constant far-red light irradiation, Mp*bir* mutants initiated gametangiophore formation but failed to fully develop mature gametangiophores (Figure 24E and 24F). Taken together, these results indicate that MpBIR functions in vegetative development and sexual reproduction.

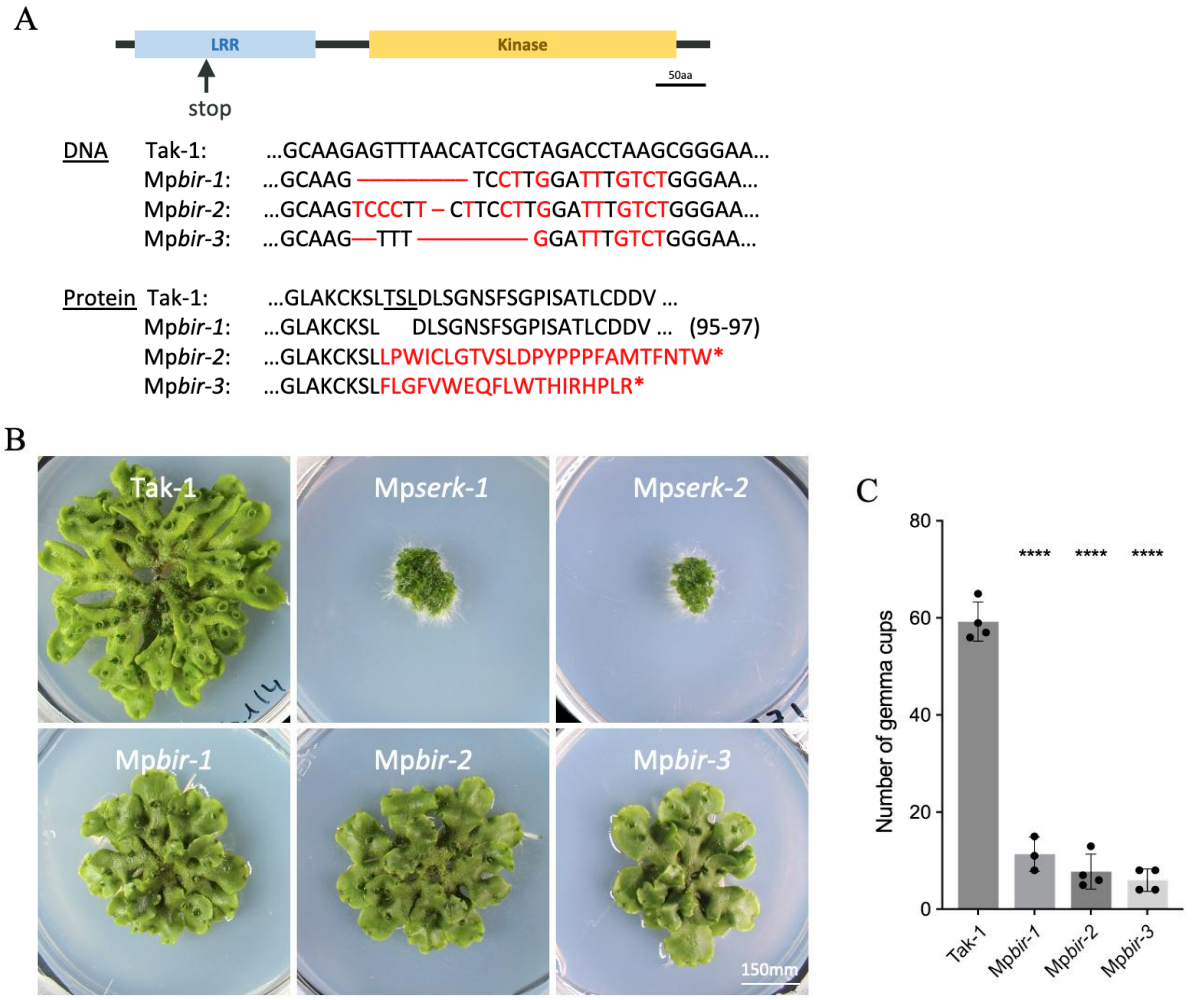

D

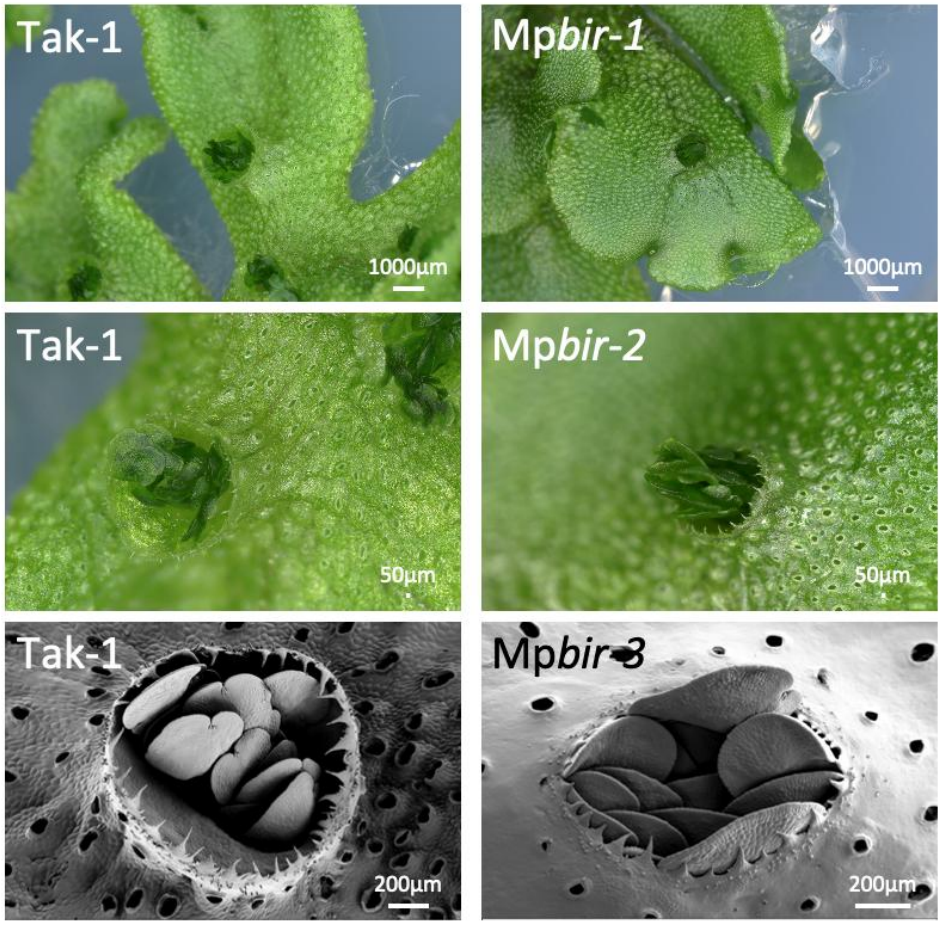
Tak-1
1000µm
Mpbir-1
1000µm
Tak-1
50µm
Mpbir-2
50µm
Tak-1
200µm
Mpbir-3
200µm

E

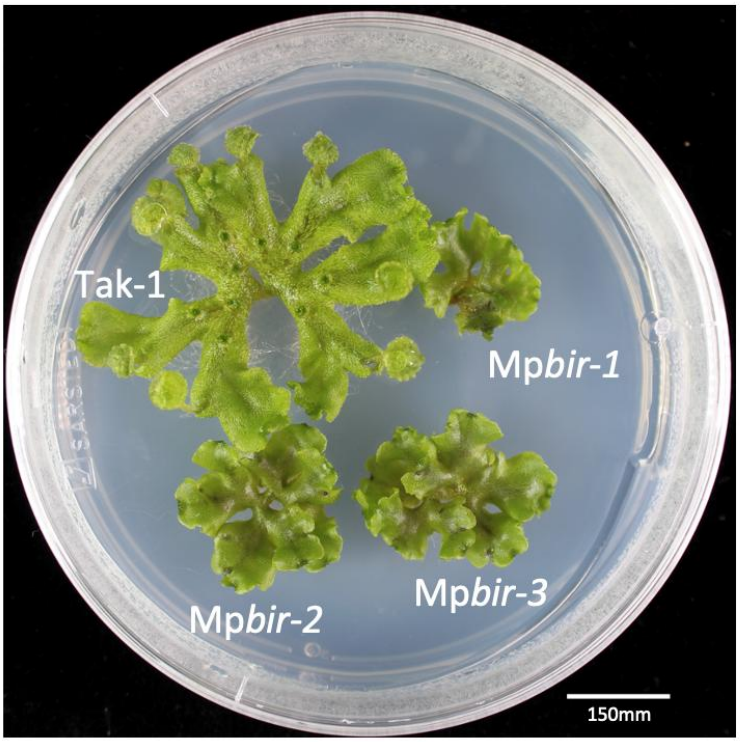
Tak-1
Mpbir-1
Mpbir-3
Mpbir-2
150mm

F

Figure 24. Phenotype and genome-editing sites of Mp*bir* mutants

A. Schematic representation of MpBIR disruption in the Mp*bir-1*, Mp*bir-2*, and Mp*bir-3*. Gene editing resulting in early stop of protein translation near the N-terminus of MpBIR is indicated by the black arrow.

B. Twenty-nine-day-old Mp*bir-1*, Mp*bir-2*, and Mp*bir-3* compared to Mps*erk-1*, Mps*erk-2*, and Tak-1. Thalli were grown from a single gemma (Mp*bir-1*, Mp*bir-2*, Mp*bir-3*, and Tak-1) or a small piece of thallus (Mps*erk-1* and Mps*erk-2*) under constant white light.

C. Statistical analysis of the amount of gemma cups in Mp*bir-1*, Mp*bir-2*, Mp*bir-3*, and Tak-1. All plants were 29 days. Significant differences calculated by one-way ANOVA, are indicated with asterisks. Error bars, SD. ****, p-value < 0.0001.

D. Gemma cups in 4-week-old Mp*bir-2* and Tak-1. Thalli were grown from single gemma under constant white light. Black and white images were taken by SEM.

E. Gametangiophore induction in 4-week-old Mp*bir-1*, Mp*bir-2*, Mp*bir-3*, and Tak-1. Thalli were grown from single gemma under constant far-red and white light.

F. Gametangiophore induction in 48-day-old Mp*bir-2*. Thalli were grown from single gemma under constant far-red and white light.

MpSERK interacts with MpBIR *in vivo* (Figure 23A and 23B). To further investigate the relationship between MpBIR and MpSERK, I generated Mp*serk/bir* double knock-out (DKO) mutants using the CRSIPR-Cas9 system. Three independent DKO mutant lines (Mp*serk/bir-1* to Mp*serk/bir-3*) were obtained. Mp*serk/bir-3* was established in the Mp*serk-1* mutant background, while Mp*serk/bir-1* and Mp*serk/bir-2* were established in the Mp*bir-3* and Mp*bir-1* mutant backgrounds, respectively. All three independent Mp*serk/bir* DKO mutant lines displayed similar phenotypes, which phenocopied Mp*serk* mutants (Figure 25A and 18E). These results suggest that Mp*SERK* is epistatic to Mp*BIR*.

Transgenic plants overexpressing MpBIR tagged with miniTurbo and Myc at its C-terminus, driven by the ubiquitous Mp*EF1α* promoter ($_{pro}$Mp*EF1α*:Mp*BIR-miniTurbo-Myc*), were generated in the Tak-1 background. Plants accumulating varying levels of MpBIR-miniTurbo-Myc were obtained (Figure 25B). Notably, transgenic lines with high accumulation of MpBIR (Line No. 6 and No. 9) phenocopied Mp*serk* mutants, showing a bushy structure of thalli and no gemma cups (Figure 25B and 25C). Taken together, these results suggest that MpBIR represses MpSERK function or activity through physical interaction.

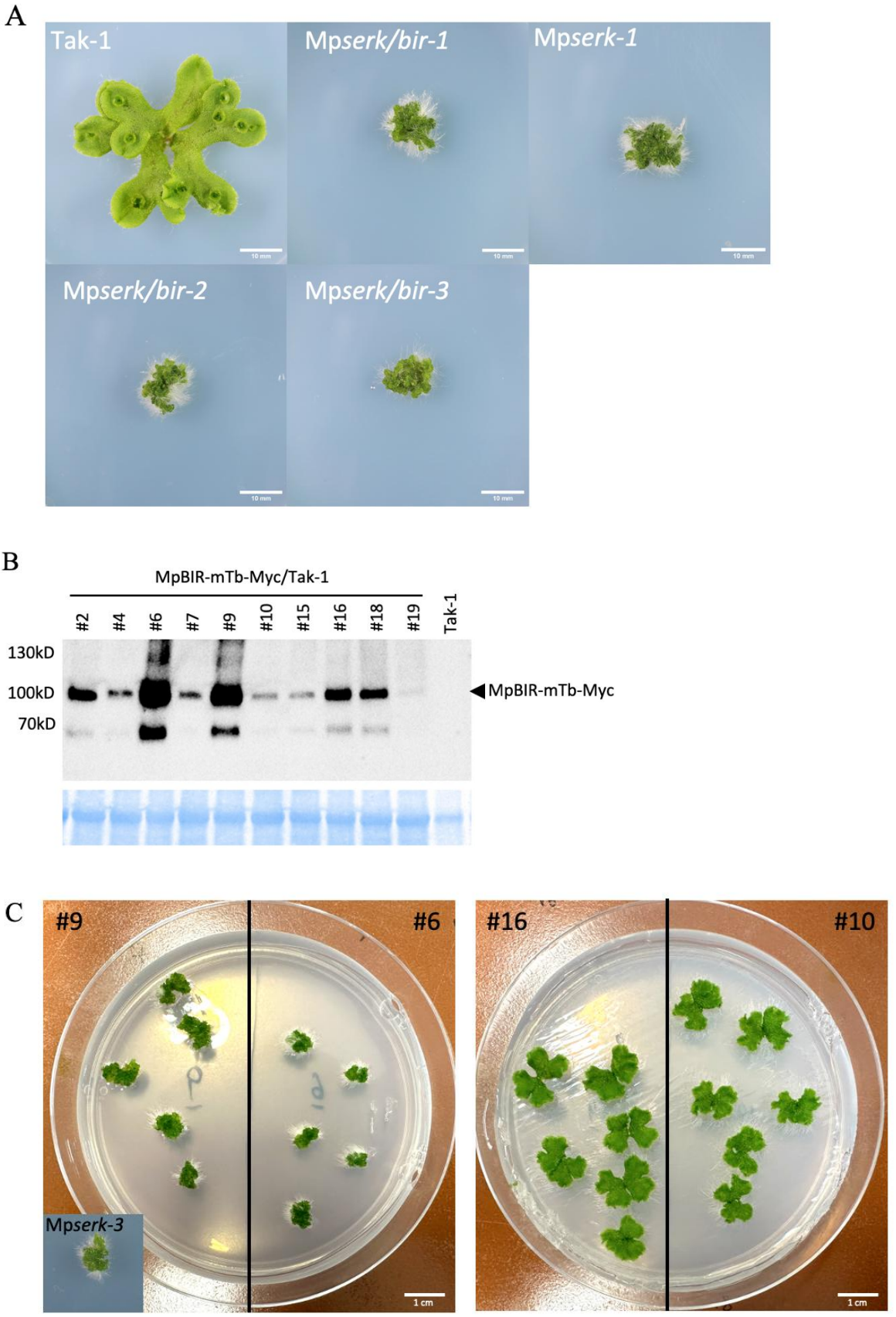

Figure 25. Mp*serk/bir* DKO mutant and overexpression of MpBIR

A. Three-week-old Mp*serk/bir* DKO mutants compared to Mp*serk-3* and Tak-1. Thalli were grown from a single gemma (Tak-1) or a small piece of thallus (Mp*serk/bir* DKO mutants and Mp*serk-3*) under constant white light.

B. Immunoblot analysis of MpBIR expression in $_{pro}$Mp*EF1α*:Mp*BIR-miniTurbo-Myc* transgenic plants. Wild-type Tak-1 served as controls. Black arrow indicates the expression of MpBIR-miniTurbo-Myc. Anti-Myc antibody was used to detect the fusion proteins. A CBB-stained blot is shown as a loading control.
C. Two-week-old transgenic lines of $_{pro}$Mp*EF1α*:Mp*BIR-miniTurbo-Myc* compared to Mp*serk-3*. Thalli were grown from a single gemma (MpBIR overexpression line 10 and 16) or a small piece of thallus (MpBIR overexpression line 6 and 9, and Mp*serk-3*) under constant white light.

3.2.3.3 MpBIR negatively regulates the defence response

AtBIR2 and AtBIR3 have been shown to negatively regulate AtSERK3 in the absence of stimuli, restricting unwanted interactions between AtSERK3 and PRRs. Disruptions in the expression level of AtBIRs impact both plant growth and defence responses (Halter et al. 2014; Imkampe et al. 2017; Ma et al. 2017; Guzmán-Benito et al. 2024). Considering the phenotypes of Mp*bir,* Mps*erk/bir* DKO mutants, and the overexpression lines of MpBIR, I hypothesised that MpBIR could negatively regulate MpSERK, and thus, that loss of MpBIR function may constitutively activate the MpSERK-mediated signalling pathway at certain levels, causing severe developmental defects and autoimmunity in *M. polymorpha*.

In order to further investigate the functional relationship between MpBIR and MpSERK, I conducted transcriptome analysis of Mp*serk-3*, Mp*bir-1,* Mp*bir-3*, and Tak-1. The PCA plot depicted distinct gene expression patterns in Mp*serk-3*, Mp*bir* mutants, and Tak-1, indicating significant transcriptional reprogramming in each genotype (Figure 26A and Table S4). K-means clustering were conducted on DEGs (Figure 26B), revealing that Mp*bir-1* and Mp*bir-3* displayed overall similar expression patterns. This indicates that the TSL deletion in the LRR domain of MpBIR and that the truncated MpBIR proteins perform similar functions in *M. polymorpha*, further supporting the idea that the TSL deletion in the LRR domain of MpBIR leads to a loss of function.

GO analysis of the genes from each cluster showed significant enrichment of growth and development-related GO terms in the clusters 3, 4, and 10 (Figure 26D and Table S4), supporting the observed roles of MpSERK in growth and development (Figure 18). In clusters 3 and 10, antagonistic gene expression patterns were observed between Mp*bir* mutants and the Mp*serk-3* mutant compared to Tak-1 (Figure 26B). In cluster 3, genes showed lower expression in Mp*serk-3* and higher expression in Mp*bir-1* and Mp*bir-3* mutants compared to Tak-1. This fits with my hypothesis that MpBIR could repress MpSERK functions or activity.

Defence-related GO terms were significantly enriched in the clusters 1, 5, and 9. GO terms such as ‘Defence response to bacterium’, ‘Defence response to fungi’, and ‘Response to stress’ were found in these clusters (Figure 26C and Table S4). In cluster 1, defence-related

genes, such as MpPR5 homologue (Mp2g24450), and MpPR4 (Mp2g21910), and NLR proteins (Mp4g08790 and Mp7g04670) were significantly up-regulated (Log2FC ≥ 1) in Mp*bir-1* and Mp*bir-3* but not in the Mps*erk-3* mutant compared to Tak-1. The MpPR5 homologue (Mp2g13870) was found to be significantly up-regulated (Log2FC ≥ 1) in both Mp*bir* mutants, but down-regulated (Log2FC ≤ -1) in the Mps*erk-3* mutant compared to Tak-1. Cluster 1 also displayed antagonistic gene expression patterns between Mp*bir* mutants and Mps*erk-3* mutant compared to Tak-1 (Figure 26B). Altogether, these findings suggest that MpBIR plays a role in restricting undesired MpSERK activation in the absence of elicitors or stimuli. MpBIR negatively regulates defence-related gene expression, possibly through repression of MpSERK.

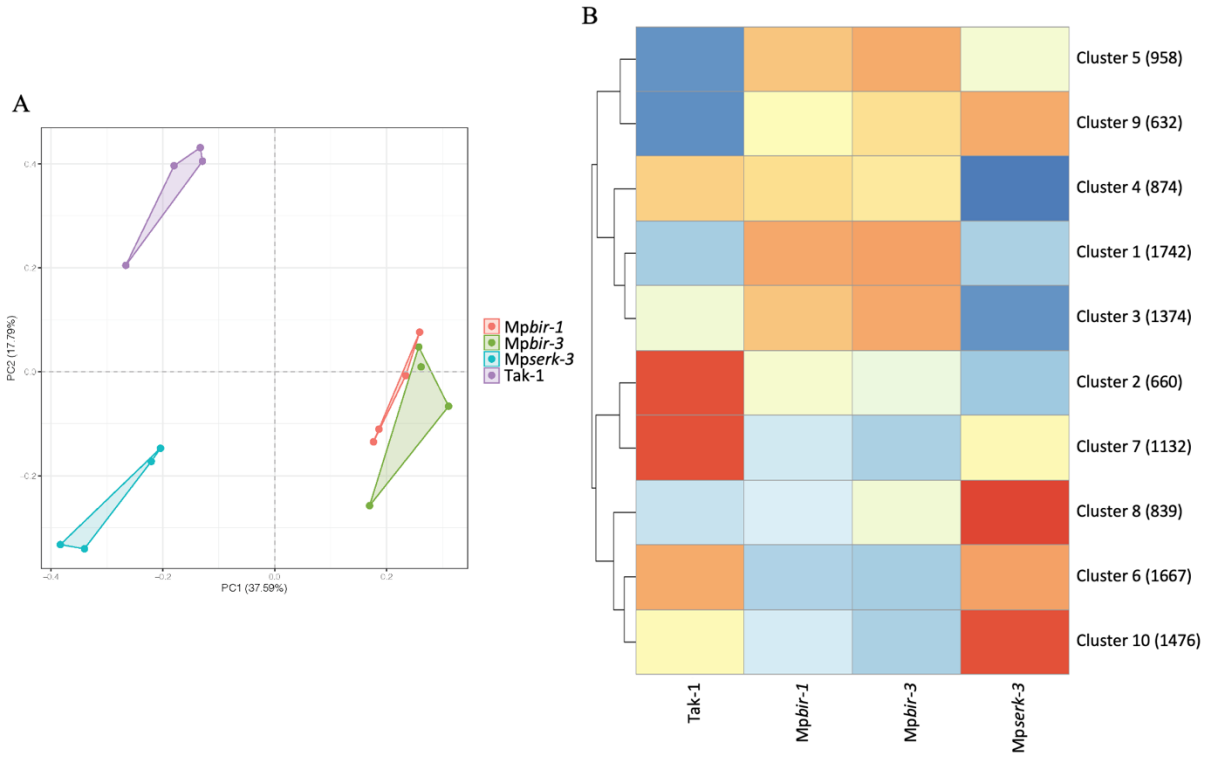

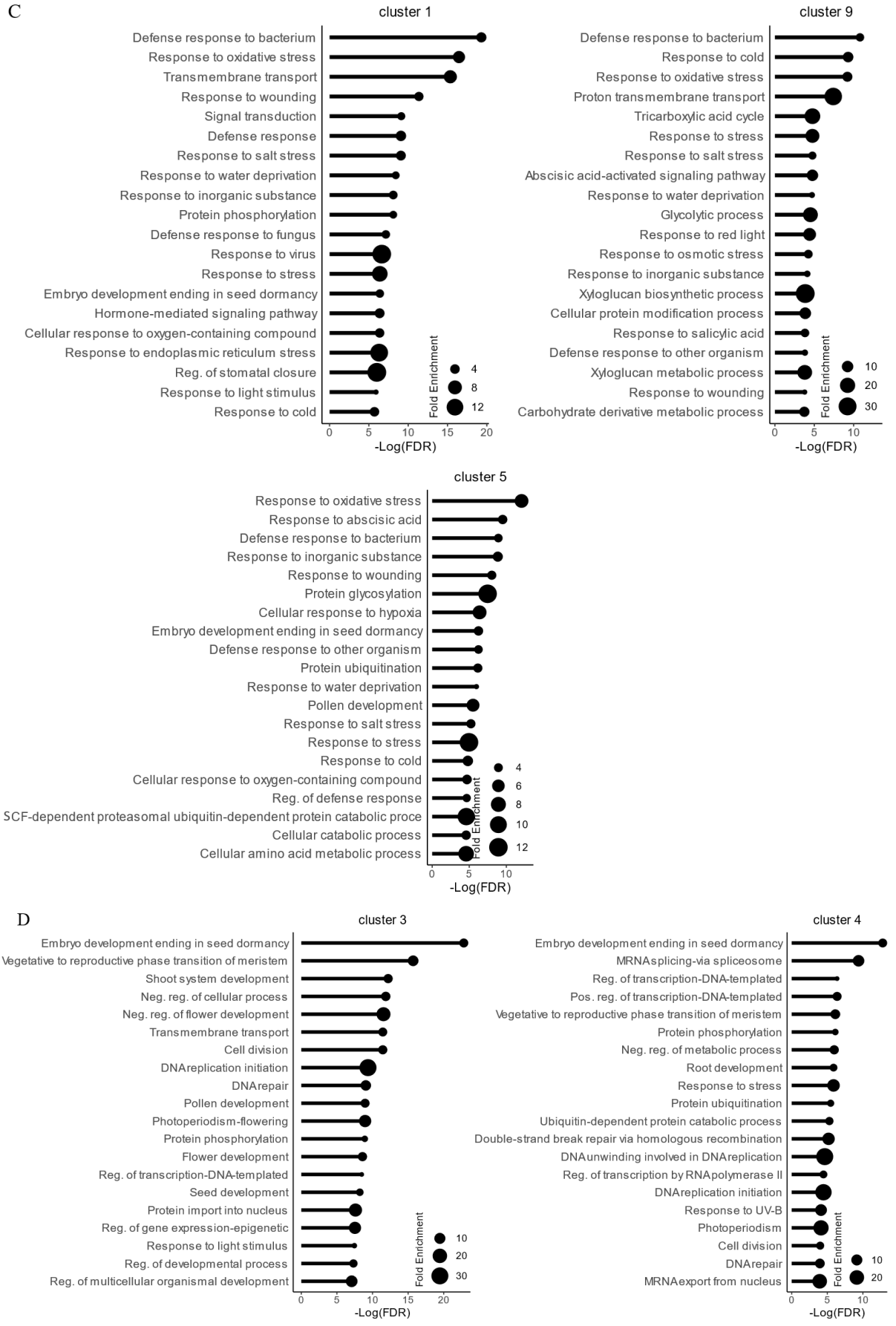
C
cluster 1
Defense response to bacterium
Response to oxidative stress
Transmembrane transport
Response to wounding
Signal transduction
Defense response
Response to salt stress
Response to water deprivation
Response to inorganic substance
Protein phosphorylation
Defense response to fungus
Response to virus
Response to stress
Embryo development ending in seed dormancy
Hormone-mediated signaling pathway
Cellular response to oxygen-containing compound
Response to endoplasmic reticulum stress
Reg. of stomatal closure
Response to light stimulus
Response to cold
Fold Enrichment
4
8
12
0 5 10 15 20
-Log(FDR)
cluster 9
Defense response to bacterium
Response to cold
Response to oxidative stress
Proton transmembrane transport
Tricarboxylic acid cycle
Response to stress
Response to salt stress
Abscisic acid-activated signaling pathway
Response to water deprivation
Glycolytic process
Response to red light
Response to osmotic stress
Response to inorganic substance
Xyloglucan biosynthetic process
Cellular protein modification process
Response to salicylic acid
Defense response to other organism
Xyloglucan metabolic process
Response to wounding
Carbohydrate derivative metabolic process
Fold Enrichment
10
20
30
0 5 10
-Log(FDR)
cluster 5
Response to oxidative stress
Response to abscisic acid
Defense response to bacterium
Response to inorganic substance
Response to wounding
Protein glycosylation
Cellular response to hypoxia
Embryo development ending in seed dormancy
Defense response to other organism
Protein ubiquitination
Response to water deprivation
Pollen development
Response to salt stress
Response to stress
Response to cold
Cellular response to oxygen-containing compound
Reg. of defense response
SCF-dependent proteasomal ubiquitin-dependent protein catabolic proce
Cellular catabolic process
Cellular amino acid metabolic process
Fold Enrichment
4
6
8
10
12
0 5 10
-Log(FDR)
D
cluster 3
Embryo development ending in seed dormancy
Vegetative to reproductive phase transition of meristem
Shoot system development
Neg. reg. of cellular process
Neg. reg. of flower development
Transmembrane transport
Cell division
DNAreplication initiation
DNArepair
Pollen development
Photoperiodism-flowering
Protein phosphorylation
Flower development
Reg. of transcription-DNA-templated
Seed development
Protein import into nucleus
Reg. of gene expression-epigenetic
Response to light stimulus
Reg. of developmental process
Reg. of multicellular organismal development
Fold Enrichment
10
20
30
0 5 10 15 20
-Log(FDR)
cluster 4
Embryo development ending in seed dormancy
MRNAsplicing-via spliceosome
Reg. of transcription-DNA-templated
Pos. reg. of transcription-DNA-templated
Vegetative to reproductive phase transition of meristem
Protein phosphorylation
Neg. reg. of metabolic process
Root development
Response to stress
Protein ubiquitination
Ubiquitin-dependent protein catabolic process
Double-strand break repair via homologous recombination
DNAunwinding involved in DNAreplication
Reg. of transcription by RNApolymerase II
DNAreplication initiation
Response to UV-B
Photoperiodism
Cell division
DNArepair
MRNAexport from nucleus
Fold Enrichment
10
20
0 5 10
-Log(FDR)

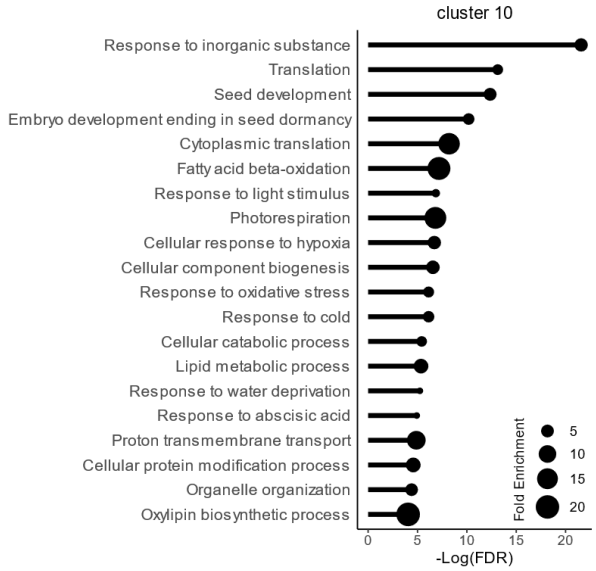

Figure 26. Transcriptome analysis in Mp*bir* and Mp*serk* mutants and phenotypes of Mp*serk/bir* mutants and MpBIR overexpression lines

A. PCA plot of DEGs observed in Mp*bir-1*, Mp*bir-2*, Mp*serk-3*, and Tak-1. Four technical replicates were performed for each condition.

B. Heatmap image showing genes grouped by the K-means clustering algorithm. Genotypes are indicated under each column. Gene expression is shown in rows. Quantitative changes in gene expression are represented in colour: red indicates high expression whereas blue indicates low expression. Gene numbers of each cluster are shown in brackets.

C and D. GO enrichment analysis of genes from clusters 1, 5, and 9 **(C)**, clusters 3, 4, and 10 **(D)** shown in Figure 26B. GO analysis was performed using ShinyGO in the pathway database of GO biological process. Size of closed circles indicates the fold enrichment in each condition. FDR < 0.05.

3.2.3.4 Bacterial pathogens grow poorly in Mp*bir* mutants

To further ascertain the role of MpBIR in negatively regulating immunity, I monitored the growth of *Pto* DC3000 in the Mp*bir* mutants compared to Tak-1. Fourteen-day-old mature thalli were inoculated with *Pto* DC3000-lux, and the bacteria levels were measured at 0 and 2 dpi. Surprisingly, I found that *Pto* DC3000-lux barely grew in Mp*bir* mutants (Figure 27A). Expression of MpBIR rescued the hyper-resistant phenotype to the wild-type Tak-1 level (Figure 27B). This result further supports the results from the transcriptome analysis, indicating that MpBIR negatively regulates immunity.

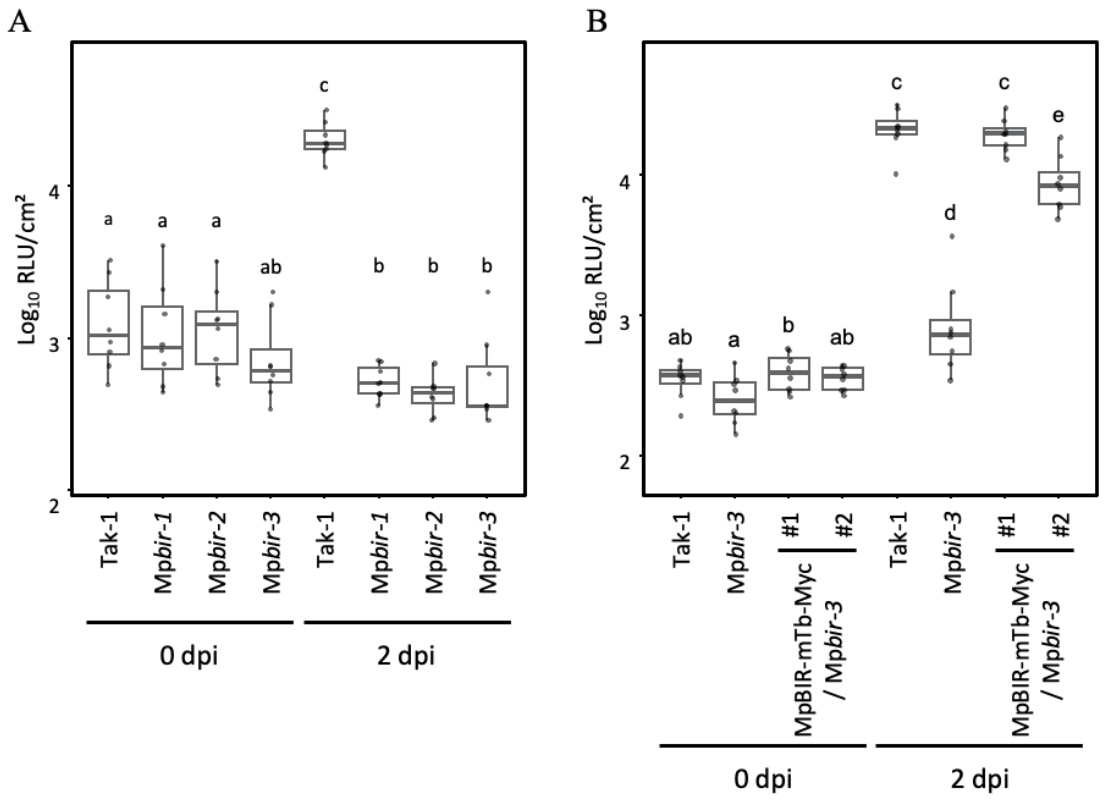

Figure 27. Growth of *Pto* DC3000-lux in Mp*bir* mutants and complementation lines

A and B. Quantification of bacterial growth in the central region of 14-day-old thalli from Mp*bir* mutants **(A)** and $_{pro}$Mp*EF1α*:Mp*BIR-miniTurbo-Myc* complementation lines **(B)**. Plants were inoculated with the bioluminescent *Pto* DC3000-lux. Boxes show upper and lower quartiles of the value, and lines in boxes represent the medians (n = 8). Statistical analysis was performed using student's t test with p-values adjusted by the BH method. Statistically significant differences are indicated by different letters. p-value < 0.05.

4 Discussion

4.1 Functional characterisation of MpFER

4.1.1 MpFER functions in development

The MLR family is believed to have arisen during the evolutionary transition of plants from aquatic to terrestrial environments, suggesting that these proteins have important functions in adaptation to terrestrial environments (Zhu et al. 2021). In *A. thaliana*, the MLR family comprises 17 members, with FER being the most extensively studied (Lindner et al. 2012). AtFER is expressed in most plant organs and plays diverse roles (Malivert and Hamant 2023). Homologues of AtFER have been identified in bryophytes and lycophytes but are absent in charophycean algae (Mecchia et al. 2022). The genomes of *M. polymorpha* and *Anthoceros* species encode a single MLR member, FER, suggesting that FER represents an ancestral form and is orthologous to all other MLRs in land plants (Mecchia et al. 2022; Zhu et al. 2021). Although the multifunctionality of FER has been extensively studied in flowering plants, its role in non-flowering plants remains largely unexplored.

In *M. polymorpha*, FER was reported to play a crucial role in rhizoid formation, regulation of cell size and organ growth, male gametogenesis, and fertility (Honkanen et al. 2016). The Mp*fer-1* mutant, initially identified through a comprehensive T-DNA insertional mutagenesis screen, exhibited short, irregularly shaped rhizoids with brown tips, indicative of rhizoid rupture (Honkanen et al. 2016). The MpFER KO mutant in the Tak-1 background, Mp*fer-9*, generated in this study, alongside other mutants (Mp*fer-2* to Mp*fer-8*) generated by Mecchia et al., showed severely affected rhizoid formation and thallus growth (Figure 4B). These findings underscore the significant role of MpFER in development, particularly in rhizoid formation and growth. Additionally, Mp*FER* expression patterns observed in rhizoids and rhizoid-initiated areas along midribs (Figure 5A, 5C to 5F), further support the function of MpFER in rhizoid formation. The developmental defects observed in the Mp*fer-9* mutant may also resulted from its inability to uptake sufficient nutrients and water from the medium due to the severe disruption of rhizoid formation.

Dead cells were observed on thalli in Mp*fer* KO mutants, likely caused by an apparent reduced stiffness of cell walls (Mecchia et al. 2022). MpFER functions in CWI maintenance mechanisms and regulates CWI in growing rhizoids through MpMRI (Westermann et al. 2019). In this study, I found that GO terms related to cell wall organisation or biogenesis were enriched among DEGs induced by MpRALF1 (Figure 12E and 12F). This suggests a potential role for MpRALF1 in MpFER-mediated CWI maintenance. It is possible that MpRALF1 regulates

CWI through MpFER. Consequently, the loss-of-rhizoids phenotype in Mp*fer-9* (Figure 4B) could be due to the loss of perception of MpRALF1, causing cell wall perturbations that lead to the severe disruption of rhizoids and thallus growth. Generating and characterising MpRALFs KO mutants could further elucidate the role of MpRALFs in CWI maintenance.

The Mp*fer-9* mutant produced gemmae and gemma cups (Figure 4B), indicating that Mp*FER* is dispensable for asexual reproduction. However, in the context of sexual reproduction, Mp*FER* plays a role in the development of antheridiophores (Mecchia et al. 2022). In amiR-Mp*FER* lines, where MpFER activity is reduced by microRNA constructs targeting Mp*FER*, spermatocytes exhibit reduced fertility (Mecchia et al. 2022). Mp*FER* is expressed in the meristem (Figure 5B), assimilatory filaments (Figure 5D), and sexual organs (Mecchia et al. 2022), consistent with the broad expression pattern of At*FER* during both vegetative and reproductive stages in *A. thaliana* (Lindner et al. 2012). These findings suggest that FER plays a crucial role in cellular growth during vegetative development.

Several residues essential for the catalytic activity of kinases and phosphorylation sites are conserved in the kinase domain of MpFER (Haruta et al. 2014b; Schoenaers et al. 2018; Mecchia et al. 2022). This suggests that MpFER possesses an active intracellular kinase domain. I was able to obtain transgenic plants expressing a kinase-dead version of MpFER but not wild-type MpFER under the ubiquitous Mp*EF1α* promoter. These results indicate that MpFER is indeed an active kinase and that its kinase activity contributes to MpFER functions. My finding is consistent with a study showing that overexpression of MpFER in wild-type Tak-1 severely affected air chamber and air pore formations and reduced the number of rhizoids (Mecchia et al. 2022). However, how the kinase activity of MpFER contributes to these developmental phenotypes remains unclear. A comparative interactome analysis between MpFER-KD and MpFER, using transgenic plants expressing $_{pro}$Mp*FER*:Mp*FER-KD-miniTurbo-Myc* and $_{pro}$Mp*FER*:Mp*FER-miniTurbo-Myc* established in this study would help to unravel the role of the MpFER kinase in growth and development.

4.1.2 The conservation and specificity of the RALF–FER module

AtFER is required for the majority of AtRALF peptide-triggered responses including growth inhibition and defence responses (Abarca, Franck, and Zipfel 2021). AtFER has been shown to directly interact with AtRALF1, AtRALF22, and AtRALF23 (Haruta et al. 2014b; Stegmann et al. 2017; Zhao et al. 2018). In this study, I found that RALF and FER function as a module also in the liverwort *M. polymorpha*. There are three RALF propeptides encoded in the genome of *M. polymorpha*. MpRALF1 and MpRALF3 are predicted to be mature RALFs and the mature

forms of MpRALF1 and MpRALF3 induced ROS bursts in an MpFER-dependent manner (Figure 10A). This may suggest a redundant role of MpRALF1 and MpRALF3 in defence priming, although MpRALF3-induced ROS bursts were lower than that induced by MpRALF1. It is also possible that MpRALF1 and MpRALF3 function in different tissues or cell types. The predicted protein structure of the extracellular domain of MpFER is highly similar to that of AtFER (Mecchia et al. 2022). Three-dimensional structure modelling suggests that MpFER, MpRALF1, and MpLRE1 can form a complex (Mecchia et al. 2022). Taken together, it is very likely that MpFER functions as a receptor for MpRALFs in *M. polymorpha*.

AtRALF34 functions as a negative regulator of immunity, suppressing MAMP-induced ROS bursts without triggering ROS itself (Stegmann et al. 2017; Abarca, Franck, and Zipfel 2021). Although MpRALFs are phylogenetically close to AtRALF34 (Figure 7D), they exhibited opposite functions, i.e., by inducing ROS bursts in *M. polymorpha*, compared to the role of AtRALF34 in *A. thaliana*. Notably, I found that AtRALF34 can induce a ROS burst in *M. polymorpha* (Figure 10A). These findings imply that the ability of RALF to suppress MAMP-induced ROS bursts was an evolutionary innovation in angiosperms or tracheophytes. The molecular mechanisms by which AtFER contributes to both ROS production and suppression in *A. thaliana* are yet to be understood. RALF peptides can suppress root and seedling growth in *A. thaliana*. In this study, I found that MpRALF1 can be sensed by *A. thaliana*, resulting in inhibited root growth (Figure 10B). Although plants have expanded their RALF and FER homologues, these findings suggest that the specificity of the RALF–FER pair remains evolutionarily conserved.

The fungal pathogen *F. oxysporum* secretes RALF-like (F-RALF) peptides to mimic plant endogenous RALF (Masachis et al. 2016; Thynne et al. 2017). F-RALF hijacks the FER-mediated pathways by inducing extracellular alkalinisation. The alkalinisation of host plant tissue is believed to contribute to fungal pathogenesis (Prusky 2001). In this study, I found that F-RALF can induce a ROS burst in *M. polymorpha*, indicating that *M. polymorpha* detects RALF peptides secreted by fungal pathogens (Figure 10A). *Fusarium oxysporum* f. sp. *Lycopersici* may employ this conserved strategy for infecting *M. polymorpha*. While the ROS production induced by 1 µM F-RALF was significantly lower than that of 1 µM MpRALF1 (Figure 10A), previous studies used 10 µM F-RALF for observing ROS production and alkalinisation in *N. benthamiana* and tomato leaves (Thynne et al. 2017). Additionally, I observed that F-RALF at a concentration of 10 µM suppressed root growth in *A. thaliana*, but 1 µM did not have this effect (Figure 10B and 10C). Loss of F-RALF in *F. oxysporum* leads to increased activation of plant defence responses, indicating that F-RALF has a function in

suppressing host immunity during fungal infection (Masachis et al. 2016). Thus, in angiosperms, it is possible that fungal pathogens secrete F-RALF to suppress chitin-induced immune responses, similar to the action of AtRALF23 (Stegmann et al. 2017). *Fusarium oxysporum* isolates infect the surface of *M. polymorpha* thalli, navigate through air pores, and grow inside the air chambers (Redkar et al. 2022). It is likely that *F. oxysporum* secretes F-RALF peptides to target MpFER expressed in assimilatory filaments, creating a favourable environment in air chambers for colonisation.

4.1.3 The regulation of immunity by MpRALF1

In *A. thaliana*, RALF–FER modules regulate complex formation between PRRs and the co-receptor AtSERK3, thereby modulating immune signalling (Stegmann et al. 2017). Many AtRALFs act as negative regulators by inhibiting the receptor complex formation. Meanwhile, AtFER functions as a scaffold protein for this complex formation, thereby positively regulating immune signalling (Du et al. 2016; Abarca, Franck, and Zipfel 2021; Stegmann et al. 2017). In the moss *P. patens*, knocking out PpRALF2 and PpRALF3 led to increased resistance to bacterial and fungal pathogens, suggesting negative roles of PpRALF2 and PpRALF3 in regulating the immune response (Mamaeva et al. 2023).

Based on the results of this study, I proposed that MpRALF1 positively regulates defence responses in *M. polymorpha*. Transcriptome analysis revealed that the DEGs up-regulated by MpRALF1 treatment partially overlap with those induced by chitin (Figures 11B and 11C), with defence-related GO terms enriched in the overlapping DEGs (Figures 12C and 12D). This emphasises the positive role of MpRALF1 in immunity. Reported MAMP-responsive or defence-related genes were up-regulated by MpRALF1 treatment (Figure 13) (Carella et al. 2019; Gimenez-Ibanez et al. 2019). The number of down-regulated DEGs upon both MpRALF1 and chitin treatment was significantly lower than the number of up-regulated DEGs (Figure 11C and Table S1), with no significant GO terms identified in the down-regulated DEGs. MpUGT11 (Mp2g23900) was identified as a down-regulated DEG after 3 hours of MpRALF1 treatment, but it was up-regulated after 1 hour of treatment (Table S1). MpUGT11 is homologous to the glycosyltransferase UGT73C7 in *A. thaliana*. AtUGT73C7 positively regulates plant immunity by redirecting the phenylpropanoid pathway (Huang et al. 2021). *Marchantia polymorpha* encodes the core enzymes of the phenylpropanoid pathway (Bowman et al. 2017). The GO term ‘Phenylpropanoid metabolic process’ was significantly enriched in DEGs upon MpRALF1 treatment for 1 hour (Figure 12E). MpUGT-dependent

phenylpropanoid biosynthesis may contribute to MpRALF1-induced defence priming against bacterial pathogens.

In *A. thaliana*, RALFs are also known to positively regulate immunity. He et al. reported that AtRALF22 induces immune responses and primes resistance against the necrotrophic fungal pathogen *S. sclerotiorum* (He et al. 2023). This finding was unexpected because AtRALF22 is a close orthologue of AtRALF23 (Figure 7D), which has been reported to play a negative role in plant immunity (Stegmann et al. 2017; Abarca, Franck, and Zipfel 2021). As a positive regulator of immunity, MpRALFs possibly amplify MAMP-induced immune responses in *M. polymorpha*. It would be interesting to test if MpRALFs can amplify chitin-induced ROS bursts. Whether the enhanced resistance against *Pto* DC3000 and the up-regulation of DEGs induced by MpRALF1 are dependent on MpFER remains unclear. Due to the severe developmental defects observed in the Mp*fer-9* mutant, conducting transcriptome analysis following MpRALF1 treatment in this mutant is challenging, as it is difficult to determine whether the DEGs are a result of developmental defects or MpRALF1 stimuli. Combined with ROS assays in this study and the structural modelling of MpRALF–MpFER shown by Mecchia et al., it is highly likely that MpRALF1 regulates immune responses through MpFER. These findings need to be further elaborated on in future studies.

4.1.4 The potential crosstalk between chitin and MpRALF1 induced pathways

The interactome analysis in this study identified MpLYK1 and MpLYR as potential interactors of MpFER (Figure 15B). MpLYK1 and MpLYR are responsible for sensing chitin and peptidoglycan fragments, triggering a series of characteristic immune responses (Yotsui et al. 2023). FRET–FLIM analysis indicated that MpFER interacts with MpLYK1 and MpLYR under non-stimulated conditions in *N. benthamiana* (Figure 15C). It is possible that the complex formations can be further induced upon elicitor treatments. Recently, an interaction between FER and LysM kinases in *Medicago truncatula* has been reported (Liu et al. 2023). MtFER was shown to be phosphorylated by MtLYK3 and participate in rhizobial symbiosis (Liu et al. 2023). Additionally, AtBSR840/LIK1, an LRR-RLK containing a single malectin domain, was shown to interact with AtCERK1 in regulating immunity (Le et al. 2014; Yang et al. 2021). These findings, along with my results, suggest that crosstalk between malectin-like RLK and LysM RLK is widely conserved in land plants.

4.2 Functional characterisation of MpAPEX and MpSERK

4.2.1 The role of MpAPEX in immunity

The similarity in morphology between Mp*apex* mutants and Tak-1, along with Mp*APEX* expression patterns (Figure 18B and 19), suggests that MpAPEX has a minimal or no role in vegetative growth and development but may function in plant–microbe interactions during later stages of thalli growth. I did not investigate gametangiophore induction in Mp*apex* mutants under far-red light irradiation. Therefore, it remains possible that MpAPEX plays a role in sexual reproduction, an idea which requires further elucidation.

In the bacterial pathogen infection assay, I observed a trend towards increased resistance to *Pto* DC3000 in Mp*apex* mutants (Figure 20). Interestingly, this trend was only observed in the apical regions not in the basal regions of the thalli in Mp*apex* mutants. This pattern of resistance partially aligned with the areas where Mp*APEX* was expressed (Figure 19G and 19H). Thus, MpAPEX may negatively regulate resistance to bacterial pathogens. The growth of *Pto* DC3000 is lower at the apical regions than at the basal regions of thalli in the wild-type Tak-1 (Matsumoto et al. 2021; Guzman-Benito et al. 2019). It is possible that in the assimilatory filaments at the apical regions, MpAPEX negatively regulates the formation of receptor complexes in response to stimuli, thereby mediating immune responses.

AtAPEX is a critical node within a predicted LRR-based cell surface interaction network, identified through a highly sensitive high-throughput interaction assay (Smakowska-Luzan et al. 2018). AtAPEX directly interacts with AtPEPR1 and AtPEPR2, the receptors for AtPEP peptides, in a ligand-independent manner. AtAPEX may also act as a regulatory scaffold, organising its counterparts into a signalling network. AtFLS2–AtSERK3 complex formation is negatively regulated by AtAPEX, despite AtAPEX being several steps away in the predicted interaction network. In the AtAPEX loss-of-function mutant, both AtBRI1 and AtFLS2 functions were affected, as evidenced by reduced hypocotyl elongation in response to BR and enhanced ROS bursts induced by flg22 (Smakowska-Luzan et al. 2018). Since orthologues of FLS2 and PEPR were not found in the genome of *M. polymorpha* (Bowman et al. 2017; Yotsui et al. 2023), MpAPEX possibly contributes to immunity via regulating other receptors. This hypothesis could be further investigated by interactome analysis using the transgenic plants expressing MpAPEX-miniTurbo-Myc generated in this study.

4.2.2 MpSERK plays a key role in both immunity and development

In *A. thaliana*, SERKs play diverse roles in development and immunity as co-receptors for multiple LRR-RLKs. In this study, I found that MpSERK is required for initiating both vegetative and sexual reproduction in *M. polymorpha* (Figure 18D to 18F). Mp*SERK* was primarily expressed in meristematic regions, consistent with the developmental defects of Mp*serk* mutants, likely caused by mis-regulations in these areas (Figure 19). AtSERK3 interacts with AtBRI1 in regulating plant growth and development (Sun et al. 2013; Fontes 2023). Homologue of BRI1 and the BR biosynthetic pathways are absent in *M. polymorpha* (Bowman et al. 2017). It is still unknown how MpSERK contributes to development in *M. polymorpha*. In contrast to the involvement of the conserved tyrosine residue (Y403) in AtSERK3 for immune signalling (Perraki et al. 2018), I found that the conserved tyrosine residue (Y418) in MpSERK plays a role in signalling related to growth and development (Figure 21B). Interactome analysis of MpSERK and MpSERK^{Y418F} suggested that Y418 in MpSERK contributes to the interaction with subfamily XI LRR-RLKs, MpTDR and MpRGI1 (Figure 22D). MpTDR is a receptor for the MpCLE1 peptide, and MpCLE1–MpTDR negatively regulates cell proliferation at the meristematic regions of *M. polymorpha* (Hirakawa et al. 2019). MpRGI is homologous to AtRGI, which is a receptor for root meristem growth factor (AtRGF) that regulates lateral root development in *A. thaliana* (Furumizu and Sawa 2021; Jeon et al. 2023). MpRGF peptides are present in the genome of *M. polymorpha* (Fang et al. 2021). The Y418 residue of MpSERK may contribute to MpTDR- and MpRGI1-mediated signalling, and the observed growth phenotype of MpSERKY^{418F} complementation plants could be due to the mis-regulation of MpTDR and MpRGI1 pathways (Fang et al. 2021; Hirakawa et al. 2019; Takahashi et al. 2021). These results highlight the diverse functions of the conserved tyrosine residue in uncoupling developmental and immune responses. Whether the conserved tyrosine residue of MpSERK also plays a role in immune signalling remains unclear.

The interactome analysis of MpSERK identified 16 potential interactors from various subfamilies of LRR-RLKs, including subfamilies I, II, III, V, VIII, IX, X, and XI (Figure 22B). This result supports the hypothesis that MpSERK acts as a co-receptor for LRR-RLKs in *M. polymorpha*. Although my aim was to identify potential PRRs that detect MAMPs in *M. polymorpha* through the interactome of MpSERK, no candidates from subfamily XII LRR-RLKs were identified. This might be because the plants were not exposed to elicitors that could be recognised by PRRs and induce complex formation. LRR-type PRRs in angiosperms often detect bacterial components. To date, the bacterial components, other than peptidoglycan, that can trigger immune responses in *M. polymorpha* have yet to be identified (Yotsui et al. 2023).

It remains unknown whether MpSERK functions as a co-receptor for PRRs in bryophytes. Further interactomics of MpSERK using plants infected with pathogens may help to identify potential LRR-type PRRs in *M. polymorpha.*

4.2.3 MpBIR function as a suppressor of MpSERK

In *A. thaliana*, BIRs interact with SERKs under resting conditions, negatively regulating SERK-mediated pathways (Halter et al. 2014; Imkampe et al. 2017; Ma et al. 2017). Through the interactome analysis in this study, MpBIR was identified as a strong candidate for interacting with MpSERK (Figure 22B). The interaction between MpBIR and MpSERK was confirmed in *N. benthamiana* using the FRET–FLIM approach (Figure 23A and 23B). It is very likely that SERK and BIR function as a module in *M. polymorpha* as well. BIR homologues have so far only been found in the genomes of land plants, suggesting that land plants acquired BIR during terrestrialisation (Furumizu and Sawa 2021).

By generating and investigating Mp*bir* KO and Mp*serk/bir* DKO mutants, I found that MpBIR is required for both vegetative growth and sexual reproduction and that Mp*serk* is epistatic to Mp*bir* (Figure 24B to 24F, and 25A). Moreover, overaccumulation of MpBIR in wild-type Tak-1 resulted in an Mp*serk*-like phenotype (Figure 25C). These results indicate that the expression level or protein homeostasis of MpBIR affects MpSERK-dependent plant growth and development and that an appropriate ratio between MpBIR and MpSERK is crucial. This further suggests that the major molecular function of MpBIR might be to suppress MpSERK activity through direct physical interactions, as in the case of SERK–BIR modules in *A. thaliana* (Halter et al. 2014; Imkampe et al. 2017; Ma et al. 2017; Hohmann et al. 2018).

Interestingly, among the three independent Mp*bir* mutant alleles that I generated, Mp*bir-1* had only a three-amino-acid (TSL) deletion in the extracellular LRR domain of MpBIR. The extracellular LRR domain of AtBIR2 and AtBIR3 was shown to bind to AtSERK3 *in vitro* (Hohmann et al. 2018). It is reasonable to speculate that the TSL deletion disrupts the proper dynamics of MpSERK–MpBIR complex formation, resulting in phenotypes similar to Mp*bir-2* and Mp*bir-3* mutants, which largely lack MpBIR (Figure 24B to 24F).

AtBIR1 was shown to have an active kinase domain, whereas AtBIR2–4 are pseudokinases (Gao et al. 2009; Halter et al. 2014; Imkampe et al. 2017). The cytosolic pseudokinase domains of AtBIR2 and AtBIR3 bind to the AtSERK3 kinase domain in yeast-2-hybrid assays, and the full-length proteins interact in planta (Halter et al. 2014; Imkampe et al. 2017). MpBIR is phylogenetically closest to AtBIR1, and several residues essential for kinase activity are conserved in MpBIR (Figure S3) (Hanks 1988). Thus, MpBIR is most likely an

active kinase. It would be important to investigate the contribution of kinase activity to MpBIR functions.

All three Mp*bir* mutants displayed hyper-resistance to the bacterial pathogen *Pto* DC3000 (Figure 27A). Several defence-related genes reported in *M. polymorpha* were found to be up-regulated in Mp*bir* mutants (Table S4) (Carella et al. 2019). These results suggest that MpBIR plays a negative role in defence. The hyper-resistance phenotype, together with the growth defects observed in Mp*bir* mutants, is reminiscent of autoimmunity. In *A. thaliana*, the loss of function in AtBIR1 leads to autoimmunity. The At*bir1* mutant exhibited strong dwarfism, cell death phenotypes, and constitutive activation of defence responses (Gao et al., 2009). Loss of AtBIR2 leads to a weak autoimmune phenotype, characterised by early senescence, mild cell death, and a slightly smaller morphology compared to the wild-type (Halter et al. 2014). In the At*bir2* mutant, cell death spreading out from the site of infection was observed after infection with the necrotrophic fungus *Alternaria brassicicola* (Halter et al. 2014). The autoimmunity-like phenotypes of Mp*bir* mutants are probably caused by the loss of suppression of MpSERK-mediated immune signalling, because apparent spontaneous cell death was not observed in Mp*bir* mutants.

If MpBIR suppresses MpSERK-mediated signalling, we can expect antagonistic downstream gene expression in Mp*bir* and Mps*erk*. Indeed, 40% of DEGs displayed contrasting expression patterns in Mps*erk* and Mp*bir* mutants compared to Tak-1 (Figure 26B). Gene cluster 1 and cluster 3 showed overall similar patterns. In cluster 1, there was a slight difference in gene expression levels between Tak-1 and Mps*erk* compared to cluster 3. This is likely because the plants used in this study were not subjected to stimuli. Plant-endogenous ligands probably regulate growth and development by activating MpSERK-dependent pathways under non-stimulated conditions. These contrasting gene expression patterns support the hypothesis that MpBIR suppresses MpSERK function by direct physical interaction in the absence of stimuli. MpSERK is probably under strict control by MpBIR when no ligands or stimuli are present. MpBIR negatively regulates defence against the bacterial pathogen, probably through the repression of MpSERK. In other words, MpSERK may positively contribute to immunity.

In summary, this study revealed potential roles of MpSERK in immunity. MpSERK also plays an important role in vegetative and sexual reproduction, and its function is suppressed by MpBIR. The MpSERK–MpBIR module regulates both immunity and development in *M. polymorpha*, suggesting that the SERK–BIR module is functionally conserved across land plants.

5 Materials and methods

5.1 Materials

5.1.1 Primers

All oligonucleotides were ordered from Sigma. The following table contains all primers that were used for gene editing, cloning, and genotyping in this study.

Name	Description	Sequence
MpFERpro5k-R	Amplifying MpFER promoter	TCTGTAGTGTATCCTCCAGCC
pENTR4-MpFERpro5k-inF	In-Fusion cloning into pENTR4	GCAGGCTCCACCATGGGAAG GTCATCCGAAGAATCATAT
pENTR4-MpFER-CDS-inR	In-Fusion cloning into pENTR4, with stop codon	AAGAAAGCTGGGTCTAGTTA CCTTCCTTGAGGGTTCACCA
MpFERpro5k-MpFER-CDS-inF	In-Fusion cloning MpFER promoter and MpFER CDS	CTGGAGGATACACTACAGAA TGAGGCGTTCGTCTTGTTTG
pENTR4-MpFER-CDS-inF	In-Fusion cloning into pENTR4	GCAGGCTCCACCATGATGAG GCGTTCGTCTTGTTTG
pENTR4-linear-R	pENTR4 linearisation	CATGGTGGAGCCTGCTTTTT
FERpro5k2-inF	In-Fusion cloning into pENTR4	CCAGGTTGAACCCAACATTGG AA
FERpro5k1-inR		TTGGGTTCAACCTGGCTTCTT GA
pENTR4-APEX-inF	In-Fusion cloning MpAPEX CDS into pENTR4	GTACAAAAAAGCAGGCTATG CAGCAGCAGCAGG
pENTR4-APEX-inR		GTACAAGAAAGCTGGGTGCG TCCAGCTGACAGCT
pro5-APEX-inF	In-Fusion cloning MpAPEX into pENTR4-pMpAPEX	AAACCCTGAGCAAGAGAATG CAGCAGCAGCAGG
pET4-pMpSERK-MpSERK_inF	In-Fusion cloning MpSERK into pENTR4-pMpSERK	AATCTCTGGAAAAGACTAGTC ATGCAGCATCCTTGGTTCC
pET4-pMpSERK-MpSERK_inR		GTACAAGAAAGCTGGGTCTCT TG
pET4-pMpFER-inR	In-Fusion cloning MpFER promoter into pENTR4	TGTACAAGAAAGCTGGGTTCT GTAGTGTATCCTCCAGCC

FERpro-FER-inR	In-Fusion cloning MpFER promoter into pENTR4-MpFER	AGACGAACGCCTCATTCTGTAGTGTATCCTCCAGCC
MpAPEX-gRNA2-seq-F	Amplifying 323bp of MpAPEX for genotyping	GTTCCCGACTGGAGTGAATC
MpAPEX-gRNA2-seq-R		TCCACTGCAGGCTACTGAAG
MpAPEX-gRNA1-seq-F	Amplifying 435bp of MpAPEX for genotyping	CCCAAACCCTGAGCAAGAGA
MpAPEX-gRNA1-seq-R		GGTGGGATGAGGTGAGAGGT
MpBIR1_65_gRNA_F	sgRNA targeting on MpBIR1 LRR domain, cloning into pMpGE_En03	CTCGAGACAAATCCAAGGAAGTAA
MpBIR1_65_gRNA_R		AAACTTACTTCCTTGGATTTGTCT
attB1-BAK1	BP cloning MpSERK CDS into pDONR207	GGGGACAAGTTTGTACAAAAAAGCAGGCTATGCAGCATCCTTGGTTCCT
attB2-BAK1		GGGGACCACTTTGTACAAGAAAGCTGGGTCTCTTGGGCCTGACAGTTCGA
attB1-BIR	BP cloning MpBIR CDS into pDONR207	GGGGACAAGTTTGTACAAAAAAGCAGGCTATGTCTTTGGAAAACCCAGAGT
attB2-BIR		GGGGACCACTTTGTACAAGAAAGCTGGGTCTGAGTTAGATACAATCAGCTCCT
attB1-MpLYR	BP cloning MpLYR CDS into pDONR207	GGGGACAAGTTTGTACAAAAAAGCAGGCTATGAATCGGGCAGTGCAA
attB2-MpLYR		GGGGACCACTTTGTACAAGAAAGCTGGGTCCCGAGCTTCGATCGGTGTA

attB1-MpLYK1	BP cloning MpLYK1 CDS into pDONR207	GGGGACAAGTTTGTACAAAAAAGCAGGCTATGATTGCGACGGGAGTTATC
attB2-MpLYK1		GGGGACCACTTTGTACAAGAAAGCTGGGTCTCGACCAGATATTAGCCCTGG
tac-promoter-F	Sequencing GST tag in pGEX-6p-1	TTAATCATCGGCTCGTATAATG
pGEX_5'	Universal sequencing primer for pGEX	GGGCTGGCAAGCCACGTTTGGTG
pGEX_3'		CCGGGAGCTGCATGTGTCAGAGG
MBP-F	3' end of maltose binding protein	GATGAAGCCCTGAAAGACGCGCAG
pBAD_Reverse	Sequencing pMAL-c2X	GATTTAATCTGTATCAGG
pMal-MpFER_cp-hf-F	HiFi cloning MpFER cytoplasmic domain into pMal-c5HisMBP	AGTTCTGTTTCAGGGGCCCGAACACAAGAGCGGCACAGG
pMal-MpFER_cp-hf-R		GAGCCTTTCGTTTTATTTGATTACCTTCCTTGAGGGTTCACC
pGEX-6p1-MpLYK1cp-hfF	HiFi cloning MpLYK1 cytoplasmic domain into pGEX-6p-1	TCTGTTCCAGGGGCCCCTGGGACCACGGCAGAGGCATTCAG
pGEX-6p1-MpLYK1cp-hfR		GTCAGTCACGATGCGGCCGCCTATCGACCAGATATTAGCCCTGG
pGEX-6p1-MpLYRcp-hfF	HiFi cloning MpLYR cytoplasmic domain into pGEX-6p-1	TCTGTTCCAGGGGCCCCTGGGAGCGCGCAAGAGGAGAAGAAC
pGEX-6p1-MpLYRcp-hfR		GTCAGTCACGATGCGGCCGCTCACCGAGCTTCGATCGG
MpLYK1-K381N-F	MpLYK1 kinase-dead mutation	TAGCTGTGAACAGGATGAATCTTCAAGCGAC
MpLYK1-K381N-R		GCTTCATGCCCCGCAGGT

MpLYR-K390E-F	MpLYR kinase-dead mutation	GGTGGCGATCGAGCAGATGAG
MpLYR-K390E-R		ACCTCGTTCCGCAAGATC
MpBIR_TSLdel-F	MpBIR TSL aa deletion	GATTTGTCTGGGAACAGTTTC
MpBIR_TSLdel-R		AAGGGACTTGCACTTCGC
MBP-seqF1	Maltose binding protein	GAAAGCGGGTCTGACCTTCC
pGEX6p1-linr-R	Linearising pGEX-6p-1	TCCCAGGGGCCCCTGGAACA
pGEX6p1-linr-F		GCGGCCGCATCGTGACTGAC
pMal-linr-R	Linearising pMal-c5	TTCGGGCCCCTGAAACAGA
pMal-linr-F		TCAAATAAAACGAAAGGCTCAGTCGA
207-BIR-linr-F	Linearising pDONR207-MpBIR	ATGTCTTTGGAAAACCCAGA
207-linr-R		AGCCTGCTTTTTTGTACAAA
pBIR-BIR-hfR	HiFi cloning MpBIR promoter into pDONR207-BIR	TTTGTACAAAAAAGCAGGCTAAACTCGTCTGATCTCACTCAACG
207-pBIR-hfF		TCTGGGTTTTCCAAAGACATCGCTCCCCGGCTTTGAATG
MpLYK1-N381K-F	Site-directed mutagenesis, MpLYK1 kinase-dead to WT	TAGCTGTGAAGAGGATGAATCTTCAAGCG
attB1-AtBIR	BP cloning AtBIR codon optimised sequence	GGGGACAAGTTTGTACAAAAAAGCAGGCTATGATGATGGGACGCTTGG
attB2-AtBIR		GGGGACCACTTTGTACAAGAAAGCTGGGTAGCGGGCCACGATCAATTC
MpBIR_CRR_TSLdel-F	Cloning MpBIR_ CRISPRR, TSL aa deletion	GACCTAAGCGGGAAC
MpBIR_CRR_TSLdel-R		TAAACTCTTGCACTTCG
MpACT-qF	for qRT analysis	AGGCATCTGGTATCCACGAG
MpACT-qR		ACATGGTCGTTCCTCCAGAC
MpEF1α -qF	for qRT analysis	CCGAGATCCTGACCAAGG

MpEF1α -qR		GAGGTGGGTACTCAGCGAAG
MpWRKY3_qF	for qRT analysis	CGGTGCTCAATCTGCTTTCT
MpWRKY3_qR		GGCTGCTGTGAAATTGGGAT
MpPR3_qF	for qRT analysis	AAGCAATGCGGTGACTCATC
MpPR3_qR		AATCGGATGAGGAAGGGCTC
MpWRKY14_qF	for qRT analysis	CTTCCAGAAAACGGGTGCAA
MpWRKY14_qR		AAATGCAACACCTAGCGAGT
MpPR5_qF	for qRT analysis	AACGCAGCAACAGATCGAAA
MpPR5_qR		AGCTTATGGACCTGCAACCT
MpBAK1_gRNA_F	sgRNA targeting on MpBAK1 kinase domain	CTCGCAAGGGTCGTCTGGCTGA
MpBAK1_gRNA_R		AAACTCAGCCAGACGACCCTTG

5.1.2 Plasmids

The pMKMM1 vector was modified from the pMpGWB300 expression vector backbone, harbouring a C-terminus miniTurbo-Myc tag. The pMKMM2 vector was modified from the pMpGWB300 backbone, harbouring *EF-1α* promoter and a C-terminus miniTurbo-Myc tag. The table below lists all the plasmids used in this study.

Name	**Description**	**Cloned Nucleic Acid / Vector Backbone**	**Selection**
pMYYM1	MpSERK promoter in GW eV	pMpSERK / pENTR4	Kan
pMYYM2	MpSERK promoter in GW dV, promoter-GUS	pMpSERK / pMpGWB304	Spt, CS
pMYYM3	MpAPEX promoter in GW eV	pMpAPEX / pENTR4	Kan
pMpGE010	GW dV for CRISPR guide	pMpGE010	Spt
pMpGE_En03	GW eV for CRISPR guide	pMpGE_En03	Kan
pMpGWB304	GW dV, GUS reporter	pMpGWB304	Spt, CS
pMYYM4	Synthesised MpFER CDS with CRISPRR	MpFER_CDS / pMA-T	Amp

pMYYM5	Synthesised MpFER-KD CDS with CRISPRR	MpFER_CDS_KD / pMA-T	Amp
pMYYM6	MpAPEX promoter in GW dV, promoter-GUS	pMpAPEX / pMpGWB304	Spt, CS
pENTR4	GW eV	pENTR4	Kan
pMYYM7	MpFER CDS with CRISPRR, no stop codon	MpFER_CDSns / pENTR4	Kan
pMYYM8	MpFER-KD CDS with CRISPRR, no stop codon	MpFER_CDS_KD / pENTR4	Kan
pMYYM9	MpAPEX CDS with CRISPRR in GW eV	MpAPEX_CDS / pENTR4	Kan
pMYYM10	MpFER-KD CDS with CRISPRR, no stop codon in GW eV	MpFER_CDS_KDns / pENTR4	Kan
pMYYM11	MpFER CDS with CRISPRR, no stop codon in GW eV	MpFER_CDSns / pENTR4	Kan
pMYYM12	MpAEPX CDS with CRISPRR, no stop codon in GW eV	MpAEPX_CDSns / pENTR4	Kan
pMYYM13	$_{pro}$MpAPEX:MpAEPX_CDS_CRISPRR_without stop codon	$_{pro}$MpAPEX:MpAEPXns / pENTR4	Kan
pMYYM14	$_{pro}$MpAPEX:MpFER_CDS_CRISPRR_without stop codon	$_{pro}$MpFER:MpFERns / pENTR4	Kan
pMYYM15	$_{pro}$MpFER:MpFER_CDS_CRISPRR_KD _without stop codon	$_{pro}$MpFER:MpFER_KDns / pENTR4	Kan
pMYYM16	$_{pro}$MpSERK:MpSERK_CDS_CRISPRR_without stop codon	$_{pro}$MpSERK:MpSERKns / pENTR4	Kan
pMYYM17	$_{pro}$MpSERK:MpSERK_CDS_CRISPRR_KD_without stop codon	$_{pro}$MpSERK:MpSERK_KDns / pENTR4	Kan
pMYYM18	$_{pro}$MpAPEX:MpAPEX_CRISPRR into GW dV pMKMM1	$_{pro}$MpAPEX:MpAEPX / pMKMM1	Spt, CS
pMYYM19	Overexpressing MpAPEX_CRISPRR into GW dV pMKMM2	MpAPEX / pMKMM2	Spt, CS
pMYYM20	Overexpressing MpFER_CRISPRR into GW dV pMKMM2	MpFER / pMKMM2	Spt, CS

pMYYM21	Overexpressing MpFER_CRISPRR_KD into GW dV pMKMM2	MpFER_KD / pMKMM2	Spt, CS
pMYYM22	$_{pro}$MpSERK_CRISPRR into GW dV pMKMM1	$_{pro}$MpSERK:MpSERK / pMKMM1	Spt, CS
pMYYM23	$_{pro}$MpSERK_CRISPRR_KD into GW dV pMKMM1	$_{pro}$MpSERK:MpSERK_KD / pMKMM1	Spt, CS
pMYYM24	$_{pro}$MpFER:MpFER_CRISPRR into GW dV pMKMM1	$_{pro}$MpFER:MpFER / pMKMM1	Spt, CS
pMYYM25	$_{pro}$MpFER:MpFER_CRISPRR_KD into GW dV pMKMM1	$_{pro}$MpFER:MpFER_KD / pMKMM1	Spt, CS
pMYYM26	MpFER promoter in GW eV	$_{pro}$MpFER / pENTR4	Kan
pMYYM27	MpFER promoter in GW dV, promoter-GUS	$_{pro}$MpFER / pMpGWB304	Spt, CS
pMYYM28	$_{pro}$MpAPEX:MpAEPX_CDS_CRISPRR without stop codon	$_{pro}$MpAPEX:MpAEPXns / pENTR4	Kan
pMYYM29	$_{pro}$MpAPEX:MpAEPX_CDS_CRISPRR without stop codon	$_{pro}$MpAPEX:MpAEPX / pMKMM1	Spt, CS
pMYYM30	Synthesised MpFER CDS with CRISPR resistance	MpAPEX_CDS / pMA	Amp
pMYYM31	GW eV for MpBIR CRISPR guide	MpBIR1_gRNA65 / pMpGE_En03	Kan
pMYYM32	GW dV for MpBIR CRISPR guide	MpBIR1_gRNA65 / pMpGE010	Spt, Hyg
pMYYM33	pDONR207-MpBIR	MpBIR / pDONR207	Gent
pMYYM34	pDONR207-MpLYK1	MpLYK1 / pDONR207	Gent
pMYYM38	pDONR207-MpBAK1	MpBAK1 / pDONR207	Gent
pMYYM39	pDONR207-MpLYK5	MpLYK5 / pDONR207	Gent
pDONR-207	GW eV	pDONR-207	Gent
pGEX-6P-1	N-terminus GST tag, protein expression vector	pGEX-6P-1	Amp

pMAL-c5HisMBP	N-terminus His-MBP tag, protein expression vector	pMAL	Amp
pABindGFP	pABindGFP containing estradiol inducible promoter and C-terminus GFP tag	pAB117	Spt, Hyg
pABindmCherry	pABindmCherry containing estradiol inducible promoter and C-terminus mCherry tag	pAB118	Spt, Hyg
pMYYM40	MpFER_KD-HisMBP, cytoplasmic domain	MpFER_KD / pMAL	Amp
pMYYM41	pDONR207-MpLYK1_K381N, KD, cytoplasmic domain	MpLYK1_K381N / pDONR-207	Gent
pMYYM42	pGEX-6p-1-MpLYR cytoplasmic domain	MpLYR / pGEX-6P-1	Amp
pMYYM43	pGEX-6p-1-MpLK1_K381N, KD, cytoplasmic domain	MpLYK1_K381N / pGEX-6P-1	Amp
pMYYM44	pGEX-6p-1-MpLK1, cytoplasmic domain	MpLYK1 / pGEX-6P-1	Amp
pMYYM45	pDONR207-MpBIR_TSL_deleted	MpBIR_TSLdel / pDONR-207	Gent
pMYYM46	Estradiol inducible expression vectors with C-GFP	MpBIR / pAB117	Spt
pMYYM47	Estradiol inducible expression vectors with C-GFP	MpBAK1 / pAB117	Spt
pMYYM48	Estradiol inducible expression vectors with C-mCherry	MpFER / pAB118	Spt
pMYYM49	Estradiol inducible expression vectors with C-mCherry	MpLYK1 / pAB118	Spt
pMYYM50	Estradiol inducible expression vectors with C-mCherry	MpBIR / pAB118	Spt
pMYYM51	Estradiol inducible expression vectors with C-mCherry	MpBAK1 / pAB118	Spt

pMYYM52	Estradiol inducible expression vectors with C-GFP	MpFER / pAB117	Spt
pMYYM53	MpBIR-miniTurbo overexpression	MpBIR / pMKMM2	Spt, CS
pMYYM54	MpBIR_TSLdeleted-miniTurbo overexpression	MpBIR_TSLdel / pMKMM2	Spt, CS
pMYYM55	Estradiol inducible expression vectors with C-GFP	MpLYK1 / pAB117	Spt
pMYYM56	Estradiol inducible expression vectors with C-GFP	MpLYR / pAB117	Spt
pMYYM57	Estradiol inducible expression vectors with C-mCherry	MpLYR / pAB118	Spt
pMYYM58	Estradiol inducible expression vectors with C-GFP	MpFER_KD / pAB117	Spt
pMYYM59	Estradiol inducible expression vectors with C-mCherry	MpFER_KD / pAB118	Spt
pMYYM60	Estradiol inducible expression vectors with C-mCherry	MpBIR_TSLdel / pAB118	Spt
pMYYM61	Estradiol inducible expression vectors with C-GFP	MpBIR_TSLdel / pAB117	Spt
pMYYM62	GW eV for MpSERK CRISPR guide	MpBAK1_gRNA / pMpGE_EN03	Kan
pMYYM63	pDONR207-AtBIR_synthesised cDNA_codon optimised for *Marchantia polymorpha*, no stop codon	AtBIRsyn / pDONR207	Gent
pMYYM64	pDONR207-MpBIR_synthesised cDNA_CRISPRR, no stop codon	MpBIR / pDONR207	Gent
pMpGE011	GW dV for CRISPR guide	pMpGE011	Spt, CS
pMYYM65	Synthesised AtBIR original version. codon optimised for *Marchantia polymorpha*	AtBIR / pMA-RQ	Amp

pMYYM66	Synthesised MpBIR original version. CRISPRR	MpBIR / pMA-RQ	Amp
pMYYM67	GW dV for MpSERK CRISPR guide	MpBAK1_gRNA / pMpGE011	Spt, CS
pMYYM68	GW dV for MpBIR CRISPR guide	MpBIR1_gRNA65 / pMpGE011	Spt, CS
pMYYM69	pDONR207-MpBIR_synthesised cDNA_CRISPRR_TSLdel, no stop codon	MpBIR_TSLdel / pDONR207	Gent
pMYYM70	MpBIRsyn-miniTurbo overexpression	MpBIRsyn / pMKMM2	Spt, CS
pMYYM71	AtBIRsyn-miniTurbo overexpression	AtBIR / pMKMM2	Spt, CS
pMYYM72	MpBIRsyn_TSLdel-miniTurbo overexpression	MpBIRsyn_TSLdel / pMKMM2	Spt, CS

5.1.3 Bacterial strains

The empty gateway binary vectors containing the toxic CcdB cassette were amplified in chemically competent *E. coli* DB3.1 strain. All other plasmids were cloned and amplified in electrocompetent or chemically competent *E. coli* DH10β or MACH-1 strains. Electrocompetent *Agrobacterium tumefaciens* GV3101 carrying expression vectors were employed for the stable transformation of *M. polymorpha*. A bioluminescent *Pto* DC3000 lux strain was utilised for bacterial infection assays, as previously detailed by Matsumoto et al. 2021.

5.1.4 Transgenic plants

The following table provides an overview of all *M. polymorpha* plants that were used for experiments in this thesis.

Description	**Cloned GMO / background**	**Selection**
Mp*apex* KO mutant #1	MpAPEX gRNA1 / Tak-1	Hyg
Mp*apex* KO mutant #2	MpAPEX gRNA2 / Tak-1	Hyg
$_{pro}$MpSERK-GUS #2	$_{pro}$MpSERK:GUS / Tak-1	CS

$_{pro}$MpAPEX-GUS #2	$_{pro}$MpAPEX:GUS / Tak-1	CS
$_{pro}$MpAPEX-GUS #10	$_{pro}$MpAPEX:GUS / Tak-1	CS
$_{pro}$MpFER-GUS #4	$_{pro}$MpFER:GUS / Tak-1	CS
$_{pro}$MpFER-GUS #10	$_{pro}$MpFER:GUS / Tak-1	CS
MpSERK^{Y418F} -miniTurbo #1	$_{pro}$MpSERK:MpSERK^{Y418F}-miniTurbo-Myc / Mp*serk#3*	CS
MpSERK^{Y418F} -miniTurbo #2	$_{pro}$MpSERK:MpSERK^{Y418F}-miniTurbo-Myc / Mp*serk#3*	CS
MpSERK^{Y418F} -miniTurbo #3	$_{pro}$MpSERK:MpSERK^{Y418F}-miniTurbo-Myc / Mp*serk#3*	CS
MpSERK^{Y418F}-miniTurbo #4	$_{pro}$MpSERK:MpSERK^{Y418F}-miniTurbo-Myc / Mp*serk#3*	CS
MpSERK-miniTurbo #4	$_{pro}$MpSERK:MpSERK-miniTurbo-Myc / Mp*serk#3*	CS
MpSERK-miniTurbo #1	$_{pro}$MpSERK:MpSERK-miniTurbo-Myc/ Mp*serk#3*	CS
MpSERK-miniTurbo #2	$_{pro}$MpSERK:MpSERK-miniTurbo-Myc / Mp*serk#3*	CS
MpSERK-miniTurbo #3	$_{pro}$MpSERK:MpSERK-miniTurbo-Myc / Mp*serk#3*	CS
MpFER-miniTurbo #2	$_{pro}$MpFER:MpFER-miniTurbo-Myc / Tak-1	CS
MpFER_KD-miniTurbo #2	$_{pro}$MpFER:MpFER_KD-miniTurbo-Myc / Tak-1	CS
MpFER_KD-miniTurbo #5	$_{pro}$MpFER:MpFER_KD-miniTurbo-Myc / Tak-1	CS
MpFER-miniTurbo #7	$_{pro}$MpFER:MpFER-miniTurbo-Myc / Tak-1	CS
MpBIR overexpressing line #6	$_{pro}$MpEF1α:MpBIR-miniTurbo-Myc / Tak-1	CS
MpBIR overexpressing line #9	$_{pro}$MpEF1α:MpBIR-miniTurbo-Myc / Tak-1	CS
Mpbir complementing by overexpressing MpBIR #10	$_{pro}$EF1α:MpBIR_CRR-miniTurbo / pMKMM2 / Mp*bir#3*	CS
Mpbir complementing by overexpressing MpBIR #4	$_{pro}$EF1α:MpBIR_CRR-miniTurbo / pMKMM2 / Mp*bir#3*	CS

Mp*serk/bir* DKO mutant #1	MpBIR1_gRNA65 / pMpGE011 / Mp*serk#3*	CS
Mp*serk/bir* DKO mutant #2	MpBAK1_gRNA / pMpGE011 / Mp*bir#3*	CS
Mp*serk/bir* DKO mutant #3	MpBAK1_gRNA / pMpGE011 / Mp*bir#1*	CS
Mp*bir* KO mutant #1	MpBIR1_gRNA65 / pMpGE010 / Tak-1	Hyg
Mp*bir* KO mutant #2	MpBIR1_gRNA65 / pMpGE010 / Tak-1	Hyg
Mp*bir* KO mutant #3	MpBIR1_gRNA65 / pMpGE010 / Tak-1	Hyg

5.2 Methods

5.2.1 Molecular cloning of genetic constructs

The 5-kb putative promoter fragment upstream of the translation initiation codon of Mp*SERK*, Mp*FER*, Mp*APEX* and Mp*BIR* was amplified. The promoters of Mp*SERK*, Mp*FER*, and Mp*APEX* were cloned into the Gateway™ pENTR4 dual-selection vector (ThermoFisher) using an In-Fusion HD cloning kit (Takara), and were then subcloned into the binary vector pMpGWB304 to construct $_{pro}$Mp*SERK*:*GUS*, $_{pro}$Mp*FER*:*GUS*, and $_{pro}$Mp*APEX*:*GUS* using the LR clonase II enzyme mix (ThermoFisher) (Ishizaki et al. 2015). The promoter of Mp*BIR* was cloned into the Gateway™ pDNOR207 vector (ThermoFisher) using the NEBuilder® HiFi DNA Assembly Cloning Kit (NEB).

To generate the targeting vectors for Mp*bir-1*, Mp*bir-2*, Mp*bir-3*, Mp*serk-4*, and Mp*serk-5*, annealed oligos for Mp*BIR*- and Mp*SERK*-targeting sgRNA were ligated into *Bsa*I-digested pMpGE_En03 (Sugano et al. 2018) using a T4 DNA ligase (NEB). Mp*BIR*- and Mp*SERK*-targeting sgRNA were then subcloned into binary vectors pMpGE010 and pMpGE011, respectively. The plasmids containing Mp*BIR*-targeting sgRNA were introduced into Tak-1 or Mp*serk-1* to generate Mp*bir* or Mp*bir*/Mp*serk-3*, respectively. The plasmids containing Mp*SERK*-targeting sgRNA were introduced into Mp*bir-3* or Mp*bir-1* to generate Mp*serk*/Mp*bir-1* or Mp*serk*/Mp*bir-2*, respectively. Screening for CRISPR/Cas9-mediated targeted mutagenesis lines was performed using genomic PCR, as described previously (Sugano et al. 2018).

The coding sequence of Mp*SERK* and Mp*SERK*^{Y418F} were synthesised. The sgRNA target site and PAM sequence of Mp*SERK* were mutated, so as not to be targeted by CRISPR/Cas9. Synthesised coding sequence of Mp*SERK* and Mp*SERK*^{Y418F} were cloned into pENTR4-$_{pro}$Mp*SERK*, and they were then subcloned into the binary vector pMKMM1 (Yan et

al. 2024) to construct $_{pro}$Mp*SERK*:Mp*SERK-miniTurbo-Myc* and $_{pro}$Mp*SERK*:Mp*SERK*^{Y418F}-*miniTurbo-Myc*. The resultant plasmids were introduced into Mp*serk-3*.

The coding sequence of Mp*BIR* was amplified from Tak-1 complementary DNA using KOD Plus Neo (Toyobo). Mp*BIR* coding sequence was cloned into pDNOR207 and pDNOR207-$_{pro}$Mp*BIR* vectors and was then subcloned into binary vector pMKMM2 and pMKMM1 (Yan et al. 2024; Melkonian et al. 2022) to construct $_{pro}$Mp*EF1*α:Mp*BIR-miniTurbo-Myc* and $_{pro}$Mp*BIR*:Mp*BIR-miniTurbo-Myc*, respectively. The $_{pro}$Mp*EF1*α:Mp*BIR-miniTurbo-Myc* plasmid was introduced into Tak-1 and the $_{pro}$Mp*BIR*:Mp*BIR-miniTurbo-Myc* plasmid was introduced into Mp*bir-3*.

To generate estradiol-inducible expression vectors with GFP or mCherry as translational fusions at the C-terminus for transient expression in *N. benthamiana* leaves, the coding sequences of Mp*BIR*, Mp*SERK*, Mp*FER*, Mp*LYK1*, and Mp*LYR* were cloned into pDNOR207 using NEBuilder® HiFi DNA Assembly Cloning Kit (NEB). These sequences were then subcloned into binary vector pABind117 and pABind118 (Somssich and Simon 2017) to construct corresponding plasmids used in Figure 15C, 23A, and 23B, using LR clonase II enzyme mix (ThermoFisher).

5.2.2 Plant growth and conditions

For maintenance, a male accession of *M. polymorpha*, Tak-1, was used as the wild- type. Plants were grown from single gemmae or small piece of mature thallus and transferred onto ½ Gamborg's B5 medium containing 1% agar. They were maintained at 22 °C under continuous white LED light at an intensity of 50–60 µmol photons $m^{-2}s^{-1}$.

For ROS assay, 7-day-old or 5-day-old gemmalings (cultured mature gemmae) in liquid ½ Gamborg's B5 medium containing 0.1% sucrose with shaking at 130 rpm at 22 °C under 50–60 µmol photons $m^{-2}s^{-1}$ continuous white LED were used.

For interactome, transcriptome, and qRT-PCR analysis, 14-day-old plants were grown from single gemmae on sterilised cellophane on ½ Gamborg's B5 medium containing 1% agar at 22 °C under 50–60 µmol photons $m^{-2}s^{-1}$ continuous white LED.

For the *Pto* DC3000-lux infection assay, 14-day-old plants were grown from single gemmae on sterilised Whatman filter paper on ½ Gamborg's B5 medium containing 1% agar at 22 °C under 50–60 µmol photons $m^{-2}s^{-1}$ continuous white LED.

For the root inhibition assay, *A. thaliana* seeds were surface-sterilised using 70% (v/v) and 100% ethanol for 10 mins, and this process was repeated twice. Seeds were dried out on sterilised Whatman filter paper on a clean bench and were germinated on ½ MS medium

containing 1% sucrose and 1% agar, adjusted to pH 5.8 using KOH, at 22 °C under 50–60 µmol photons $m^{-2}s^{-1}$ continuous white LED.

For *Agrobacterium*-mediated stable transformation, 14-day-old plants were grown from single gemmae on ½ Gamborg's B5 medium containing 1% agar at 22 °C under 50–60 µmol photons $m^{-2}s^{-1}$ continuous white LED before cutting thallus transformation.

For gametangiophore induction, thalli were grown from single gemmae on ½ Gamborg's B5 medium containing 1% agar at 22 °C under 50–60 µmol photons $m^{-2}s^{-1}$ continuous white LED and 60–65 µmol photons $m^{-2}s^{-1}$ continuous far-red LED.

5.2.3 *Agrobacterium*-mediated stable transformation

Marchantia polymorpha mutants and transgenic lines were produced using the cut thallus method for *Agrobacterium*-mediated stable transformation, as shown by Kubota et al. 2013, with minor modifications. Candidate transformants were selected using the same conditions as mentioned in 5.2.2 but on ½ Gamborg's B5 medium containing 1% agar and corresponding antibiotics as well as 100 mg/L cefotaxime for killing of residual agrobacteria. In the course of two months of culturing on antibiotic-selection ½ Gamborg's B5 plates, the thallus fragments gave rise to new, resistant plants, which were then separated onto new plates. To rule out chimerism in the obtained transformants, the first gemmae derived generation was used for screening the transformants.

5.2.4 GUS staining assay

Three-day-old gemmae and thalli of different ages from *M. polymorpha* were submerged in GUS staining solution consisting of 0.5 mg/mL X-Gluc, 0.1% Triton X-100, 10 mM EDTA, 0.5 mM potassium ferricyanide, and 0.5 mM potassium ferrocyanide in 100 mM sodium phosphate buffer (pH 7.0), followed by vacuum infiltration for 5–15 mins. After overnight incubation in the dark at 37 °C, tissues were de-stained by incubation in 70% ethanol with gentle shaking for a minimum of 1 hour before observation.

5.2.5 RALF peptide synthesis

All RALF peptides were synthesised by ABclonal Technology (https://www.abclonal.com/) with a purity of >85% (Data S1). All peptides were dissolved in Milli-Q water for usage and stored at -20 °C at a concentration of 1 mM.

5.2.6 ROS burst and ROS production pattern measurement

Gemmae from corresponding genotypes of *M. polymorpha* were collected from the gemma cups using a sterile tweezer and resuspended in 50 mL liquid ½ Gamborg's B5 medium supplemented with 0.1% sucrose in a 250-mL Erlenmeyer flask and were then cultured in a walk-in growth chamber under 50–60 µmol photons $m^{-2}s^{-1}$ continuous white LED at 22 °C for 5 or 7 days, while shaking at 300 rpm. After culturing, the gemmae were transferred to 50-mL falcon tubes and washed three times with Milli-Q water. Six gemmae of each genotype were carefully transferred into 100 µL containing 20 µM L-O12 in water. For each genotype and treatment, at least three replicates were used. All gemmae were incubated overnight in dark at room temperature. The elicitors, chitin, and all RALF peptide solutions, were dissolved in Milli-Q water supplemented with 2.5 units/mL HRP to a final concentration of 1 µM (1x). The mock solution was prepared in elicitor-free Milli-Q water supplemented with 2.5 units/mL HRP. After incubation with luminol, 100 µL of the 2x concentrated elicitor and mock solutions were added to the samples and relative RLU were measured in a plate reader.

5.2.7 Root growth inhibition assay

Seeds were surface-sterilised and vertically grown on ½ MS agar plates for 5 days under 50–60 µmol photons $m^{-2}s^{-1}$ continuous white LED before six seedlings were transferred to each well of a 12-well plate containing 4 mL per well of ½ MS medium with 1 µM AtRALF23, 1 µM AtRALF34, 1 µM MpRALF1, 1 µM MpRALF3, 1 µM F-RALF, or 10 µM F-RALF. Peptide-free ½ MS liquid medium served as the mock control. All plants were transferred to a squared ½ MS agar plate for imaging. Primary root length was measured and quantified using ImageJ software. Roots from approximately ten seedlings per treatment and genotype were measured. Experiments were repeated three times using independent biological replicates.

5.2.8 Phylogenetic analysis

Multiple sequence alignments of mature peptide sequences were created using the MUSCLE algorithm with MEGA7 software. Phylogenetic unrooted trees were constructed with the MEGA7 software by using the Maximum Likelihood method based on the JTT matrix-based model (Kumar, Stecher, and Tamura 2016).

5.2.9 Annotations of the interactomic and transcriptomic dataset

For *M. polymorpha* protein annotation, gene annotations from MpTak1_v6.1, MpTak1_v5.1, and JGI 3.1 (https://marchantia.info/) were integrated. Homologue information was then utilised for the annotation. BLAST was employed to identify homologues in TAIR10 (https://www.arabidopsis.org/), with the best hit having an e-value ≤ 10^{-10} considered as a homologue. Additional annotation resources, including TAIR10 (Lamesch et al., 2012), PANTHER v.16.0 (http://pantherdb.org/) (Mi et al., 2021), Kyoto Encyclopedia of Genes and Genomes (KEGG) (Ogata et al., 1999), HAMPA (https://hamap.expasy.org/), and Araport 11 (https://www.arabidopsis.org/) (Cheng et al., 2017) were utilised for annotating homologues. Integration of annotation files was performed using RSTUDIO (v.1.4.1103) (https://www.rstudio.com/) with R (v.x64 4.0.3) (https://cran.r-project.org/) using the TIDYVERSE (v.1.3.0), RIO (v.0.5.16), and ZOO (v.1.8-8) packages.

5.2.10 GO enrichment analysis

GO term enrichment was performed with ShinyGO 0.80 (http://bioinformatics.sdstate.edu/go/) (Ge, Jung, and Yao 2020). Corresponding homologues were used as input protein lists for the analysis. For GO analysis of DEGs in *M. polymorpha*, the best BLASTP hit genes in *A. thaliana* were used.

5.2.11 Transcriptome analysis

Total RNA was isolated from 14-day-old *M. polymorpha* by RNeasy Plant Mini Kits (QIAGEN). For RNA-seq analysis in chapter 3.1.4.1, wild-type Tak-1 plants were subjected to vacuum infiltration with Milli-Q water for 10 mins, followed by overnight incubation in water at room temperature. Next, water was removed and samples were treated with mock, 1 µM chitin, or 1 µM MpRALF1 for 1 and 3 hours. For RNA-seq analysis in chapter 3.2.3.3, wild-type Tak-1, Mp*bir-1*, Mp*bir-3*, and Mp*serk-3*were collected from ½ Gamborg's B5 medium containing 1% agar.

Library preparation and sequencing were conducted by Novegene, UK (https://www.novogene.com/eu-en/) using the Illumina NovaSeq 6000 platform. Raw reads underwent quality control and trimming using fastp (Chen et al. 2018). Mapping of reads and quantification of transcripts per gene were performed against the *M. polymorpha* genomes and gene annotations (MpTak_v6.1) (Montgomery et al. 2020) using the STAR aligner (Dobin et al. 2013). Genes with fewer than an average of 10 read counts were excluded, and the log2 fold

change in gene expression between conditions was calculated using the R package DESeq2 (Love, Huber, and Anders 2014). Genes with statistical significance (FDR adjusted p-value < 0.05) were selected for further analyses. Differentially expressed genes were grouped using K-means clustering with the pheatmap R package.

5.2.12 RNA extraction and cDNA synthesis

Total RNA was extracted from two 14-day-old thalli using the RNeasy Plant Mini Kit (QIAGEN). On-column DNase I treatment was performed using the RNase-free DNase I (QIAGEN) according to the manufacturer's recommendations. Total RNA samples were quantified by a Nanodrop spectrophotometer. First-strand complementary DNA was synthesised from 1 µg total RNA using SuperScript IV Reverse Transcriptase (ThermoFisher). Reverse transcription was performed according to the manufacturer's protocol. Complementary DNA was then diluted 10 times by adding nuclease-free water.

5.2.13 Quantitative RT-PCR analysis

Quantitative RT-PCR was performed using a CFX96 Read-Time System LightCycler 96 (Bio-Rad). Reactions were performed in 10 µL volume using iQ SYBR Green Supermix (Bio-Rad). MpACT served an internal standard. Primers used for qRT-PCR are listed in chapter 5.1.1. The two-step cycle was composed of denaturation at 95 °C for 3 mins followed by hybridisation/elongation at 60 °C for 30 seconds; the cycle was repeated 40 times and then followed by a dissociation step. Three technical replicates and three biological replicates were performed for each reaction.

5.2.14 *Pto* DC3000-lux infection assay

Bacterial quantification in infected thalli was carried out as described before (Matsumoto et al. 2021). Briefly, *M. polymorpha* were grown on autoclaved Whatman filter paper on ½ Gamborg's B5 medium for two weeks. In the meantime, *Pto* DC3000-lux was cultivated in King's B medium containing 30 mg/mL rifampicin at 28 °C to achieve an OD_{600} of 0.8. The saturated bacterial culture was subsequently washed and resuspended in Milli-Q water to prepare a bacterial suspension with of an OD_{600} of 1.0. Next, two-week-old thalli were submerged in the bacterial suspension followed by vacuum for 5 mins and incubation for 0 to 2 days on pre-wetted Whatman filter papers. All plants were incubated in a growth chamber under long day conditions (8 hours in dark, 16 hours under light) at 22 °C under 50–60 µmol photons $m^{-2}s^{-1}$ white light LED. After incubation, thallus discs (4 mm diameter) were punched

from the centre region using a sterile biopsy punch (pfm medical) and transferred to a 96-well plate (VWR). Before measuring, the thallus discs were kept in the dark for 10 mins. Bioluminescence was measured in a FLUOstar Omega plate reader (BMG Labtech).

For the elicitor primming assay, 14-day-old plants were harvested from on ½ Gamborg's B5 medium. Prior to immersion in the bacterial suspension, the plants underwent vacuum infiltration with Milli-Q water for 5 mins, followed by overnight incubation at room temperature. Next, the plants were removed from water and treated with 1 µM chitin, 1 µM MpRALF1, 1 µM AtRALF23 or water as mock treatment for 3 and 24 hours at room temperature.

5.2.15 Transient expression in *N. benthamiana*

Agrobacterium strains transformed with the desired vectors were cultured on LB plates containing the respective antibiotics at 28 °C for 2 days. A single colony was selected and inoculated into 5 mL of LB medium with the appropriate antibiotics, then incubated overnight at 28 °C with shaking. To prepare a fresh liquid culture, 1 mL of the overnight culture was added to 4 mL of LB medium and incubated at 28 °C with shaking for 4 hours. The bacteria were then collected by centrifugation and resuspended in 5 mL of infiltration solution (5% sucrose, 0.01% Silwet® L-77, 450 µM acetosyringone, a spatula tip of glucose). The bacterial suspension was kept on ice before infiltration. The optical density was measured using a spectrophotometer and adjusted to an OD_{600} of 0.4 per strain using fresh infiltration solution. *Nicotiana benthamiana* leaves were infiltrated with the suspension using a needleless syringe, and the infiltrated areas were marked with a permanent marker. The plants were kept at 22 °C under 50–60 µmol photons $m^{-2}s^{-1}$ continuous white LED for at least 48 hours. To induce protein expression, the abaxial side of the infilled leaves were painted with 20 µM β-estradiol and 0.1% Tween 20 for 24 hours.

5.2.16 Purification of fusion proteins

The cytoplasmic domains of MpFER and MpLYK1 were amplified and cloned into pMal-c2x with a MBPHis tag and pGEX with a GST tag, respectively. To generate kinase-dead mutant of MpFER and MpLYK1, site-directed mutagenesis was performed using the Q5 Site-Directed Mutagenesis Kit (NEB), and mutations were confirmed by sequence analysis. The primers used for mutagenesis are listed in chapter 5.1.1. All plasmids were transformed into *E. coli* strain Rosetta (DE3). Cultures of *E. coli* strains harbouring constructs were supplemented with 1 µM IPTG at OD_{600} 0.8 at 16 °C for 16 hours. The recombinant proteins were purified with glutathione agarose (PureCube) or Ni-NTA agarose (PureCube) according to the manufacturers'

instructions. Purified proteins were aliquoted and snap-frozen in liquid nitrogen and stored at -80 °C until further analysis.

5.2.17 *in vitro* kinase assay

For the kinase assay, approximately 1 µg of each fusion protein, MBPHis-FER-KD, GST-LYK1, and GST-LYK1-KD were utilised. MBPHis-FER was treated with FastAP thermosensitive alkaline phosphatase (ThermoFisher), and the reactions were terminated by heating at 70 °C for 30 mins. Then MBPHis-FER was incubated with either GST-LYK1 or GST-LYK1-KD in kinase reaction buffer containing 50 mM, Tris-HCl (pH 7.55), 10 mM MgCl2, 1 mM DTT, and 10 mM ATP in a final volume of 10 µL. The reaction was incubated for 1 hour at 24 °C, terminated by adding equal volume of SDS sample buffer, and then heated at 70 °C for 10 mins.

5.2.18 Immunoblotting

The samples from *in vitro* kinase assay were then separated by 6% 20 µM Mn^{2+}-Phos-Tag polyacrylamide gel. Preparation and use of Mn^{2+}-Phos-Tag polyacrylamide gels and subsequent immunoblot was performed as described by the manufacture (FUJIFILM wako). The gel was run at 140 V (25 mA) for 150 mins at 4 °C. The resolving gel was then washed six times in 15 mL of transfer buffer containing 10 mM EDTA with gentle shaking for 10 mins each time and then washed twice for 15 mins each time in transfer buffer without EDTA. Proteins were then blotted onto polyvinylidene fluoride (PVDF) membranes (Bio-Rad) using a Trans-Blot Turbo (Bio-Rad) transfer system at room temperature. Membranes were blocked using 5% non-fat milk in T-BST buffer. For detection of MBPHis-FER-KD, membranes were probed with 1:1000 dilution of Anti-His (Cell Signaling) and 1:10000 dilution of anti-mouse HRP secondary antibody (Cell Signaling). For detection of GST-LYK1 and GST-LYK1-KD, membranes were probed with 1:1000 dilution Anti-GST (Cell Signaling) and 1:10000 dilution of anti-mouse HRP secondary antibody (Cell Signaling).

For immunoblotting of protein extracts from transgenic lines expressing target protein tagged with miniTurbo-Myc, proteins were separated by SDS-polyacrylamide-gel electrophoresis (PAGE) and blotted onto PVDF membranes (Bio-Rad) using a Trans-Blot Turbo (Bio-Rad) transfer system. Membranes were blocked using 5% non-fat milk in T-BST buffer. For detection of biotinylated proteins, membranes were probed with HRP-conjugated streptavidin (Cell Signalling). For detection of Myc-tagged proteins, membrane was probed with anti-Myc-tag mouse monoclonal antibody (Cell Signaling) and HRP-conjugated anti-

mouse immunoglobulin G (IgG) antibody (Cell Signaling). All membranes were probed with primary antibody for 1 hour at room temperature or overnight at 4 °C and then probed with secondary antibody for 1 hour at room temperature. Proteins were visualised on the membranes using a luminol-based chemiluminescent substrate that is oxidised by HRP in the presence of peroxide (ThermoFisher).

5.2.19 Statistical analysis

Excel, R (4.2.3) and RStudio (2024.04.1) were used for statistical analysis and drawing figures. Bacterial growth and ROS burst quantifications were statistically analysed using Student's t-test, with p-values adjusted by the BH method. Statistical analysis of total ROS production was performed using the Tukey-HSD test. Statistically significant differences were defined as values with $p < 0.05$.

In qRT-PCR and root inhibition assay, statistical analysis was performed by applying one-way ANOVA followed by Dunnet's test, comparing each treatment to the mock control using Prism 9.0 (GraphPad).

5.2.20 Cryo-scanning electron microscopy (Cryo-SEM)

Samples were mounted on copper sample holders, snap-frozen in liquid nitrogen and sublimated, sputtered with Gold/Palladium mixture (80% Gold/20% Palladium) using an Emitech K1250X cryo system, and then images were taken using a Zeiss Supra 40VP scanning electron microscope.

5.2.21 FRET–FLIM

Nicotiana benthamiana leaf samples expressing either only GFP as donor in absence of mCherry as acceptor, or in combination with mCherry, were mounted on microscope slides in water, covered with a high precision cover glass and immediately used for analysis of fluorescence lifetimes. For this, a Leica SP8 FALCON-DIVE confocal system, equipped with an InSight X3 pulsed laser from Spectra Physics with a fixed laser line of 1045 and a line tunable from 680 to 1300 nm, was used in combination with either a 40x/1.25 NA GLYC or 40x/1.10 W immersion objective. For imaging and FLIM experiments, GFP was excited with 930 nm and the emission window from 490 to 550 nm was recorded with the RLD detector. To observe FRET between GFP as donor and mCherry as acceptor, only the donor fluorescence was recorded for lifetime imaging. Images with a frame size of 512 by 512 pixels were acquired until a level of 1000 photons were reached for the maximum pixel value. Mean τ intensity

weighted lifetimes (ns) were averaged across multiple regions of interest, containing two neighbouring cells.

5.2.22 Interactome analysis

Interactome analysis was carried out as described before (Melkonian et al. 2022). Briefly,14-day-old thalli were collected, vacuum-infiltrated with 700 µM biotin solutions, and incubated overnight in biotin solution with gentle shaking at room temperature. After incubation, thalli were washed with Milli-Q water, drained on filter paper, and snap-frozen in liquid nitrogen. Plants were ground into tissue powder and the total protein was extracted. Then, 500 µg of total protein were used for biotin depletion by MeOH:$ChCl_3$ precipitation. Biotinylated proteins were pulled down using streptavidin magnetic Sepharose (GE Healthcare Life Sciences) and then processed for on-bead digested with trypsin. Biotin-treated samples were also analysed through immunoblotting analysis.

Sample processing. After removal of the supernatant the beads were submitted to on-bead digestion. To this end, beads were resuspended in 25 µL digest buffer 1 (50 mM Tris pH 7.5, 2M Urea, 1 mM DTT, 5µg/mL Trypsin) and incubated in a Thermomixer at 32 °C with 400 rpm for 30 mins. The supernatant was transferred to a fresh tube and the beads were treated with 50 µL digest buffer 2 (50 mM Tris pH 7.5, 2 M Urea, 5 mM CAA), mixed briefly, the supernatant was combined with the previous one and the total digest was incubated overnight in a Thermomixer at 32 °C with 400 rpm. After acidification with 10% TFA (5 µL) samples were desalted with C18 Empore disk membranes according to the StageTip protocol (Rappsilber 2003). The eluted peptides were dried and then taken up in 10 µL A* buffer and peptide concentration was determined by Nanodrop.

LC-MS/MS data acquisition. Samples were analysed using an EASY-nLC 1200 (ThermoFisher) coupled to a QExactive Plus mass spectrometer (ThermoFisher). Peptides were separated on 16-cm frit-less silica emitters (New Objective, 75 µm inner diameter), packed in-house with reversed-phase ReproSil-Pur C18 AQ 1.9 µm resin (Dr. Maisch). Peptides were loaded on the column and eluted for 60 mins (For analysis of MpSERK) or 115 mins (For analysis of MpFER and MpLYK1) using a segmented linear gradient of 5% to 95% solvent B (0 min: 5% B; 0–5 mins -> 5% B; 5–25 mins -> 15% B; 25–50 mins -> 35%B; 50–55 mins -> 95% B; 55–60 mins -> 95% B) (For analysis of MpSERK) or (0 min: 5% B; 0–5 mins -> 5% B; 5–65 mins -> 20% B; 65–90 mins -> 35% B; 90–100 mins -> 55%; 100–105 mins -> 95%, 105–115 mins -> 95%) (For analysis of MpFER and MpLYK1) (solvent A 0% ACN, 0.1% FA; solvent B 80% ACN, 0.1% FA) at a flow rate of 300 nL/min. Mass spectra were acquired in

data-dependent acquisition mode with the TOP12 method (For analysis of MpSERK) or TOP15 method (For analysis of MpFER and MpLYK1). MS spectra were acquired in the Orbitrap analyser with a mass range of 300–1500 m/z (For analysis of MpSERK) or 300–1750 m/z (For analysis of MpFER and MpLYK1) at a resolution of 70,000 FWHM and a target value of 3×10^6 ions. Precursors were selected with an isolation window of 1.3 m/z. HCD fragmentation was performed at a normalised collision energy of 25. MS/MS spectra were acquired with a target value of $5x10^5$ ions at a resolution of 17,500 FWHM, a maximum injection time of 85 ms (For analysis of MpSERK) or 55 ms (For analysis of MpFER and MpLYK1) and a fixed first mass of m/z 100. Peptides with a charge of 1, greater than 6, or with unassigned charge state were excluded from fragmentation for MS^2; dynamic exclusion for 20 s (For analysis of MpSERK) or 30 s (For analysis of MpFER and MpLYK1) prevented repeated selection of precursors.

Data analysis. Raw data were processed using MaxQuant software (version 1.6.3.4) (http://www.maxquant.org/) (Cox and Mann 2008) with label-free quantification (LFQ) and iBAQ-enabled (Tyanova, Temu, and Cox 2016), normalisation was skipped for the LFQ quantification. MS/MS spectra were searched by the Andromeda search engine against a combined database containing the sequences from *M. polymorpha* (MpTak1v5.1_r1_primary_transcripts_proteinV3; https://marchantia.info/) and sequences of 248 common contaminant proteins and decoy sequences and the sequence of the miniTurbo tag. Trypsin specificity was required and a maximum of two missed cleavages allowed. Minimal peptide length was set to seven amino acids. Carbamidomethylation of cysteine residues was set as fixed, oxidation of methionine and protein N-terminus acetylation as variable modifications. Peptide-spectrum-matches and proteins were retained if they were below a false discovery rate of 1%.

The non-normalised MaxLFQ values of every two-genotype combination (five replicates per condition) were pre-processed in Perseus (version 1.5.8.5) (http://www.maxquant.org/) and submitted for normalisation analysis using the Normalyser tool (http://normalyzer.immunoprot.lth.se/) (Chawade, Alexandersson, and Levander 2014). The output was analysed for outliers and one replicate per condition was removed in the subsequent data analysis. The final data analysis was carried out in MaxQuant as described above on the reduced raw dataset; each two-genotype combination was searched independently.

Statistical analysis of the MaxLFQ values was carried out using Perseus. Quantified proteins were filtered for reverse hits and hits “identified by site” and MaxLFQ values were log2-transformed and the data was normalised by subtraction of the median per column. After grouping samples by condition only those proteins were retained for the subsequent analysis

that had three valid values in one of the conditions. Two-sample *t*-tests were performed using a permutation-based FDR of 5%. The output was exported to Excel for further processing. Alternatively, data was filtered for either three or four valid values in one of the conditions and missing values were imputed from a normal distribution (1.8 downshift, separately for each column). Volcano plots were generated in Perseus using an FDR of 5% and an *S0*=1. The Perseus output was exported and further processed using Excel and R.

References

Abarca, A., C. M. Franck, and C. Zipfel. 2021. "Family-wide evaluation of RAPID ALKALINIZATION FACTOR peptides." *Plant Physiol* 187 (2):996-1010. doi: 10.1093/plphys/kiab308.

Alhoraibi, H., J. Bigeard, N. Rayapuram, J. Colcombet, and H. Hirt. 2019. "Plant Immunity: The MTI-ETI Model and Beyond." *Curr Issues Mol Biol* 30:39-58. doi: 10.21775/cimb.030.039.

Althoff, F., S. Kopischke, O. Zobell, K. Ide, K. Ishizaki, T. Kohchi, and S. Zachgo. 2014. "Comparison of the MpEF1alpha and CaMV35 promoters for application in Marchantia polymorpha overexpression studies." *Transgenic Res* 23 (2):235-44. doi: 10.1007/s11248-013-9746-z.

Bhalla, Hemal, Karthik Sudarsanam, Ashutosh Srivastava, and Subramanian Sankaranarayanan. 2024. "Structural insights into the recognition of RALF peptides 1 by FERONIA receptor kinase during Brassicaceae Pollination." *bioRxiv*. doi: 10.1101/2024.07.02.601642.

Blackburn, M. R., M. Haruta, and D. S. Moura. 2020. "Twenty Years of Progress in Physiological and Biochemical Investigation of RALF Peptides." *Plant Physiol* 182 (4):1657-1666. doi: 10.1104/pp.19.01310.

Bohm, H., I. Albert, L. Fan, A. Reinhard, and T. Nurnberger. 2014. "Immune receptor complexes at the plant cell surface." *Curr Opin Plant Biol* 20:47-54. doi: 10.1016/j.pbi.2014.04.007.

Boutrot, Freddy, and Cyril Zipfel. 2017. "Function, Discovery, and Exploitation of Plant Pattern Recognition Receptors for Broad-Spectrum Disease Resistance." *Annual Review of Phytopathology* 55 (Volume 55, 2017):257-286. doi: https://doi.org/10.1146/annurev-phyto-080614-120106.

Bowman, J. L. 2022. "The liverwort Marchantia polymorpha, a model for all ages." *Curr Top Dev Biol* 147:1-32. doi: 10.1016/bs.ctdb.2021.12.009.

Bowman, J. L., T. Kohchi, K. T. Yamato, J. Jenkins, S. Shu, K. Ishizaki, S. Yamaoka, R. Nishihama, Y. Nakamura, F. Berger, C. Adam, S. S. Aki, F. Althoff, T. Araki, M. A. Arteaga-Vazquez, S. Balasubrmanian, K. Barry, D. Bauer, C. R. Boehm, L. Briginshaw, J. Caballero-Perez, B. Catarino, F. Chen, S. Chiyoda, M. Chovatia, K. M. Davies, M. Delmans, T. Demura, T. Dierschke, L. Dolan, A. E. Dorantes-Acosta, D. M. Eklund, S. N. Florent, E. Flores-Sandoval, A. Fujiyama, H. Fukuzawa, B. Galik, D. Grimanelli, J. Grimwood, U. Grossniklaus, T. Hamada, J. Haseloff, A. J. Hetherington, A. Higo, Y.

Hirakawa, H. N. Hundley, Y. Ikeda, K. Inoue, S. I. Inoue, S. Ishida, Q. Jia, M. Kakita, T. Kanazawa, Y. Kawai, T. Kawashima, M. Kennedy, K. Kinose, T. Kinoshita, Y. Kohara, E. Koide, K. Komatsu, S. Kopischke, M. Kubo, J. Kyozuka, U. Lagercrantz, S. S. Lin, E. Lindquist, A. M. Lipzen, C. W. Lu, E. De Luna, R. A. Martienssen, N. Minamino, M. Mizutani, M. Mizutani, N. Mochizuki, I. Monte, R. Mosher, H. Nagasaki, H. Nakagami, S. Naramoto, K. Nishitani, M. Ohtani, T. Okamoto, M. Okumura, J. Phillips, B. Pollak, A. Reinders, M. Rovekamp, R. Sano, S. Sawa, M. W. Schmid, M. Shirakawa, R. Solano, A. Spunde, N. Suetsugu, S. Sugano, A. Sugiyama, R. Sun, Y. Suzuki, M. Takenaka, D. Takezawa, H. Tomogane, M. Tsuzuki, T. Ueda, M. Umeda, J. M. Ward, Y. Watanabe, K. Yazaki, R. Yokoyama, Y. Yoshitake, I. Yotsui, S. Zachgo, and J. Schmutz. 2017. "Insights into Land Plant Evolution Garnered from the Marchantia polymorpha Genome." *Cell* 171 (2):287-304 e15. doi: 10.1016/j.cell.2017.09.030.

Campbell, L., and S. R. Turner. 2017. "A Comprehensive Analysis of RALF Proteins in Green Plants Suggests There Are Two Distinct Functional Groups." *Front Plant Sci* 8:37. doi: 10.3389/fpls.2017.00037.

Cao, J., and F. Shi. 2012. "Evolution of the RALF Gene Family in Plants: Gene Duplication and Selection Patterns." *Evol Bioinform Online* 8:271-92. doi: 10.4137/EBO.S9652.

Cao, Y. , Y. Liang, K. Tanaka, C. T. Nguyen, R. P. Jedrzejczak, A. Joachimiak, and G. Stacey. 2014. "The kinase LYK5 is a major chitin receptor in Arabidopsis and forms a chitin-induced complex with related kinase CERK1." *Elife* 3. doi: 10.7554/eLife.03766.

Carella, P., A. Gogleva, D. J. Hoey, A. J. Bridgen, S. C. Stolze, H. Nakagami, and S. Schornack. 2019. "Conserved Biochemical Defenses Underpin Host Responses to Oomycete Infection in an Early-Divergent Land Plant Lineage." *Curr Biol* 29 (14):2282-2294 e5. doi: 10.1016/j.cub.2019.05.078.

Carella, P., A. Gogleva, M. Tomaselli, C. Alfs, and S. Schornack. 2018. "Phytophthora palmivora establishes tissue-specific intracellular infection structures in the earliest divergent land plant lineage." *Proc Natl Acad Sci U S A* 115 (16):E3846-E3855. doi: 10.1073/pnas.1717900115.

Chawade, A., E. Alexandersson, and F. Levander. 2014. "Normalyzer: a tool for rapid evaluation of normalization methods for omics data sets." *J Proteome Res* 13 (6):3114-20. doi: 10.1021/pr401264n.

Chen, S., Y. Zhou, Y. Chen, and J. Gu. 2018. "fastp: an ultra-fast all-in-one FASTQ preprocessor." *Bioinformatics* 34 (17):i884-i890. doi: 10.1093/bioinformatics/bty560.

Chinchilla, D., L. Shan, P. He, S. de Vries, and B. Kemmerling. 2009. "One for all: the receptor-associated kinase BAK1." *Trends Plant Sci* 14 (10):535-41. doi: 10.1016/j.tplants.2009.08.002.

Chinchilla, D., C. Zipfel, S. Robatzek, B. Kemmerling, T. Nurnberger, J. D. Jones, G. Felix, and T. Boller. 2007. "A flagellin-induced complex of the receptor FLS2 and BAK1 initiates plant defence." *Nature* 448 (7152):497-500. doi: 10.1038/nature05999.

Chiyoda, S., K. Ishizaki, H. Kataoka, K. T. Yamato, and T. Kohchi. 2008. "Direct transformation of the liverwort Marchantia polymorpha L. by particle bombardment using immature thalli developing from spores." *Plant Cell Rep* 27 (9):1467-73. doi: 10.1007/s00299-008-0570-5.

Coll, N. S., P. Epple, and J. L. Dangl. 2011. "Programmed cell death in the plant immune system." *Cell Death Differ* 18 (8):1247-56. doi: 10.1038/cdd.2011.37.

Cox, J., and M. Mann. 2008. "MaxQuant enables high peptide identification rates, individualized p.p.b.-range mass accuracies and proteome-wide protein quantification." *Nat Biotechnol* 26 (12):1367-72. doi: 10.1038/nbt.1511.

DeFalco, T. A., and C. Zipfel. 2021. "Molecular mechanisms of early plant pattern-triggered immune signaling." *Mol Cell* 81 (17):3449-3467. doi: 10.1016/j.molcel.2021.07.029.

Delwiche, C. F., and E. D. Cooper. 2015. "The Evolutionary Origin of a Terrestrial Flora." *Curr Biol* 25 (19):R899-910. doi: 10.1016/j.cub.2015.08.029.

Dobin, A., C. A. Davis, F. Schlesinger, J. Drenkow, C. Zaleski, S. Jha, P. Batut, M. Chaisson, and T. R. Gingeras. 2013. "STAR: ultrafast universal RNA-seq aligner." *Bioinformatics* 29 (1):15-21. doi: 10.1093/bioinformatics/bts635.

Du, C., X. Li, J. Chen, W. Chen, B. Li, C. Li, L. Wang, J. Li, X. Zhao, J. Lin, X. Liu, S. Luan, and F. Yu. 2016. "Receptor kinase complex transmits RALF peptide signal to inhibit root growth in Arabidopsis." *Proc Natl Acad Sci U S A* 113 (51):E8326-E8334. doi: 10.1073/pnas.1609626113.

Duckett, J. G., R. Ligrone, K. S. Renzaglia, and S. Pressel. 2014. "Pegged and smooth rhizoids in complex thalloid liverworts (Marchantiopsida): structure, function and evolution." *Botanical Journal of the Linnean Society* 174:68-92.

Dunser, K., S. Gupta, A. Herger, M. I. Feraru, C. Ringli, and J. Kleine-Vehn. 2019. "Extracellular matrix sensing by FERONIA and Leucine-Rich Repeat Extensins controls vacuolar expansion during cellular elongation in Arabidopsis thaliana." *EMBO J* 38 (7). doi: 10.15252/embj.2018100353.

Edwards, Dianne, Jennifer L. Morris, John B. Richardson, and Paul Kenrick. 2014. "Cryptospores and cryptophytes reveal hidden diversity in early land floras." *New Phytologist* 202 (1):50-78. doi: https://doi.org/10.1111/nph.12645.

Escobar-Restrepo, J. M., N. Huck, S. Kessler, V. Gagliardini, J. Gheyselinck, W. C. Yang, and U. Grossniklaus. 2007. "The FERONIA Receptor-like Kinase Mediates Male-Female Interactions During Pollen Tube Reception." *Science* 317. doi: 10.1126/science.1143562.

Escocard de Azevedo Manhaes, A. M., F. A. Ortiz-Morea, P. He, and L. Shan. 2021. "Plant plasma membrane-resident receptors: Surveillance for infections and coordination for growth and development." *J Integr Plant Biol* 63 (1):79-101. doi: 10.1111/jipb.13051.

Fang, Y., J. Chang, T. Shi, W. Luo, Y. Ou, D. Wan, and J. Li. 2021. "Evolution of RGF/GLV/CLEL Peptide Hormones and Their Roles in Land Plant Growth and Regulation." *Int J Mol Sci* 22 (24). doi: 10.3390/ijms222413372.

Fontes, E. P. B. 2023. "SERKs and NIKs: Coreceptors or signaling hubs in a complex crosstalk between growth and defense?" *Curr Opin Plant Biol*:102447. doi: 10.1016/j.pbi.2023.102447.

Fujioka, S., and T. Yokota. 2003. "Biosynthesis and metabolism of brassinosteroids." *Annu Rev Plant Biol* 54:137-64. doi: 10.1146/annurev.arplant.54.031902.134921.

Furumizu, C., and S. Sawa. 2021. "Insight into early diversification of leucine-rich repeat receptor-like kinases provided by the sequenced moss and hornwort genomes." *Plant Mol Biol*. doi: 10.1007/s11103-020-01100-0.

Gao, M., X. Wang, D. Wang, F. Xu, X. Ding, Z. Zhang, D. Bi, Y. T. Cheng, S. Chen, X. Li, and Y. Zhang. 2009. "Regulation of cell death and innate immunity by two receptor-like kinases in Arabidopsis." *Cell Host Microbe* 6 (1):34-44. doi: 10.1016/j.chom.2009.05.019.

Gao, Yuxia, Wenqiang Wang, Tian Zhang, Zhen Gong, Huayao Zhao, and Guan-Zhu Han. 2018. "Out of Water: The Origin and Early Diversification of Plant R-Genes." *Plant Physiology* 177 (1):82-89. doi: 10.1104/pp.18.00185.

Ge, S. X., D. Jung, and R. Yao. 2020. "ShinyGO: a graphical gene-set enrichment tool for animals and plants." *Bioinformatics* 36 (8):2628-2629. doi: 10.1093/bioinformatics/btz931.

Gimenez-Ibanez, S., A. M. Zamarreno, J. M. Garcia-Mina, and R. Solano. 2019. "An Evolutionarily Ancient Immune System Governs the Interactions between

Pseudomonas syringae and an Early-Diverging Land Plant Lineage." *Curr Biol* 29 (14):2270-2281 e4. doi: 10.1016/j.cub.2019.05.079.

Ginanjar, E. F., O. K. Teh, and T. Fujita. 2022. "Characterisation of rapid alkalinisation factors in Physcomitrium patens reveals functional conservation in tip growth." *New Phytol* 233 (6):2442-2457. doi: 10.1111/nph.17942.

Gómez-Gómez, L., and T. Boller. 2000. "FLS2: An LRR Receptor–like Kinase Involved in the Perception of the Bacterial Elicitor Flagellin in Arabidopsis." *molecular Cell* 5:1003-1011.

Gonneau, M., T. Desprez, M. Martin, V. G. Doblas, L. Bacete, F. Miart, R. Sormani, K. Hematy, J. Renou, B. Landrein, E. Murphy, B. Van De Cotte, S. Vernhettes, I. De Smet, and H. Hofte. 2018. "Receptor Kinase THESEUS1 Is a Rapid Alkalinization Factor 34 Receptor in Arabidopsis." *Curr Biol* 28 (15):2452-2458 e4. doi: 10.1016/j.cub.2018.05.075.

Guzman-Benito, I., L. Donaire, V. Amorim-Silva, J. G. Vallarino, A. Esteban, A. T. Wierzbicki, V. Ruiz-Ferrer, and C. Llave. 2019. "The immune repressor BIR1 contributes to antiviral defense and undergoes transcriptional and post-transcriptional regulation during viral infections." *New Phytol* 224 (1):421-438. doi: 10.1111/nph.15931.

Guzmán-Benito, Irene, Carmen Robinson, Chenlei Hua, Ana Rocio Sede, Laura Elvira-González, Isabel Punzón, Manfred Heinlein, Thorsten Nürnberger, and César Llave. 2024. "The receptor-like kinase BIR1 inhibits elicitor-induced plasmodesmata callose deposition and PTI gene expression and requires EDS1 and SOBIR1 to cause dose-dependent cell-death in Arabidopsis." *bioRxiv*. doi: 10.1101/2023.06.23.546234.

Halter, T., J. Imkampe, S. Mazzotta, M. Wierzba, S. Postel, C. Bucherl, C. Kiefer, M. Stahl, D. Chinchilla, X. Wang, T. Nurnberger, C. Zipfel, S. Clouse, J. W. Borst, S. Boeren, S. C. de Vries, F. Tax, and B. Kemmerling. 2014. "The leucine-rich repeat receptor kinase BIR2 is a negative regulator of BAK1 in plant immunity." *Curr Biol* 24 (2):134-143. doi: 10.1016/j.cub.2013.11.047.

Hanks, S. K. A. M. Quinn, T. Hunter. 1988. "The protein kinase family: conserved features and deduced phylogeny of the catalytic domains." *Science* 241 (4861):41-52. doi: 10.1126/science.3291115.

Haruta, M., G. Sabat, K. Stecker, B. B. Minkoff, and M. R. Sussman. 2014a. "A Peptide Hormone and Its Receptor Protein Kinase Regulate Plant Cell Expansion." *Science* 343:408-411.

Haruta, M., G. Sabat, K. Stecker, B. B. Minkoff, and M. R. Sussman. 2014b. "A Peptide Hormone and Its Receptor Protein Kinase Regulate Plant Cell Expansion." *Science* 343 (6169):408-411. doi: 10.1126/science.1244454.

He, Y. H., S. Y. Chen, X. Y. Chen, Y. P. Xu, Y. Liang, and X. Z. Cai. 2023. "RALF22 promotes plant immunity and amplifies the Pep3 immune signal." *J Integr Plant Biol* 65 (11):2519-2534. doi: 10.1111/jipb.13566.

Heese, A., D. R. Hann, S. Gimenez-Ibanez, A. M. Jones, K. He, J. Li, J. I. Schroeder, S. C. Peck, and J. P. Rathjen. 2007. "The receptor-like kinase SERK3/BAK1 is a central regulator of innate immunity in plants." *Proc Natl Acad Sci U S A* 104:12217-12222.

Herger, A., K. Dunser, J. Kleine-Vehn, and C. Ringli. 2019. "Leucine-Rich Repeat Extensin Proteins and Their Role in Cell Wall Sensing." *Curr Biol* 29 (17):R851-R858. doi: 10.1016/j.cub.2019.07.039.

Hirakawa, Y., N. Uchida, Y. L. Yamaguchi, R. Tabata, S. Ishida, K. Ishizaki, R. Nishihama, T. Kohchi, S. Sawa, and J. L. Bowman. 2019. "Control of proliferation in the haploid meristem by CLE peptide signaling in Marchantia polymorpha." *PLoS Genet* 15 (3):e1007997. doi: 10.1371/journal.pgen.1007997.

Hirakawa, Y., T. Fujimoto, S. Ishida, N. Uchida, S. Sawa, T. Kiyosue, K. Ishizaki, R. Nishihama, T. Kohchi, and J. L. Bowman. 2020. "Induction of Multichotomous Branching by CLAVATA Peptide in Marchantia polymorpha." *Current Biology* 30 (19):3833-3840.e4. doi: 10.1016/j.cub.2020.07.016.

Hisanaga, Tetsuya, Shohei Yamaoka, Tomokazu Kawashima, Asuka Higo, Keiji Nakajima, Takashi Araki, Takayuki Kohchi, and Frédéric Berger. 2019. "Building new insights in plant gametogenesis from an evolutionary perspective." *Nature Plants* 5 (7):663-669. doi: 10.1038/s41477-019-0466-0.

Hohmann, U., J. Nicolet, A. Moretti, L. A. Hothorn, and M. Hothorn. 2018. "The SERK3 elongated allele defines a role for BIR ectodomains in brassinosteroid signalling." *Nat Plants* 4 (6):345-351. doi: 10.1038/s41477-018-0150-9.

Honkanen, S., V. A. S. Jones, G. Morieri, C. Champion, A. J. Hetherington, S. Kelly, H. Proust, D. Saint-Marcoux, H. Prescott, and L. Dolan. 2016. "The Mechanism Forming the Cell Surface of Tip-Growing Rooting Cells Is Conserved among Land Plants." *Curr Biol* 26 (23):3238-3244. doi: 10.1016/j.cub.2016.09.062.

Huang, X. X., Y. Wang, J. S. Lin, L. Chen, Y. J. Li, Q. Liu, G. F. Wang, F. Xu, L. Liu, and B. K. Hou. 2021. "The novel pathogen-responsive glycosyltransferase UGT73C7 mediates

the redirection of phenylpropanoid metabolism and promotes SNC1-dependent Arabidopsis immunity." *Plant J* 107 (1):149-165. doi: 10.1111/tpj.15280.

Imkampe, J., T. Halter, S. Huang, S. Schulze, S. Mazzotta, N. Schmidt, R. Manstretta, S. Postel, M. Wierzba, Y. Yang, Wmam van Dongen, M. Stahl, C. Zipfel, M. B. Goshe, S. Clouse, S. C. de Vries, F. Tax, X. Wang, and B. Kemmerling. 2017. "The Arabidopsis Leucine-Rich Repeat Receptor Kinase BIR3 Negatively Regulates BAK1 Receptor Complex Formation and Stabilizes BAK1." *Plant Cell* 29 (9):2285-2303. doi: 10.1105/tpc.17.00376.

Ishizaki, K., R. Nishihama, M. Ueda, K. Inoue, S. Ishida, Y. Nishimura, T. Shikanai, and T. Kohchi. 2015. "Development of Gateway Binary Vector Series with Four Different Selection Markers for the Liverwort Marchantia polymorpha." *PLoS One* 10 (9):e0138876. doi: 10.1371/journal.pone.0138876.

Ishizaki, K., R. Nishihama, K. T. Yamato, and T. Kohchi. 2016. "Molecular Genetic Tools and Techniques for Marchantia polymorpha Research." *Plant Cell Physiol* 57 (2):262-70. doi: 10.1093/pcp/pcv097.

Iwakawa, H., K. Melkonian, T. Schluter, H. W. Jeon, R. Nishihama, H. Motose, and H. Nakagami. 2021. "Agrobacterium-Mediated Transient Transformation of Marchantia Liverworts." *Plant Cell Physiol*. doi: 10.1093/pcp/pcab126.

Jeon, B. W., J. S. Kim, E. Oh, N. Y. Kang, and J. Kim. 2023. "ROOT MERISTEM GROWTH FACTOR1 (RGF1)-RGF1 INSENSITIVE 1 peptide-receptor pair inhibits lateral root development via the MPK6-PUCHI module in Arabidopsis." *J Exp Bot* 74 (5):1475-1488. doi: 10.1093/jxb/erac495.

Ji, D., T. Chen, Z. Zhang, B. Li, and S. Tian. 2020. "Versatile Roles of the Receptor-Like Kinase Feronia in Plant Growth, Development and Host-Pathogen Interaction." *Int J Mol Sci* 21 (21). doi: 10.3390/ijms21217881.

Jian, Y., D. Gong, Z. Wang, L. Liu, J. He, X. Han, and K. Tsuda. 2024. "How plants manage pathogen infection." *EMBO Rep* 25 (1):31-44. doi: 10.1038/s44319-023-00023-3.

Jones, J. D., and J. L. Dangl. 2006. "The plant immune system." *Nature* 444 (7117):323-9. doi: 10.1038/nature05286.

Jones, V. A., and L. Dolan. 2012. "The evolution of root hairs and rhizoids." *Ann Bot* 110 (2):205-12. doi: 10.1093/aob/mcs136.

Jones, Jonathan D. G., Russell E. Vance, and Jeffery L. Dangl. 2016. "Intracellular innate immune surveillance devices in plants and animals." *Science* 354 (6316):aaf6395. doi: doi:10.1126/science.aaf6395.

Kanazawa, T., H. Morinaka, K. Ebine, T. L. Shimada, S. Ishida, N. Minamino, K. Yamaguchi, S. Shigenobu, T. Kohchi, A. Nakano, and T. Ueda. 2020. "The liverwort oil body is formed by redirection of the secretory pathway." *Nat Commun* 11 (1):6152. doi: 10.1038/s41467-020-19978-1.

Kato, H., Y. Yasui, and K. Ishizaki. 2020. "Gemma cup and gemma development in Marchantia polymorpha." *New Phytol* 228 (2):459-465. doi: 10.1111/nph.16655.

Kohchi, T., K. T. Yamato, K. Ishizaki, S. Yamaoka, and R. Nishihama. 2021. "Development and Molecular Genetics of Marchantia polymorpha." *Annu Rev Plant Biol* 72:677-702. doi: 10.1146/annurev-arplant-082520-094256.

Kubota, A., K. Ishizaki, M. Hosaka, and T. Kohchi. 2013. "Efficient Agrobacterium-mediated transformation of the liverwort Marchantia polymorpha using regenerating thalli." *Biosci Biotechnol Biochem* 77 (1):167-72. doi: 10.1271/bbb.120700.

Kumar, S., G. Stecher, and K. Tamura. 2016. "MEGA7: Molecular Evolutionary Genetics Analysis Version 7.0 for Bigger Datasets." *Mol Biol Evol* 33 (7):1870-4. doi: 10.1093/molbev/msw054.

Le, M. H., Y. Cao, X. C. Zhang, and G. Stacey. 2014. "LIK1, a CERK1-interacting kinase, regulates plant immune responses in Arabidopsis." *PLoS One* 9 (7):e102245. doi: 10.1371/journal.pone.0102245.

Li, C., F. L. Yeh, A. Y. Cheung, Q. Duan, D. Kita, M. C. Liu, J. Maman, E. J. Luu, B. W. Wu, L. Gates, M. Jalal, A. Kwong, H. Carpenter, and H. M. Wu. 2015. "Glycosylphosphatidylinositol-anchored proteins as chaperones and co-receptors for FERONIA receptor kinase signaling in Arabidopsis." *Elife* 4. doi: 10.7554/eLife.06587.

Li, J., J. Wen, K. A. Lease, J. T. Doke, F. E. Tax, and J. C. Walker. 2002. "BAK1, an Arabidopsis LRR Receptor-like Protein Kinase, Interacts with BRI1 and Modulates Brassinosteroid Signaling." *Cell* 110:213-222.

Liao, Ye, Xiangyu Wen, Jingyuan Zheng, Xin Li, Xuelei Deng, Xinqiu Tan, Xiuhui Liang, Xi Yi, and Hongdong Liao. 2023. "RALF-like peptide improves the colonization of endophytic Colletotrichum tofieldiae through interacting with plant receptor-like kinase." *Plant Pathology* 72 (9):1649-1661. doi: 10.1111/ppa.13788.

Ligrone, Roberto, Anna Carafa, Erica Lumini, Valeria Bianciotto, Paola Bonfante, and Jeffrey G. Duckett. 2007. "Glomeromycotean associations in liverworts: a molecular, cellular, and taxonomic analysis." *American Journal of Botany* 94 (11):1756-1777. doi: https://doi.org/10.3732/ajb.94.11.1756.

Lindner, H., L. M. Muller, A. Boisson-Dernier, and U. Grossniklaus. 2012. "CrRLK1L receptor-like kinases: not just another brick in the wall." *Curr Opin Plant Biol* 15 (6):659-69. doi: 10.1016/j.pbi.2012.07.003.

Liu, Y., X. Huang, M. Li, P. He, and Y. Zhang. 2016. "Loss-of-function of Arabidopsis receptor-like kinase BIR1 activates cell death and defense responses mediated by BAK1 and SOBIR1." *New Phytol* 212 (3):637-645. doi: 10.1111/nph.14072.

Liu, Z., J. Yang, Y. Long, C. Zhang, D. Wang, X. Zhang, W. Dong, L. Zhao, C. Liu, J. Zhai, and E. Wang. 2023. "Single-nucleus transcriptomes reveal spatiotemporal symbiotic perception and early response in Medicago." *Nat Plants* 9 (10):1734-1748. doi: 10.1038/s41477-023-01524-8.

Love, M. I., W. Huber, and S. Anders. 2014. "Moderated estimation of fold change and dispersion for RNA-seq data with DESeq2." *Genome Biol* 15 (12):550. doi: 10.1186/s13059-014-0550-8.

Ma, C., Y. Liu, B. Bai, Z. Han, J. Tang, H. Zhang, H. Yaghmaiean, Y. Zhang, and J. Chai. 2017. "Structural basis for BIR1-mediated negative regulation of plant immunity." *Cell Res* 27 (12):1521-1524. doi: 10.1038/cr.2017.123.

Ma, X., G. Xu, P. He, and L. Shan. 2016. "SERKing Coreceptors for Receptors." *Trends Plant Sci* 21 (12):1017-1033. doi: 10.1016/j.tplants.2016.08.014.

Malivert, A., and O. Hamant. 2023. "Why is FERONIA pleiotropic?" *Nat Plants*. doi: 10.1038/s41477-023-01434-9.

Mamaeva, Anna, Irina Lyapina, Andrey Knyazev, Nina Golub, Timur Mollaev, Elena Chudinova, Sergey Elansky, Vladislav V. Babenko, Vladimir A. Veselovsky, Ksenia M. Klimina, Tatiana Gribova, Daria Kharlampieva, Vassili Lazarev, and Igor Fesenko. 2023. "RALF peptides modulate immune response in the moss Physcomitrium patens." *Frontiers in Plant Science* 14. doi: 10.3389/fpls.2023.1077301.

Masachis, S., D. Segorbe, D. Turra, M. Leon-Ruiz, U. Furst, M. El Ghalid, G. Leonard, M. S. Lopez-Berges, T. A. Richards, G. Felix, and A. Di Pietro. 2016. "A fungal pathogen secretes plant alkalinizing peptides to increase infection." *Nat Microbiol* 1 (6):16043. doi: 10.1038/nmicrobiol.2016.43.

Matsui, H., H. Iwakawa, G. S. Hyon, I. Yotsui, S. Katou, I. Monte, R. Nishihama, R. Franzen, R. Solano, and H. Nakagami. 2020. "Isolation of Natural Fungal Pathogens from Marchantia polymorpha Reveals Antagonism between Salicylic Acid and Jasmonate during Liverwort-Fungus Interactions." *Plant Cell Physiol* 61 (2):265-275. doi: 10.1093/pcp/pcz187.

Matsumoto, Ayumi, Titus Schlüter, Katharina Melkonian, Atsushi Takeda, Hirofumi Nakagami, and Akira Mine. 2021. "A versatile Tn7 transposon-based bioluminescence tagging tool for quantitative and spatial detection of bacteria in plants." *Plant Communications*. doi: 10.1016/j.xplc.2021.100227.

McConaha, Marjorie. 1941. "Ventral Structures Effecting Capillarity in the Marchantiales." *American Journal of Botany* 28 (4):301-306. doi: 10.2307/2436787.

Mecchia, M. A., M. Rovekamp, A. Giraldo-Fonseca, D. Meier, P. Gadient, H. Vogler, D. Limacher, J. L. Bowman, and U. Grossniklaus. 2022. "The single Marchantia polymorpha FERONIA homolog reveals an ancestral role in regulating cellular expansion and integrity." *Development* 149 (19). doi: 10.1242/dev.200580.

Mecchia, M. A., G. Santos-Fernandez, N. N. Duss, S. C. Somoza, A. Boisson-Dernier, V. Gagliardini, A. Martínez-Bernardini, T. N. Fabrice, C. Ringli, J. P. Muschietti, and U. Grossniklaus. 2017. "RALF4/19 peptides interact with LRX proteins to control pollen tube growth in Arabidopsis." *Science*.

Melkonian, K., S. C. Stolze, A. Harzen, and H. Nakagami. 2022. "miniTurbo-based interactomics of two plasma membrane-localized SNARE proteins in Marchantia polymorpha." *New Phytol* 235 (2):786-800. doi: 10.1111/nph.18151.

Miya, A., I. Albert, T. Shinya, Y. Desaki, K. Ichimura, K. Shirasu, Y. Narusaka, N. Kawkami, H. Kaku, and N. Shibuya. 2007. "CERK1, a LysM receptor kinase, is essential for chitin elicitor signaling in Arabidopsis." *Proc Natl Acad Sci U S A*

Murphy, E., and I. De Smet. 2014. "Understanding the RALF family: a tale of many species." *Trends Plant Sci* 19 (10):664-71. doi: 10.1016/j.tplants.2014.06.005.

Montgomery, S. A., Y. Tanizawa, B. Galik, N. Wang, T. Ito, T. Mochizuki, S. Akimcheva, J. L. Bowman, V. Cognat, L. Marechal-Drouard, H. Ekker, S. F. Hong, T. Kohchi, S. S. Lin, L. D. Liu, Y. Nakamura, L. R. Valeeva, E. V. Shakirov, D. E. Shippen, W. L. Wei, M. Yagura, S. Yamaoka, K. T. Yamato, C. Liu, and F. Berger. 2020. "Chromatin Organization in Early Land Plants Reveals an Ancestral Association between H3K27me3, Transposons, and Constitutive Heterochromatin." *Curr Biol* 30 (4):573-588 e7. doi: 10.1016/j.cub.2019.12.015.

Morato do Canto, A., P. H. Ceciliato, B. Ribeiro, F. A. Ortiz Morea, A. A. Franco Garcia, M. C. Silva-Filho, and D. S. Moura. 2014. "Biological activity of nine recombinant AtRALF peptides: implications for their perception and function in Arabidopsis." *Plant Physiol Biochem* 75:45-54. doi: 10.1016/j.plaphy.2013.12.005.

Morris, J. L., M. N. Puttick, J. W. Clark, D. Edwards, P. Kenrick, S. Pressel, C. H. Wellman, Z. Yang, H. Schneider, and P. C. J. Donoghue. 2018. "The timescale of early land plant evolution." *Proc Natl Acad Sci U S A* 115 (10):E2274-E2283. doi: 10.1073/pnas.1719588115.

Nam, K. H., J. Li. 2002. "BRI1/BAK1, a Receptor Kinase Pair Mediating Brassinosteroid Signaling." *Cell* 110 (2):203-212. doi: 10.1016/s0092-8674(02)00814-0.

Ngou, B. P. M., H. K. Ahn, P. Ding, and J. D. G. Jones. 2021. "Mutual potentiation of plant immunity by cell-surface and intracellular receptors." *Nature* 592 (7852):110-115. doi: 10.1038/s41586-021-03315-7.

Ngou, B. P. M., P. Ding, and J. D. G. Jones. 2022. "Thirty years of resistance: Zig-zag through the plant immune system." *Plant Cell* 34 (5):1447-1478. doi: 10.1093/plcell/koac041.

Ngou, Bruno Pok Man, Michele Wyler, Marc W. Schmid, Yasuhiro Kadota, and Ken Shirasu. 2024. "Evolutionary trajectory of pattern recognition receptors in plants." *Nature Communications* 15 (1). doi: 10.1038/s41467-023-44408-3.

Nishiyama, T., P. G. Wolf, M. Kugita, R. B. Sinclair, M. Sugita, C. Sugiura, T. Wakasugi, K. Yamada, K. Yoshinaga, K. Yamaguchi, K. Ueda, and M. Hasebe. 2004. "Chloroplast phylogeny indicates that bryophytes are monophyletic." *Molecular Biology and Evolution* 21 (10):1813-1819. doi: 10.1093/molbev/msh203.

Olsen, Addie Nina, John Mundy, and Karen Skriver. 2002. "Peptomics, Identification of Novel Cationic Arabidopsis Peptides with Conserved Sequence Motifs." *In Silico Biology* 2:441-451.

Ortiz-Morea, F. A., J. Liu, L. Shan, and P. He. 2022. "Malectin-like receptor kinases as protector deities in plant immunity." *Nat Plants* 8 (1):27-37. doi: 10.1038/s41477-021-01028-3.

Osakabe, Yuriko, Kazuko Yamaguchi-Shinozaki, Kazuo Shinozaki, and Lam-Son Phan Tran. 2013. "Sensing the environment: key roles of membrane-localized kinases in plant perception and response to abiotic stress." *Journal of Experimental Botany* 64 (2):445-458. doi: 10.1093/jxb/ers354.

Pearce, G., D. S. Moura, J. Stratmann, and C. A. Ryan, Jr. 2001. "RALF, a 5-kDa ubiquitous polypeptide in plants, arrests root growth and development." *Proc Natl Acad Sci U S A* 98 (22):12843-7. doi: 10.1073/pnas.201416998.

Pearce, Gregory, Yube Yamaguchi, Gerhard Munske, and Clarence A. Ryan. 2010. "Structure–activity studies of RALF, Rapid Alkalinization Factor, reveal an essential – YISY –

motif." *Peptides* 31 (11):1973-1977. doi: https://doi.org/10.1016/j.peptides.2010.08.012.

Perraki, A., T. A. DeFalco, P. Derbyshire, J. Avila, D. Sere, J. Sklenar, X. Qi, L. Stransfeld, B. Schwessinger, Y. Kadota, A. P. Macho, S. Jiang, D. Couto, K. U. Torii, F. L. H. Menke, and C. Zipfel. 2018. "Phosphocode-dependent functional dichotomy of a common co-receptor in plant signalling." *Nature* 561 (7722):248-252. doi: 10.1038/s41586-018-0471-x.

Pruitt, R. N., A. A. Gust, and T. Nurnberger. 2021. "Plant immunity unified." *Nat Plants* 7 (4):382-383. doi: 10.1038/s41477-021-00903-3.

Prusky, D., J. L. McEvoy, B. Leverentz, W. S. Conway. 2001. "Local Modulation of Host pH by Colletotrichum Species as a Mechanism to Increase Virulence." *Mol Plant Microbe Interact* 14 (9):1105-1113. doi: 10.1094/MPMI.2001.14.9.1105.

Puttick, M. N., J. L. Morris, T. A. Williams, C. J. Cox, D. Edwards, P. Kenrick, S. Pressel, C. H. Wellman, H. Schneider, D. Pisani, and P. C. J. Donoghue. 2018. "The Interrelationships of Land Plants and the Nature of the Ancestral Embryophyte." *Curr Biol* 28 (5):733-745 e2. doi: 10.1016/j.cub.2018.01.063.

Rappsilber, J., Y. Ishihama, M. Mann. 2003. "Stop and Go Extraction Tips for Matrix-AssistedLaser Desorption/Ionization, Nanoelectrospray,and LC/MS Sample Pretreatment in Proteomics." *Analytical Chemistry* 75 (3):663-670. doi: 10.1021/ac026117i.

Redkar, A., S. Gimenez Ibanez, M. Sabale, B. Zechmann, R. Solano, and A. Di Pietro. 2022. "Marchantia polymorpha model reveals conserved infection mechanisms in the vascular wilt fungal pathogen Fusarium oxysporum." *New Phytol* 234 (1):227-241. doi: 10.1111/nph.17909.

Redkar, Amey, Selena Gimenez Ibanez, Mugdha Sabale, Bernd Zechmann, Roberto Solano, and Antonio Di Pietro. 2021. "Marchantia polymorpha model reveals conserved infection mechanisms in the vascular wilt fungal pathogen Fusarium oxysporum." doi: 10.1101/2021.03.20.436100.

Romani, F., E. Banic, S. N. Florent, T. Kanazawa, J. Q. D. Goodger, R. A. Mentink, T. Dierschke, S. Zachgo, T. Ueda, J. L. Bowman, M. Tsiantis, and J. E. Moreno. 2020. "Oil Body Formation in Marchantia polymorpha Is Controlled by MpC1HDZ and Serves as a Defense against Arthropod Herbivores." *Curr Biol* 30 (14):2815-2828 e8. doi: 10.1016/j.cub.2020.05.081.

Romani, F., J. R. Flores, J. I. Tolopka, G. Suarez, X. He, and J. E. Moreno. 2022. "Liverwort oil bodies: diversity, biochemistry, and molecular cell biology of the earliest secretory structure of land plants." *J Exp Bot* 73 (13):4427-4439. doi: 10.1093/jxb/erac134.

Roux, M., B. Schwessinger, C. Albrecht, D. Chinchilla, A. Jones, N. Holton, F. G. Malinovsky, M. Tor, S. de Vries, and C. Zipfel. 2011. "The Arabidopsis leucine-rich repeat receptor-like kinases BAK1/SERK3 and BKK1/SERK4 are required for innate immunity to hemibiotrophic and biotrophic pathogens." *Plant Cell* 23 (6):2440-55. doi: 10.1105/tpc.111.084301.

Sauret-Gueto, S., E. Frangedakis, L. Silvestri, M. Rebmann, M. Tomaselli, K. Markel, M. Delmans, A. West, N. J. Patron, and J. Haseloff. 2020. "Systematic Tools for Reprogramming Plant Gene Expression in a Simple Model, Marchantia polymorpha." *ACS Synth Biol* 9 (4):864-882. doi: 10.1021/acssynbio.9b00511.

Schoenaers, S., D. Balcerowicz, G. Breen, K. Hill, M. Zdanio, G. Mouille, T. J. Holman, J. Oh, M. H. Wilson, N. Nikonorova, L. D. Vu, I. De Smet, R. Swarup, W. H. De Vos, I. Pintelon, D. Adriaensen, C. Grierson, M. J. Bennett, and K. Vissenberg. 2018. "The Auxin-Regulated CrRLK1L Kinase ERULUS Controls Cell Wall Composition during Root Hair Tip Growth." *Curr Biol* 28 (5):722-732 e6. doi: 10.1016/j.cub.2018.01.050.

Schulze, B., T. Mentzel, A. K. Jehle, K. Mueller, S. Beeler, T. Boller, G. Felix, and D. Chinchilla. 2010. "Rapid heteromerization and phosphorylation of ligand-activated plant transmembrane receptors and their associated kinase BAK1." *J Biol Chem* 285 (13):9444-9451. doi: 10.1074/jbc.M109.096842.

Shimamura, M. 2016. "Marchantia polymorpha: Taxonomy, Phylogeny and Morphology of a Model System." *Plant Cell Physiol* 57 (2):230-56. doi: 10.1093/pcp/pcv192.

Smakowska-Luzan, E., G. A. Mott, K. Parys, M. Stegmann, T. C. Howton, M. Layeghifard, J. Neuhold, A. Lehner, J. Kong, K. Grunwald, N. Weinberger, S. B. Satbhai, D. Mayer, W. Busch, M. Madalinski, P. Stolt-Bergner, N. J. Provart, M. S. Mukhtar, C. Zipfel, D. Desveaux, D. S. Guttman, and Y. Belkhadir. 2018. "An extracellular network of Arabidopsis leucine-rich repeat receptor kinases." *Nature* 553 (7688):342-346. doi: 10.1038/nature25184.

Somssich, Marc, and Rüdiger Simon. 2017. "Studying Protein–Protein Interactions In Planta Using Advanced Fluorescence Microscopy." In *Plant Genomics*, 267-285.

Srivastava, R., J. X. Liu, H. Guo, Y. Yin, and S. H. Howell. 2009. "Regulation and processing of a plant peptide hormone, AtRALF23, in Arabidopsis." *Plant J* 59 (6):930-9. doi: 10.1111/j.1365-313X.2009.03926.x.

Stegmann, M., J. Monaghan, E. Smakowska-Luzan, H. Rovenich, A. Lehner, N. Holton, Y. Belkhadir, and C. Zipfel. 2017. "The receptor kinase FER is a RALF-regulated scaffold controlling plant immune signaling." *Science*.

Sugano, S. S., R. Nishihama, M. Shirakawa, J. Takagi, Y. Matsuda, S. Ishida, T. Shimada, I. Hara-Nishimura, K. Osakabe, and T. Kohchi. 2018. "Efficient CRISPR/Cas9-based genome editing and its application to conditional genetic analysis in Marchantia polymorpha." *PLoS One* 13 (10):e0205117. doi: 10.1371/journal.pone.0205117.

Sun, Y., Z. Han, J. Tang, Z. Hu, C. Chai, B. Zhou, and J. Chai. 2013. "Structure reveals that BAK1 as a co-receptor recognizes the BRI1-bound brassinolide." *Cell Res* 23 (11):1326-9. doi: 10.1038/cr.2013.131.

Takahashi, G., S. Betsuyaku, N. Okuzumi, T. Kiyosue, and Y. Hirakawa. 2021. "An Evolutionarily Conserved Coreceptor Gene Is Essential for CLAVATA Signaling in Marchantia polymorpha." *Front Plant Sci* 12:657548. doi: 10.3389/fpls.2021.657548.

Tanaka, K., and M. Heil. 2021. "Damage-Associated Molecular Patterns (DAMPs) in Plant Innate Immunity: Applying the Danger Model and Evolutionary Perspectives." *Annu Rev Phytopathol* 59:53-75. doi: 10.1146/annurev-phyto-082718-100146.

Thomma, B. P., T. Nurnberger, and M. H. Joosten. 2011. "Of PAMPs and effectors: the blurred PTI-ETI dichotomy." *Plant Cell* 23 (1):4-15. doi: 10.1105/tpc.110.082602.

Thynne, Elisha, Isabel M. L. Saur, Jaime Simbaqueba, Huw A. Ogilvie, Yvonne Gonzalez-Cendales, Oliver Mead, Adam Taranto, Ann-Maree Catanzariti, Megan C. McDonald, Benjamin Schwessinger, David A. Jones, John P. Rathjen, and Peter S. Solomon. 2017. "Fungal phytopathogens encode functional homologues of plant rapid alkalinization factor (RALF) peptides." *Molecular Plant Pathology* 18 (6):811-824. doi: 10.1111/mpp.12444.

Tyanova, S., T. Temu, and J. Cox. 2016. "The MaxQuant computational platform for mass spectrometry-based shotgun proteomics." *Nat Protoc* 11 (12):2301-2319. doi: 10.1038/nprot.2016.136.

Wang, G., Z. Zhao, X. Zheng, W. Shan, and J. Fan. 2022. "How a single receptor-like kinase exerts diverse roles: lessons from FERONIA." *Mol Hortic* 2 (1):25. doi: 10.1186/s43897-022-00046-9.

Westermann, J., E. Koebke, R. Lentz, M. Hulskamp, and A. Boisson-Dernier. 2020. "A Comprehensive Toolkit for Quick and Easy Visualization of Marker Proteins, Protein-Protein Interactions and Cell Morphology in Marchantia polymorpha." *Front Plant Sci* 11:569194. doi: 10.3389/fpls.2020.569194.

Westermann, J., S. Streubel, C. M. Franck, R. Lentz, L. Dolan, and A. Boisson-Dernier. 2019. "An Evolutionarily Conserved Receptor-like Kinases Signaling Module Controls Cell Wall Integrity During Tip Growth." *Curr Biol* 29 (22):3899-3908 e3. doi: 10.1016/j.cub.2019.09.069.

Wickett, N. J., S. Mirarab, N. Nguyen, T. Warnow, E. Carpenter, N. Matasci, S. Ayyampalayam, M. S. Barker, J. G. Burleigh, M. A. Gitzendanner, B. R. Ruhfel, E. Wafula, J. P. Der, S. W. Graham, S. Mathews, M. Melkonian, D. E. Soltis, P. S. Soltis, N. W. Miles, C. J. Rothfels, L. Pokorny, A. J. Shaw, L. DeGironimo, D. W. Stevenson, B. Surek, J. C. Villarreal, B. Roure, H. Philippe, C. W. dePamphilis, T. Chen, M. K. Deyholos, R. S. Baucom, T. M. Kutchan, M. M. Augustin, J. Wang, Y. Zhang, Z. Tian, Z. Yan, X. Wu, X. Sun, G. K. Wong, and J. Leebens-Mack. 2014. "Phylotranscriptomic analysis of the origin and early diversification of land plants." *Proc Natl Acad Sci U S A* 111 (45):E4859-68. doi: 10.1073/pnas.1323926111.

Willmann, R., H. M. Lajunen, G. Erbs, M. A. Newman, D. Kolb, K. Tsuda, F. Katagiri, J. Fliegmann, J. J. Bono, J. V. Cullimore, A. K. Jehle, F. Gotz, A. Kulik, A. Molinaro, V. Lipka, A. A. Gust, and T. Nurnberger. 2011. "Arabidopsis lysin-motif proteins LYM1 LYM3 CERK1 mediate bacterial peptidoglycan sensing and immunity to bacterial infection." *Proc Natl Acad Sci U S A* 108 (49):19824-9. doi: 10.1073/pnas.1112862108.

Xi, L., X. N. Wu, M. Gilbert, and W. X. Schulze. 2019. "Classification and Interactions of LRR Receptors and Co-receptors Within the Arabidopsis Plasma Membrane - An Overview." *Front Plant Sci* 10:472. doi: 10.3389/fpls.2019.00472.

Xiao, Y., M. Stegmann, Z. Han, T. A. DeFalco, K. Parys, L. Xu, Y. Belkhadir, C. Zipfel, and J. Chai. 2019. "Mechanisms of RALF peptide perception by a heterotypic receptor complex." *Nature* 572 (7768):270-274. doi: 10.1038/s41586-019-1409-7.

Yamaoka, S., K. Inoue, and T. Araki. 2021. "Regulation of gametangia and gametangiophore initiation in the liverwort Marchantia polymorpha." *Plant Reprod* 34 (4):297-306. doi: 10.1007/s00497-021-00419-y.

Yan, Yijia, Jaqueline Mellüh, Martin A. Mecchia, Hyung-Woo Jeon, Katharina Melkonian, Clemens Holzberger, Anne Harzen, Sara Christina Stolze, Rainer Franzen, Yuki Hirakawa, Ana I. Caño Delgado, and Hirofumi Nakagami. 2024. "Conserved role of the SERK–BIR module in development and immunity across land plants." *bioRxiv*:2024.08.14.607940. doi: 10.1101/2024.08.14.607940.

Yang, H., D. Wang, L. Guo, H. Pan, R. Yvon, S. Garman, H. M. Wu, and A. Y. Cheung. 2021. "Malectin/Malectin-like domain-containing proteins: A repertoire of cell surface

molecules with broad functional potential." *Cell Surf* 7:100056. doi: 10.1016/j.tcsw.2021.100056.

Yotsui, I., H. Matsui, S. Miyauchi, H. Iwakawa, K. Melkonian, T. Schluter, S. Michavila, T. Kanazawa, Y. Nomura, S. C. Stolze, H. W. Jeon, Y. Yan, A. Harzen, S. S. Sugano, M. Shirakawa, R. Nishihama, Y. Ichihashi, S. G. Ibanez, K. Shirasu, T. Ueda, T. Kohchi, and H. Nakagami. 2023. "LysM-mediated signaling in Marchantia polymorpha highlights the conservation of pattern-triggered immunity in land plants." *Curr Biol* 33 (17):3732-3746 e8. doi: 10.1016/j.cub.2023.07.068.

Yuan, M., Z. Jiang, G. Bi, K. Nomura, M. Liu, Y. Wang, B. Cai, J. M. Zhou, S. Y. He, and X. F. Xin. 2021. "Pattern-recognition receptors are required for NLR-mediated plant immunity." *Nature* 592 (7852):105-109. doi: 10.1038/s41586-021-03316-6.

Yuan, M., B. P. M. Ngou, P. Ding, and X. F. Xin. 2021. "PTI-ETI crosstalk: an integrative view of plant immunity." *Curr Opin Plant Biol* 62:102030. doi: 10.1016/j.pbi.2021.102030.

Zhang, Lisha, Chenlei Hua, Denis Janocha, Judith Fliegmann, and Thorsten Nürnberger. 2023. "Plant cell surface immune receptors—Novel insights into function and evolution." *Current Opinion in Plant Biology* 74. doi: 10.1016/j.pbi.2023.102384.

Zhang, X., H. Peng, S. Zhu, J. Xing, X. Li, Z. Zhu, J. Zheng, L. Wang, B. Wang, J. Chen, Z. Ming, K. Yao, J. Jian, S. Luan, D. Coleman-Derr, H. Liao, Y. Peng, D. Peng, and F. Yu. 2020. "Nematode-Encoded RALF Peptide Mimics Facilitate Parasitism of Plants through the FERONIA Receptor Kinase." *Mol Plant* 13 (10):1434-1454. doi: 10.1016/j.molp.2020.08.014.

Zhang, X. S., J. H. Choi, J. Heinz, and C. S. Chetty. 2006. "Domain-specific positive selection contributes to the evolution of Arabidopsis leucine-rich repeat receptor-like kinase (LRR RLK) genes." *J Mol Evol* 63 (5):612-21. doi: 10.1007/s00239-005-0187-z.Zhang, X., Z. Yang, D. Wu, and F. Yu. 2020. "RALF-FERONIA Signaling: Linking Plant Immune Response with Cell Growth." *Plant Commun* 1 (4):100084. doi: 10.1016/j.xplc.2020.100084.

Zulawski, Monika, Gunnar Schulze, Rostyslav Braginets, Stefanie Hartmann, and Waltraud X. Schulze. 2014. "The Arabidopsis Kinome: phylogeny and evolutionary insights into functional diversification." *BMC Genomics* 15 (1):548. doi: 10.1186/1471-2164-15-548.

Zhang, X., Z. Yang, D. Wu, and F. Yu. 2020. "RALF-FERONIA Signaling: Linking Plant Immune Response with Cell Growth." *Plant Commun* 1 (4):100084. doi: 10.1016/j.xplc.2020.100084.

Zhao, C., O. Zayed, Z. Yu, W. Jiang, P. Zhu, C. C. Hsu, L. Zhang, W. A. Tao, R. Lozano-Duran, and J. K. Zhu. 2018. "Leucine-rich repeat extensin proteins regulate plant salt tolerance in Arabidopsis." *Proc Natl Acad Sci U S A* 115 (51):13123-13128. doi: 10.1073/pnas.1816991115.

Zhu, S., Q. Fu, F. Xu, H. Zheng, and F. Yu. 2021. "New paradigms in cell adaptation: decades of discoveries on the CrRLK1L receptor kinase signalling network." *New Phytol* 232 (3):1168-1183. doi: 10.1111/nph.17683.

Zipfel, C. 2014. "Plant pattern-recognition receptors." *Trends Immunol* 35 (7):345-51. doi: 10.1016/j.it.2014.05.004.

Zipfel, C., G. Kunze, D. Chinchilla, A. Caniard, J. D. Jones, T. Boller, and G. Felix. 2006. "Perception of the bacterial PAMP EF-Tu by the receptor EFR restricts Agrobacterium-mediated transformation." *Cell* 125 (4):749-60. doi: 10.1016/j.cell.2006.03.037.

Supplemental data

Peptides	Sequence
MpRALF1	AASGYYVGYGALTANRVPCPPQSGRSYYTPGCSTASGPVRPYTRGCSTITRCARDG
MpRALF3	ATKKKSNTKSSGYFISYSALSASRTSCPPRSGRSYYTRNCNSASGPVRPYSRGCSTISRCARDSG
AtRALF23	ATRRYISYGALRRNTIPCSRRGASYYNCRRGAQANPYSRGCSAITRCRRS
AtRALF34	YWRRTKYYISYGALSANRVPCPPRSGRSYYTHNCFRARGPVHPYSRGCSSITRCRR
F-RALF	PAAKPQSGEISYGALNRDHIPCSVKGASAANCRPGAEANPYNRGCNAIEKCRGGVGGN

Data S1. Sequences of RALF peptides

Chemically synthesised RALF peptides used in this study. All peptides were dissolved in Milli-Q water for usage and stored at -20 °C at a concentration of 1 mM.

	MpRALF1	AtRALF23	Mock
3h	7.0	7.0	7.0
24h	7.42	7.41	7.32

Data S2. The pH of surrounding buffer in primming assay

The pH of the surrounding buffer was measured after 3 hours or 24 hours of RALF peptide treatment at room temperature. The pH values represent the average of three measurements.

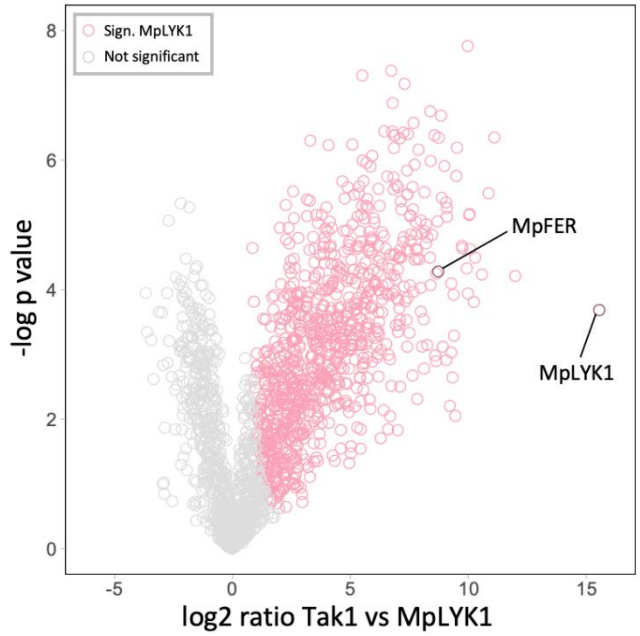

Figure S1. Interactome analysis of MpLYK1

Identification of MpLYK1 interacting proteins by the miniTurbo-based proximity *in vivo* labelling approach. *Marchantia polymorpha* wild-type Tak-1 was used as a control. Three biological replicates were used for the analysis. MpFER and bait protein MpLYK1 are shown in black.

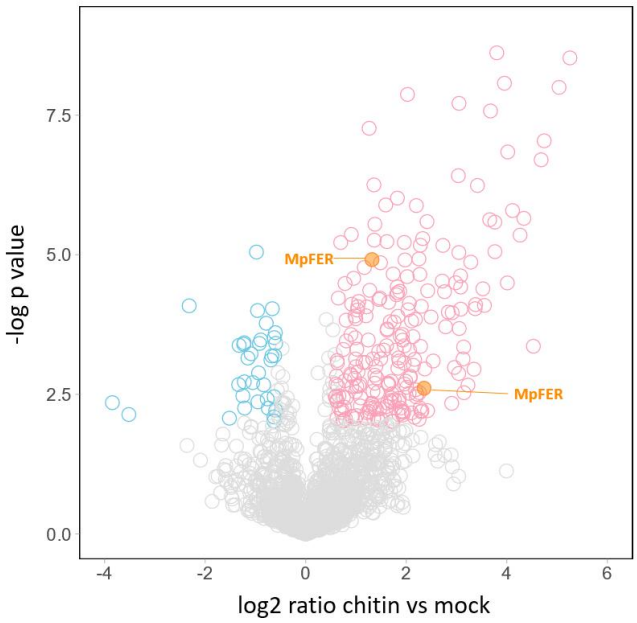

Figure S2. Chitin-induced phosphoproteome changes in *M. polymorpha*

Volcano plots showing differential abundance of phosphopeptides between *M. polymorpha* gemmalings treated with mock and 1 mg/mL chitin. Each circle represents a single unique phosphopeptide. Significantly increased and decreased phosphopeptides are coloured red and blue, respectively ($|log2FC| > 0.58$, $p < 0.01$). Phosphopeptides of MpFER were shown in orange filled circles.

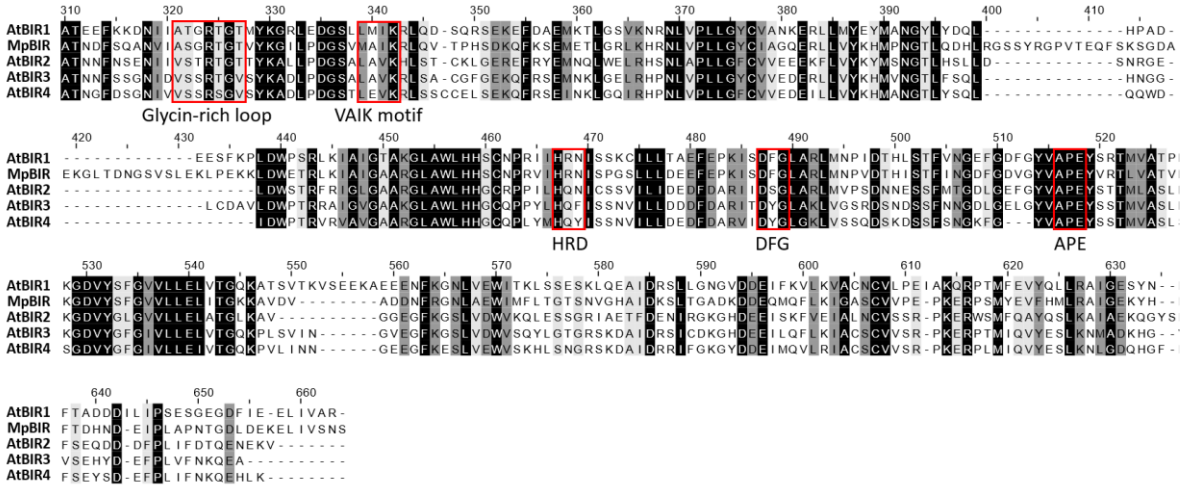

Figure S3. Sequence alignment of MpBIR and AtBIRs

An alignment of MpBIR and AtBIR1 to AtBIR4 reveals that MpBIR contains important catalytic residues (highlighted by red boxes) of the kinase domain.

Table S1 Transcriptome analysis

Table S2 Interactome analysis

Table S3 Interactome analysis

Table S4 Transcriptome analysis

Eidesstattliche Erklärung

gemäß der Promotionsordnung vom 12. März 2020

„Hiermit versichere ich an Eides statt, dass ich die vorliegende Dissertation selbstständig und ohne die Benutzung anderer als der angegebenen Hilfsmittel und Literatur angefertigt habe. Alle Stellen, die wörtlich oder sinngemäß aus veröffentlichten und nicht veröffentlichten Werken dem Wortlaut oder dem Sinn nach entnommen wurden, sind als solche kenntlich gemacht. Ich versichere an Eides statt, dass diese Dissertation noch keiner anderen Fakultät oder Universität zur Prüfung vorgelegen hat; dass sie - abgesehen von unten angegebenen Teilpublikationen und eingebundenen Artikeln und Manuskripten - noch nicht veröffentlicht worden ist sowie, dass ich eine Veröffentlichung der Dissertation vor Abschluss der Promotion nicht ohne Genehmigung des Promotionsausschusses vornehmen werde. Die Bestimmungen dieser Ordnung sind mir bekannt. Darüber hinaus erkläre ich hiermit, dass ich die Ordnung zur Sicherung guter wissenschaftlicher Praxis und zum Umgang mit wissenschaftlichem Fehlverhalten der Universität zu Köln gelesen und sie bei der Durchführung der Dissertation zugrundeliegenden Arbeiten und der schriftlich verfassten Dissertation beachtet habe und verpflichte mich hiermit, die dort genannten Vorgaben bei allen wissenschaftlichen Tätigkeiten zu beachten und umzusetzen. Ich versichere, dass die eingereichte elektronische Fassung der eingereichten Druckfassung vollständig entspricht."

Teilpublikationen:

Conserved role of the SERK–BIR module in development and immunity across land plants

Yan, Y., J. Mellüh, M. A. Mecchia, H. W. Jeon, K. Melkonian, C. Holzberger, A. Harzen, S. C. Stolze, R. Franzen, Y. Hirakawa. a, A. I. C. Delgado, and H. Nakagami. (2024) bioRxiv, Submitted

Köln, 29. August 2024

Yijia Yan